Mixing, Digestion, and Emptying in Human-Stomach: A Computational Fluid Dynamics Study

Vom Fachbereich Produktionstechnik

der

UNIVERSITÄT BREMEN

zur Erlangung des Grades

Doktor-Ingenieur

genehmigte

Dissertation

von

MSc., Changyong, Li

Gutachter: Prof. Dr. Marc Avila (Universität Bremen)

Prof. Dr.-Ing. Christian J. Cyron (Technische Universität Hamburg)

Tag der mündlichen Prüfung: 25.08.2022

Zusammenfassung

Der Magen ist für die Nahrungsverdauung unerlässlich, seine Funktionsweise ist jedoch sehr kompliziert, während seine Mechanismen noch nicht vollständig verstanden sind. Das Verständnis der Magenverdauungsmechanismen ist wichtig für die Entwicklung funktioneller Lebensmittel. Muskelbewegungen der Magenwand spielen eine entscheidende Rolle im menschlichen Verdauungsprozess. Sie verbessern die Vermischung der aufgenommenen Nahrung mit dem von der Magenwand abgesonderten Magensaft. In dieser Arbeit wird ein Computational Fluid Dynamics (CFD) Modell entwickelt, um die Strömungsdynamik beim Mischen flüssiger Nahrungsmittel mit dem Magensaft besser zu verstehen. Die Magenmotilität wird mit einem dynamischen Netz modelliert. Die Magensaftsekretion wird als Massenquelle modelliert und Wasserstoffionen werden dem Magenlumen kontinuierlich zugeführt. Die Magenentleerungsraten verschiedener Lebensmittel werden nach ihrem Kaloriengehalt bestimmt.

Das numerische Modell wird zunächst verwendet, um die Strömungsdynamik im Magen zu untersuchen. Die numerischen Ergebnisse zeigen, dass die terminalen Antrumkontraktionen (TACs) die kinetische Energie im Magen erheblich steigern können. Der TAC erzeugt rückläufige „Jets“ und senkt den pH-Wert des flüssigen Mageninhalts. Die Mischeffizienz von flüssigem Mageninhalt und Magensaft ist gering. Es dauert etwa 40-50 min bis sich eine saure Umgebung mit einem pH-Wert von 1,6 im Magenlumen eingestellt hat. Die Simulationen in dieser Arbeit zeigen, dass der Dichteunterschied in Nahrung/Magensaft signifikante Auswirkungen auf die dynamische räumliche Verteilung des Magen-pH-Wertes hat.

Mit dem entwickelten numerischen Modell, wird der Vorgang des Mischens und Entleerens von Mageninhalt weiter untersucht. Die numerischen Ergebnisse bestätigen, dass sich bei der Wasserentleerung ein schneller Entleerungsweg nahe der kleinen Krümmung (relativ kurzer konkaver Rand rechts) des Magens befindet. Dieser schnelle Entleerungsweg existiert jedoch nicht, wenn der Mageninhalt aus Wasser und Nahrungsbolus mit unterschiedlichen Eigenschaften besteht. Die Muskelkontraktionen verbessern das Mischen von leichten Boli und Wasser, während

sie nur begrenzte Auswirkungen auf schwere Boli haben. Dadurch werden Lebensmittel schichtweise verteilt; schwere Nahrungsboli befinden sich in der untersten Schicht. Neben der Magenmotilität und der hohen Viskosität der Nahrung ist auch die Nahrungsmatrix aus schweren Nahrungspartikeln für die Bildung der Magenstraße wichtig. Die Nahrungsmatrix und die Faltenzone verhalten sich wie ein poröses Medium, das den leichten Nahrungspartikeln einen höheren Strömungswiderstand als dem Wasser entgegensetzt, was zu einer schnelleren Entleerung des Wassers führt. Das Wasser wird entlang der Magenwand entleert, da der Strömungswiderstand in den Magenfalten kleiner ist als in der Nahrungsmatrix. Dieser Mechanismus wird durch die numerischen Ergebnisse gestützt und könnte die in Experimenten beobachteten Phänomene physikalisch erklären.

Das CFD-Modell wird weiterentwickelt, um die Verdauung großer Nahrungspartikel in einer sauren und dynamischen Umgebung zu untersuchen. Das in dieser Arbeit eingeführte Konzept der Lebensmittelmatrix wird verwendet, um die großen Nahrungspartikel zu modellieren. Zur Berechnung der Zerfallsgeschwindigkeit wird ein Reaktions-Diffusions-Konvektionsmodell verwendet. Die numerischen Ergebnisse zeigen, dass die Verdauung und Entleerung schneller ablaufen, wenn das Fleisch bei einer höheren Temperatur behandelt wird. Die Verdauungsgeschwindigkeit wird erheblich reduziert, wenn die Magenmotilität oder die Sekretion von Wasserstoffionen aufgrund einer Magenerkrankung geschwächt ist. TACs stimulieren starke retropulsive Rückflüsse, die den Transport von Enzymen und Wasserstoffionen verbessern und dadurch den Verdauungsprozess beschleunigen. Aufgrund des Strömungswiderstandes durch die Nahrungsmatrix aus großen Nahrungspartikeln wird flüssiger Mageninhalt in einem Weg nahe der Mageninnenoberfläche entleert. Große Nahrungspartikel werden hauptsächlich im Bereich neben der Mageninnenfläche zersetzt. Daher sollte die charakteristische Längenskala des Stofftransports (für Enzyme oder Wasserstoffionen) der Größe der Lebensmittelmatrix entsprechen, anstatt der Größe großer Lebensmittelpartikel.

Abstract

The stomach is essential for food digestion, however, its operation is highly complicated while its mechanisms are still not fully understood. Understanding gastric digestion mechanisms is important for the design of functional foods. Muscular movements of the stomach wall play critical roles in the human digestive process. They enhance the mixing of ingested foods with the gastric juice secreted from the stomach wall. In this thesis, a computational fluid dynamics (CFD) model is developed to better understand the flow dynamics in the process of mixing liquid foods with the gastric juice. The gastric motility is modeled with a dynamic mesh. The gastric juice secretion is modelled with sources of mass and hydrogen ions continually added into the stomach lumen. Gastric emptying rates of different foods are determined according to their calorie content.

The numerical model is first used to investigate flow dynamics in the stomach. The numerical results show that the terminal antral contractions (TACs) can considerably increase the kinetic energy in the stomach. The TAC creates retropulsive “jets” and reduces the pH of liquid gastric contents. The mixing efficiency of liquid gastric contents and gastric juice is low, and it takes about 40-50 min to approach an acidic environment with a pH of 1.6 inside the stomach lumen. The simulations in this thesis show that the density difference in food/stomach-juice has significant effects on the dynamic spatial distribution of gastric pH.

With the developed numerical model, the process of mixing and emptying of gastric contents is further investigated. The numerical results confirm that a fast pathway is located close to the lesser curvature (relatively short concave border on the right) of the stomach when water is emptied. However, this fast pathway doesn’t exist when the gastric contents are composed of water and food boluses with different properties. The muscle contractions enhance the mixing of light food boluses and water, while they have limited effects on heavy food boluses. As a result, food is distributed in layers; heavy food boluses are located in the bottom layer. Besides the gastric motility and high viscosity of foods, the food matrix made of heavy food particles is also important to the formation of the Magenstrasse (stomach road). The food matrix and the zone of wrinkles

behave like a porous medium which has higher flow resistance to the light food particles than to the water, leading to faster emptying of water. The water is emptied along the stomach wall since the flow resistance in the stomach wrinkles is smaller than the one in the food matrix. This mechanism is supported by the numerical results, and it may explain the phenomena observed in the experiments.

The CFD model is further developed to investigate the digestion of large food particles in an acidic and dynamic environment. The concept of food matrix introduced in this thesis is used to model the large food-particles. A reaction-diffusion-convection model is used to calculate the rate of disintegration. The numerical results suggest that the digestion and emptying become faster when the meat is treated at a higher temperature. The digestion rate is reduced considerably when the gastric motility or the secretion of hydrogen ions is weakened due to a stomach disorder. TACs stimulate strong retropulsive backflows which enhance the transport of enzymes and hydrogen ions, thereby accelerating the digestion process. Due to the flow resistance by the food matrix made of large food particles, liquid gastric contents are emptied in a pathway close to the stomach inner-surface. Large food-particles are mainly disintegrated in the region next to the stomach inner-surface. Therefore, the characteristic length scale of mass transfer (for enzymes or hydrogen ions) should be the size of the food matrix, instead of the size of large food-particles.

Acknowledgements

First, I would like to thank my advisors from Hamburg University of Technology, Dr. Yan Jin, and from University of Bremen, Prof. Marc Avila, for their tireless supports throughout my PhD. I also appreciate the research institute, Center of Applied Space Technology and Microgravity (ZARM), for securing conference funding, workplace, and computing resources that enabled me to complete the research. Special thanks to China Scholarship Council (CSC), which provides me with the scholarship to make this thesis possible.

Second, I am grateful to Prof. Xiao Dong Chen and Prof. Jie Xiao of Soochow University for many interesting discussions regarding the digestion in the gastrointestinal tract. I also thank the colleagues in Prof. Avila's group, they have contributed many insights in fluid mechanics, I have learned a lot from them.

Finally, I would like to thank my parents for their love, continued support and encouragement for many years. I also want to thank my friends who have given me a lot of time for listening to my sharing of happiness and sadness.

Table of Contents

Nomenclature

Acronyms

ACs	Antral contractions
ACWs	Antral contraction waves
B-SPH	Biomechanical-smoothed particle hydrodynamics
CFD	Computational fluid dynamics
CV	Control volume
FVM	Finite volume method
GALT	Gut-associated lymphoid tissue
KGM	Konjac glucomannan
MMC	Migrating motor complex
MPI	Message passing interface
MRI	Magnetic resonance imaging
NA	Not available
ODEs	Ordinary differential equations
PDEs	Partial differential equations
PISO	Pressure-implicit with splitting of operators
SCL	Space conservation law
TACs	Terminal antral contractions
TCs	Tonic contractions
0D	0-dimensional
2D	2-dimensional
3D	3-dimensional

Greek Symbols

α	Species in gastric contents (-)
β	Model constant (-)
γ	Model coefficient ($kg \cdot m^{-1-3\beta} \cdot s^{-2}$)
η	Model coefficient ($m^{3-1.5\beta} \cdot s^{-1}$)
μ_0	Dynamic viscosity of the water (Pa·s)
ν_0	Kinematic viscosity of the water ($m^2 \cdot s^{-1}$)
ν_F	Kinematic viscosity of small food particles ($m^2 \cdot s^{-1}$)
ν_l	Kinematic viscosity of the liquid ($m^2 \cdot s^{-1}$)
ν_m	Kinematic viscosity of the mixture ($m^2 \cdot s^{-1}$)
ξ	Diffusion coefficient in the Laplace equation (-)
ρ_0	Water density or reference density ($kg \cdot m^{-3}$)
ρ_F	Density of small food particles ($kg \cdot m^{-3}$)
ρ_g	Density of gastric contents ($kg \cdot m^{-3}$)
ρ_l	Density of the liquid ($kg \cdot m^{-3}$)
ρ_m	Density of the mixture ($kg \cdot m^{-3}$)
ρ_P	Density of the meat protein ($kg \cdot m^{-3}$)
τ_{ij}	Viscous stress tensor ($m^2 \cdot s^{-2}$)
φ	A general tensorial property (-)
ϕ	Local porosity (-)
ϕ_F	Porosity of the food matrix (-)
ϕ_W	Porosity of stomach wrinkles (-)

Roman Symbols

A_{ACW}	Amplitude of an ACW (m)
A_e	Area of the outlet (pylorus) (m^2)

A_{is}	Surface area of the stomach inner-surface (m^2)
A_s	Surface area of a food particle in the food matrix (m^2)
A_{TAC}	Amplitude of a TAC (m)
c_0	Mass fraction of the water (-)
c_E	Total enzyme concentration ($U \cdot mg^{-1}$)
c_{EG}	Enzyme concentration in the gastric juice ($U \cdot mg^{-1}$)
c_{EM}	Enzyme concentration in the food matrix ($U \cdot mg^{-1}$)
c_E^{pH}	Concentration of active enzymes ($U \cdot mg^{-1}$)
c_{Emax}^{pH}	Fraction of active enzymes that can access all available cleavage sites on proteins (-)
c_F	Mass concentration of small food particles (-)
c_H	Mole concentration of hydrogen ions ($kmol \cdot m^{-3}$)
c_{HG}	Mole concentration of hydrogen ions in the gastric juice ($kmol \cdot m^{-3}$)
c_{HM}	Mole concentration of hydrogen ions in the food matrix ($kmol \cdot m^{-3}$)
Co	Courant number (-)
Co_{max}	Maximum local Courant number (-)
c_n	Mass concentration of the n^{th} food species (-)
$\bar{c}_n$	Mean mass concentration of the n^{th} food species (-)
c_{n0}	Local mass concentration of the n^{th} food species for the initial field (-)
$\bar{c}_{n0}$	Mean mass concentration of the n^{th} food species for the initial field (-)
c_P	Mass concentration of the meat protein (-)
$\boldsymbol{d}_{AC}$	Displacement of the points at the stomach surface (m)
D_E	Diffusion coefficient of enzymes (pepsins, $m^2 \cdot s^{-1}$)
D_F	Diffusion coefficient of small food particles ($m^2 \cdot s^{-1}$)
D_H	Diffusion coefficient of hydrogen ions ($m^2 \cdot s^{-1}$)
d_p	Particle diameter in the food matrix (m)

D_p	Effective diameter of porous media (wrinkles and the food matrix) (m)
$\boldsymbol{D}_{sc}$	Distance vector pointing from a point at the stomach surface to the closest point at the centerline (m)
$e(t)$	The mass difference between $G(t)$ and $G_o(t)$ at time t (s)
g_i	Gravitational acceleration ($m \cdot s^{-2}$)
G_{emp}	Mass of emptied gastric contents (kg)
$G(t)$	The mass of gastric contents at time t (kg)
$G_o(t)$	The objective mass of gastric contents at time t (kg)
h_{ACW}	Width of an ACW (m)
K	Permeability (m^2)
k_B	Boltzmann's constant ($J \cdot K^{-1}$)
K_{a1}	First pepsin dissociation constant (-)
K_{a2}	Second pepsin dissociation constant (-)
Ke	Averaged kinetic energy ($m^2 \cdot s^{-2}$)
k_E	Mass transfer coefficient of enzymes (pepsins, $m \cdot s^{-1}$)
k_H	Mass transfer coefficient of hydrogen ions ($m \cdot s^{-1}$)
K_d	Parameter for the PID controller ($m \cdot kg^{-1}$)
K_i	Parameter for the PID controller ($m \cdot kg^{-1} \cdot s^{-2}$)
K_p	Parameter for the PID controller ($m \cdot kg^{-1} \cdot s^{-1}$)
l_{01}	Arc length between two points (m)
l_f	Constant of kinetic rate of formation of products form protein cleavage (s^{-1})
L	Constant of pseudo reaction rate (-)
m_H	Amounts of hydrogen ions in a mesh cell (kmol)
$\dot{m}$	Mass outflow rate of the gastric contents ($kg \cdot s^{-1}$)
$\dot{m}_H$	Secretion rate of hydrogen ions ($mol \cdot s^{-1}$)
m_E	Amounts of enzymes in a mesh cell ($U \cdot m^3 \cdot mg^{-1}$)
$m_{r,n}$	Mixing rate of the n^{th} food species (-)

M_t	Mixing index of hydrogen ions (-)
M_0	Initial value of M_t (-)
q_g	Caloric density of gastric contents (kcal·m^{-3})
$\dot{q}$	A constant of the caloric outflow rate (kcal·s^{-1})
p	Static pressure divided by density (m^2·s^{-2})
p'	Alternative pressure (m^2·s^{-2})
$\overline{\text{pH}}$	Volume averaged pH value in the stomach (-)
r_{ACW}	Maximum contraction rate of an ACW (-)
r_{dig}	Digestion rate of large food particles (-)
Re	Reynolds number (-)
r_{emp}	Emptying rate (m^3·s^{-1})
r_{gr}	Gastric retention rate (-)
r_{grl}	Gastric retention rate of liquids (-)
r_{grs}	Gastric retention rate of solids (-)
r_{mix}	Mixing rate of hydrogen ions (-)
r_{TAC}	Maximum contraction rate of a TAC (-)
Sc_E	Schmidt number of enzymes (-)
Sc_H	Schmidt number of hydrogen ions (-)
s_{ij}	Strain rate (s^{-1})
Sh_E	Sherwood number of enzymes (-)
Sh_H	Sherwood number of hydrogen ions (-)
$\dot{s}_G$	Source term due to the secretion of the gastric juice (kg·m^{-3}·s^{-1})
$\dot{s}_m$	Source term of the mass (kg·m^{-3}·s^{-1})
$\dot{s}_P$	Source term due to disintegration of the food matrix into small food particles (kg·m^{-3}·s^{-1})
$\dot{s}_{pi}$	Drag force due to porous media (m·s^{-2})
$\dot{s}_{ui}$	Source term in the momentum equation (m·s^{-2})

$\dot{s}_W$	Source term due to movements of wrinkles ($kg \cdot m^{-3} \cdot s^{-1}$)
t	Time (s)
t_0^{ACW}	Start time of an ACW (s)
t_0^{TAC}	Start time of a TAC (s)
T_a	Absolute temperature (K)
T_{ACW}	Generation period of an ACW (s)
T_{ACW}^{lc}	Life cycle of an ACW (s)
T_{he}	Time for half-emptying of gastric contents (s)
T_h	Heating temperature used to treat meat samples (°C)
T_{is}	Surface tension force of the stomach inner-surface (Pa)
T_{TAC}	Generation period of a TAC (s)
T_{TAC}^{lc}	Life cycle of a TAC (s)
u_{ACW}	Velocity of the ACW movement along the centerline ($m \cdot s^{-1}$)
u_e	Velocity magnitude at the outlet (pylorus) ($m \cdot s^{-1}$)
u_{gj}	Mesh velocity of the moving grid ($m \cdot s^{-1}$)
u_i	Velocity component ($m \cdot s^{-1}$)
u_{is}	Velocity magnitude of the stomach inner-surface ($m \cdot s^{-1}$)
u_j	Velocity component ($m \cdot s^{-1}$)
u_{si}	Velocity of the solid matrix of the porous matrix ($m \cdot s^{-1}$)
$\mathbf{u}_{TC}$	Velocity vector of tonic contraction ($m \cdot s^{-1}$)
V_{cell}	Volume of a mesh cell (m^3)
V_F	Volume of small food particles in the stomach (m^3)
V_l	Volume of the liquid in the stomach (m^3)
V_{l0}	Initial value of V_l (m^3)
V_{pl}	Volume of large food particles (m^3)
V_{pl0}	Initial value of V_{pl} (m^3)
V_s	Volume of solid food particles (m^3)

V_{s0}	Initial value of V_s (m^3)
V_t	Total stomach volume (m^3)
V_W	Volume of stomach wrinkles region (m^3)
V_w	Volume of the water in the stomach (m^3)
V_{w0}	Initial volume of V_w (m^3)

List of Figures

List of Tables

CHAPTER 1

Introduction

Health problems related to gastric mechanics have been studied extensively in recent years. Functional foods design and digestion control have caused widespread concerns, and the factors that influence drug absorption via gastrointestinal tract is drawing increasing interest. For people with decreased digestive ability, foods which can be easily digested are needed; for persons who have metabolic syndrome, which is a common metabolic disorder due to the increasing prevalence of obesity (Eckel et al., 2005), foods which are hard to digest are preferred, to avoid absorbing too many nutrients. Functional foods have been proposed and designed according to these demands. For example, foods which contain dextrin can reduce lipid absorption for losing weight (Mukai et al., 2017), and Konjac glucomannan (KGM) is widely used in designing satiety-enhanced foods due to its high viscosity (Ho et al., 2017; Morell et al., 2014; Shang et al., 2020).

Besides functional foods, the gastric mechanics is also important to biopharmacy. The forces experienced by a pill in the human stomach is very important for the rational design for targeted drug delivery to the proximal gastrointestinal tract (Laulicht et al., 2010). Many gastro-retentive techniques have been designed and tested to extend the gastrointestinal retention time, therapeutic agents can benefit from the increased residence time (Bardonnet et al., 2006; Davis, 2005; Talukder and Fassihi, 2004). The effect of food on the release and absorption of solid oral dosage forms is a common biopharmaceutical problem (Koziolek et al., 2013).

Researchers and technologists have investigated food digestion and drug metabolism in human stomach by *in vivo*, *in vitro*, and *in silico* methods. This introduction reviews the related researches to justify the thesis. The objectives and achievements of the thesis are described.

1.1 Food Digestion in Human Digestive Tract

Digestion is the breakdown of large, insoluble food particles into small, water-soluble molecules which can be absorbed into water-like plasma. It happens in the digestive tract. The state of food, such as size, composition, macrostructure and microstructure, changes significantly as it passes through the digestive tract. Digestion includes chemical digestion, physical digestion, biological digestion and absorption.

Chemical digestion involves secretions of digestive enzymes (biocatalysts) throughout the digestive tract. Physical digestion is the process that does not alter the chemical nature of the food. Mechanical and hydrodynamic forces make the food smaller to increase the surface area and mobility of the food. Biological digestion involves microbiology in the gastrointestinal tract. Absorption is the process in which nutrients are transferred into the blood or lymph capillaries through cell membranes of the lining in the small and large intestines.

The digestive tract is roughly a long and hollow tubular chamber which mainly includes the mouth, esophagus, stomach, small intestine and large intestine (see Fig. 1.1). The small intestine is composed of the duodenum, jejunum and ileum. The large intestine consists of the cecum, colon and rectum. Clinically, the part that includes the oral cavity, pharynx, esophagus, stomach and duodenum is usually called upper digestive tract, while the part below the jejunum is called lower digestive tract. The upper digestive tract is the main place for food digestion, whereas almost all nutrients, 95% water and electrolyte absorption are done in the lower digestive tract (Tharakan, 2009). Human digestive glands include both large digestive glands and small digestive glands. The small digestive glands are distributed in the wall of each part of the digestive tract. The large digestive gland is composed of three pairs of salivary glands (the parotid gland, sublingual gland, and submandibular gland), stomach gland, pancreas, liver and gallbladder. With the help of digestive juices secreted by the digestive glands, the digestive tract completes the food intake, nutrients absorption and excretion of waste to ensure the normal metabolism process.

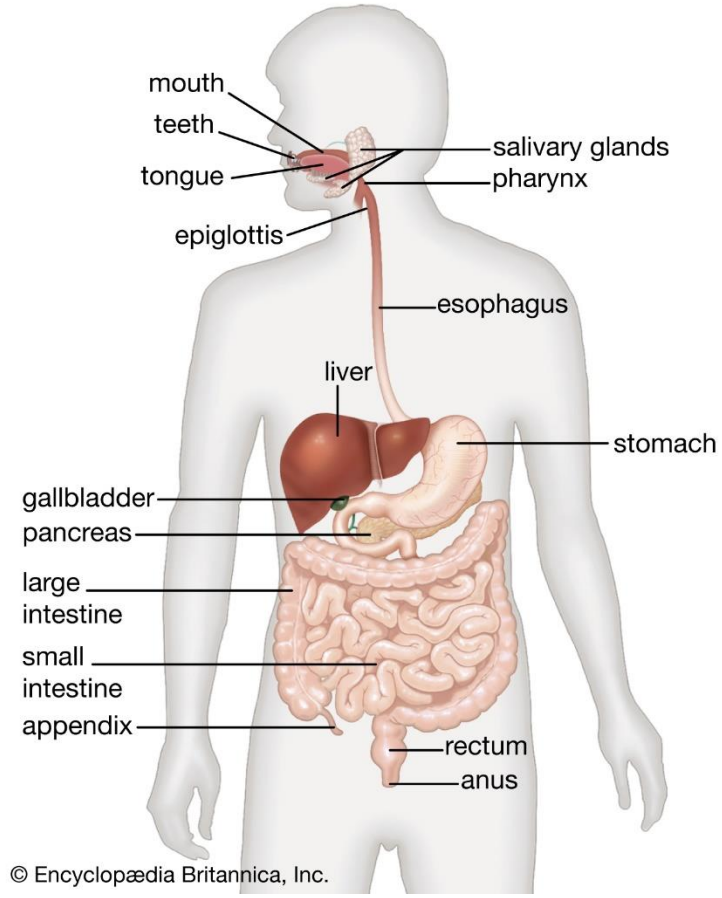

Fig. 1.1. The human digestive tract from mouth to anus as seen from the front. By courtesy of Encyclopædia Britannica, Inc., copyright 2010.

The mouth is the starting point of the digestive system and the respiratory system, and is also the first step for the digestion of solid foods inside the digestive tract. The teeth in the mouth can complete different tasks, e.g., cutting, tearing, grinding, and shearing (Mosca and Chen, 2016). The biting force is 100-400 N and varies individually (Marze, 2017a, b; Mosca and Chen, 2016). Mastication determines the initial particle properties (e.g., size, size distribution, density and porosities) of the gastric content. Ingested foods are masticated and mixed with saliva, saliva secretion is important for the composition and the physicochemical properties of stomach contents.

Table 1.1 shows the selected components of saliva and related functions. The saliva has pH of 5-7, it processes the food chemically (alpha-amylase catalyzes the decomposition of carbohydrates, and lingual lipase slightly decomposes fat) and helps swallow. The residence time of food in mouth

varies from 20 seconds to 2 min (Guerra et al., 2012). A former study showed that number of chewing cycles influences the emptying rate, and the emptying time decreases as the chewing number increases (Pera et al., 2002). The chewing cycles are affected by individual factors, e.g., physiology, degree of hunger, and certain habits (Engelen et al., 2005). In addition, the chewing performance shows high individual differences, it depends on the volume and food properties (including dryness, hardness or texture) (Fontijn-Tekamp et al., 2004; Helkimo et al., 1978). Usually, a longer time is needed for chewing hard foods, like peanuts and carrots, because the disintegration of the particles takes longer. The size of solid food is roughly reduced under 5.0 mm, which is related to the food type, e.g., the typical size for peanuts and gherkins is 0.8 mm and 3.0 mm respectively (Jalabert-Malbos et al., 2007). The product of oral digestion is called bolus; this term applies to this mixture of food until it is passed into the stomach for further digestion. 10 kPa pressure can be generated on the tongue surface when swallowing (Chen, 2009).

Table 1.1. The composition of saliva and the corresponding function (Koziolek et al., 2013).

Substances		Function
Water (99.5%)		Lubrication, cleansing, taste mediation
Proteins (0.3%)	Ig A (immunoglobulins)	Immune defense, antibacterial effects
	Lysozyme, lactoferrin	Antibacterial effects
	Mucins	Lubrication, tissue protection
	Alpha-amylase	Starch digestion
Electrolytes		Demineralization, remineralization, buffering
Urea		Buffering

The pharynx is a shared channel by both the respiratory tract and the digestive tract. In addition to respiratory, protective and defensive functions, the most important physiological function of the pharynx is to assist in swallowing food (Musselman, 1951). The esophagus (about 25 cm in length and 1.5-2 cm in diameter) is a long and narrow tubular organ connected to the pharynx on the

upper side and the cardia on the lower side. It is the channel for food to enter into the stomach; the main function of the esophagus is to swallow food and it does not have functions of digestion and secretion. The driving force for the transport of the bolus comes from the esophageal peristalsis. Esophageal peristalsis is performed by striated muscles in the cervical esophagus (upper part) and smooth muscles in the thoracic esophagus (lower part) (Koziolek et al., 2013).

The time of transporting bolus usually takes a few seconds, which can be affected by body posture, properties of the bolus, age and certain disorders (Nguyen et al., 1997; Osmanoglou et al., 2004). However, it has been reported that gelatin capsules can stay in the esophagus unnoticed for hours, which may cause serious problems (Jaspersen, 2000). At the lower end of the esophagus (~4-6 cm long from the cardia), the pressure is greater than the pressure in the stomach, which can effectively prevent the food in the stomach from flowing back to the esophagus (Hirano et al., 2015).

After food goes through the esophagus, it enters the stomach for further mixing and breakdown which is accomplished both mechanically and chemically. The role of the food's composition and structure in nutritional and functional performance during digestion has been widely recognized (Dupont et al., 2018; Kunz et al., 2005; Le Feunteun et al., 2014; Marciani et al., 2012; Marciani et al., 2007). The food bolus acts as a buffer to resist pH change, so that the main body tends to have higher pH and higher viscosity, surrounded by low pH and viscosity materials around the outside, while the pH can be very low close to the stomach wall. Marciani et al. (2001b) showed that gastric secretions are combined with gentle wall-motility by *in vivo* echo-planar nuclear magnetic resonance imaging (MRI). The wall movements make the more easily hydrated part of the bolus to be sloughed off in layers, this process is sometimes known as "onion peeling" effect (Rickett, 2013). Thus, we can see that this stage of digestion is a gradual process since parts of bolus are not immediately contacted with enzymes.

The obtained mixture of food and gastric secretions, called chyme, will later enter the duodenum through the pylorus under the control of the pyloric sphincter (Kong and Singh, 2008).

The acidic chyme will be neutralized by sodium bicarbonate ($NaHCO_3$) in the duodenum to approach a suitable pH for enzyme activities (Kaunitz and Akiba, 2006).

In the small intestine, the food mixes with bile as well as pancreatic juice and the nutrients are absorbed through the wall of the intestine (Schneeman, 2002). The retention time of the food in the small intestine is 2-5 h (Guerra et al., 2012). The motility of the duodenum has a strong relationship with the stomach, which is called "antro-duodenal co-ordination" (Ehrlein and Schemann, 2005). The duodenal contractions are inhibited during the emptying of the stomach. Chemical digestion happens in the duodenum: The remaining lipids after mouth digestion are decomposed (Carrière et al., 2001); carbohydrates are hydrolyzed in the lumen of duodenum and uppermost jejunum by the amylase in the pancreatic juice (Gray, 1975); proteins are digested by proteinase (e.g., trypsin, chymotrypsin, carboxypeptidase and elastase) in the pancreatic juice (Lorkowski, 2012). The typical pH in the lumen is 6.5-7 (Guerra et al., 2012). The bile acid contained in the bile acts as an emulsifier, dissolving lipids into the aqueous phase to form micelles, which are easily absorbed by the wall of the small intestine. Most bile salts are reabsorbed actively in the ileum and reused in the bile by the enterohepatic circulation. There are two movement types of the small intestine wall (physical digestion of the small intestine), one is segmentation contractions, which mix inner contents, another is peristaltic contractions that move contents forward (Griffiths, 2012).

The large intestine is the place for microbial fermentation and reabsorbing water as well as electrolytes, the rest will be emptied as excrement. The retention time in the large intestine is 12-24 h, and the typical pH in the lumen is 5-7 (Guerra et al., 2012).

The main process of the digestion, e.g., gastrointestinal transit, gut secretion, and motility are closely regulated by hormonal (Schubert, 2008) and neural (Mayer, 2011) effects. Digestive hormones may enhance or inhibit secretions of glandular organs and contractions of smooth muscles. There are two nervous systems (autonomic nervous system and enteric nervous system) involved in the regulation of the digestive process. There are approximately 70% of all immune

cells in the body located in the digestive tract (known as gut-associated lymphoid tissue, GALT), which play an important role in the immune system, i.e., mucosal defense (Mason et al., 2008).

1.2 Human Stomach

The shape of the stomach varies with the volume of the food in the stomach and the posture of the person (Langer, 1988). For an adult human, the stomach's relaxed and empty volume is about 0.08 liters, since it has a good distensibility, the stomach can expand to hold roughly 4 L of foods (Johnson and Brusca, 1994). In moderate filling condition, the adult stomach is about 25 to 30 cm in length and approximately 1.5 L in capacity (Tortora and Derrickson, 2017). Despite of the differences in detail, their general shape is similar to the Roman-letter "J" as shown in Fig. 1.2. The J-shaped stomach connects the esophagus at its upper end and the duodenum at its lower end.

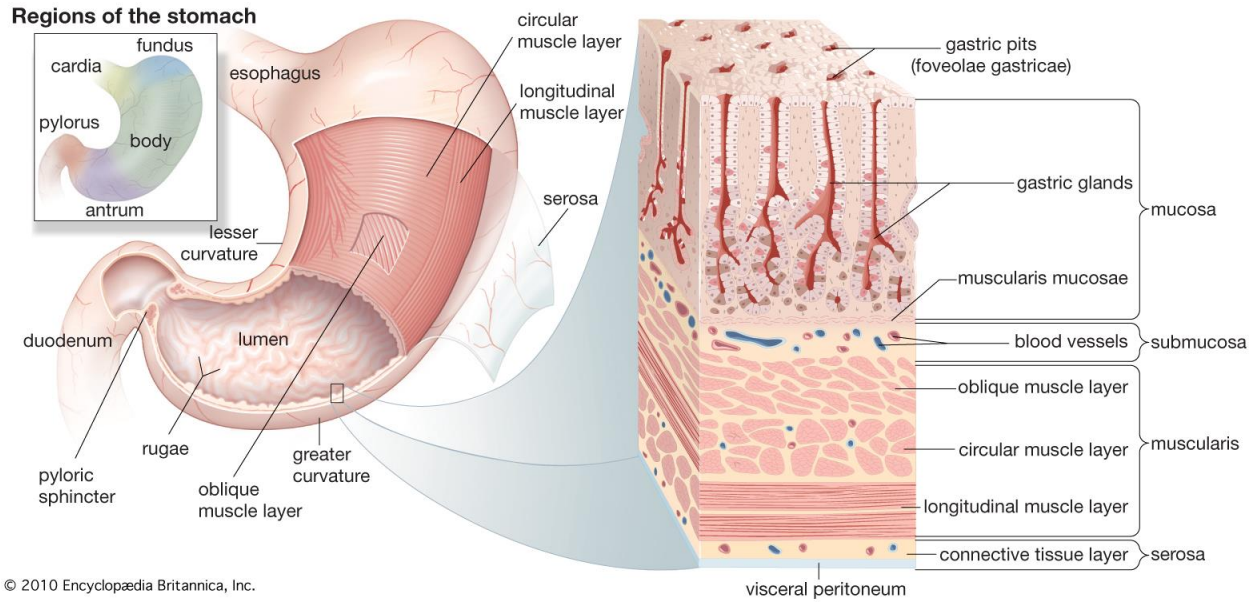

Fig. 1.2. Structure of the human stomach (left) and a zoomed view of the gastric wall (right). By courtesy of Encyclopædia Britannica, Inc., copyright 2010.

The three major roles of stomach are storing, mixing and emptying of the food during the digestion (Kong and Singh, 2008). The stomach can also absorb certain small molecules, i.e.,

aspirin (Hogben et al., 1957), amino acids (Krehbiel and Matthews, 2003), caffeine (Chvasta and Cooke, 1971) and ethanol (Levitt et al., 1997). Generally, the digestion speed of the stomach is regulated by the emptying rate, and can be affected by meal temperature, viscosity and energy content, the amount of nutrients (e.g., sugars and fat), the structure and texture of the food (Marciani et al., 2001b; Marciani et al., 2007).

The concave border of human stomach on the right is called lesser curvature, and the convex border on the left is called greater curvature, see Fig. 1.2. Anatomically, a human-stomach can be decomposed into five parts: The cardia, fundus, body, antrum, and pylorus.

The cardia is the part which is closest to the esophagus. A 1.5-3 cm wide sphincter can be found in the cardia, the sphincter can tighten the cardia entrance, and thus prevent the food and gastric acid in the stomach from flowing back into the esophagus during the gastric peristaltic contraction (Owen, 1986).

The upper section of the stomach next to the cardia is called the fundus. The middle part of the stomach is the body (corpus), which is the main portion of the stomach. The proximal stomach consisted of fundus and orad body (around one third of the body) is a reservoir for undigested material and responsible for the emptying of liquids (Urbain et al., 1989). Additionally, it may influence the distribution and selective emptying of gastric contents during the digestion process (Schwizer et al., 2002; Wickham et al., 2012). The reservoir function is achieved due to the flexibility and distensibility of the stomach volume. The large volume of food ingestion only induces a small increase of the intragastric pressure due to the regulation of vagus nerves (Kwiatek et al., 2009).

The distal stomach made of the remaining body, the antrum and the pylorus acts as the grinder, mixer and siever of solid particles (Brandstaeter et al., 2019; Urbain et al., 1989). The antrum has a higher density of smooth muscle that can generate strong peristaltic waves to grind and compress the food (Beckett et al., 2003). Mixing and homogenizing function are achieved by physical (gastric contractions) and chemical (gastric juices) effects (Kong and Singh, 2008). The pylorus

links the stomach and the duodenum, which is the narrowest portion of the stomach, with a diameter ranges between 5 mm and 23 mm reported in the literature (Harrison et al., 2018). Pylorus controls the emptying of chyme into the small intestine, which acts like a valve. The size of solid contents need to be reduced under 2.0 mm to pass through the pylorus, larger solid foods remain in the stomach for further digestion (Kelly, 1980). The experiments of Tougas et al. (1992) showed that the pylorus sphincter keeps open for pure water, while it contracts when receptors in the duodenum detect fats and sugars.

1.2.1 Stomach Wrinkles

The human stomach wall is about 3-4 mm in thickness and mainly consists of four layers (see Fig. 1.2), the serosa, muscularis, submucosa, and mucosa, from the outside to the inside (Brandstaeter et al., 2019). The inner surface of the stomach is full of wrinkles (also known as rugae or gastric folds), the mucosal lining forms these countless wrinkles, each wrinkle is around 5-10 mm in width and 2-4 mm in depth (Chen et al., 2016). Rugae allow stretching and unfolding of the stomach for accommodating meals and also help to grind and move food during digestion.

1.2.2 Gastric Secretions

The stomach secretes digestive enzymes, which are called gastric enzymes. Pepsin (secreted as the inactive precursor, pepsinogen) is the main gastric enzyme, which is produced by gastric chief cells (Podolsky et al., 2015). Pepsin breaks down food-proteins into smaller particles (e.g., peptide fragments and amino acids). Pepsin is most active in acidic conditions between pH 1.5 to 2.5 and inactive when at pH greater or equal to 6.5, but it is fully denatured until pH 8.0 (Piper and Fenton, 1965).

Gastric juice, which is also called gastric acid or stomach acid, is a digestive fluid produced by gastric glands located in the stomach wall and is mainly made up of water (around 99.5% of the gastric juice), mucus, pepsinogens, and hydrochloric acid (HCl), more detailed information can be found in Table 1.2.

Table 1.2. The main components of the gastric secretion.

Component	Secretion cell	Function
Mucus	Foveolar cells	Mucosa protection, lubrication
Pepsinogen	Chief cells	Digestion of proteins (after acid activation to pepsin)
Hydrochloric acid (HCl)	Parietal cells	Pepsin activition, protein degradation, protection against overgrowth of bacteria, support of duodenal micronutrient absorption
Bicarbonate	Foveolar cells	Prevention of gastric acid from damaging the stomach
Gastric lipase	Chief cells	Lipolysis
Intrinsic factor	Parietal cells	Necessary for the absorption of vitamin B_{12} in the distal ileum
Bile salts	From duodenal reflux	Surface tension reduction (surfactant), lipid emulsification via creation of mixed micelles

The pH value of gastric juice is between 1.3 and 2.5 inside the human stomach lumen of healthy human, while eating can increase the pH value to the range 4.5-5.8 (Kong and Singh, 2008). Gastric acid is subsequently secreted to reduce the pH within 1 h (Malagelada et al., 1976). However, areas of stomach can still have a pH more than 5 up to 3-5 hours (Bornhorst et al., 2014). Ingestion of food and swell of the stomach leads to the secretion of gastric juice. The stomach secretes 2 to 3 liters of gastric juice per day. After food intake, the secretion rate can increase from 10 $ml \cdot min^{-1}$ under fasting condition to 50 $ml \cdot min^{-1}$ (Versantvoort et al., 2004).

Typical viscosity of gastric juice in the human-stomach ranges 0.01 to 2 Pa·s, and it has a similar density as water (Abrahamsson et al., 1998; Abrahamsson et al., 2005). It is a non-Newtonian fluid with shear-thinning behavior (Dikeman and Fahey Jr, 2006; Takahashi and Sakata, 2002). The gastric juice penetrates and dilutes the gastric contents (Kong and Singh, 2008). *In vitro* experiments have shown the viscosity of digesta decreased after 40 minutes from a maximum of 17 Pa·s to 2.2 Pa·s (Marciani et al., 2000). The influences of peristalsis, dilution and proteolysis

on the viscosity of digesta were quantified by Ye et al. (2022), they indicated that peristalsis and dilution play a domiant role in reducing the viscosity.

1.2.3 Gastric Motility

Gastric motility shows different patterns in the fasted and fed states. In the fasted state, there is a four-phase and cyclical movement called inter-digestive migrating motor complex (MMC), where the electric activity of stomach wall cleans and empties non-digestible objects from the lumen (Takahashi, 2012, 2013). The MMC is dominated by the contractive pattern due to circular muscle contractions. The four phases of MMC are identified by their strength of contraction, and each phase lasts for different times (Kong and Singh, 2008). As can be seen in Table 1.3, phase III has the strongest contractions, which allow the stomach to empty large monolithic items, e.g., capsules and tablets (Brun et al., 2012). All the undigested objects are swept into the small intestine during this phase. Phase I and IV show weakest contractions. As for phase II, the contraction intensity is up to 50% of the maximum. The whole period of a MMC is around 1-2 h, which starts from the proximal stomach and moves towards the ileum (Sarna, 1985; Vantrappen et al., 1977).

Table 1.3. The intensity and duration of four phases in a MMC cycle. mm Hg is a measure of pressure, a peak pressure amplitude can be measured in the stomach.

Phase	Intensity	Duration (min)
I	Rare contraction	40-60
II	Higher frequency and contraction strength (up to 40 mm Hg)	40-60
III	Highest contraction strength (up to 80 mm Hg)	4-6
IV	Motoric rest, a transition period between in phase III and I	15-30

After ingestion of a meal, MMC patterns change to digestive motility patterns (fed patterns). The gastric relaxation for a meal can be decomposed into three mechanisms, i.e., receptive, adaptive and feedback relaxation of the proximal stomach, which acts as the reservoir (Ehrlein and Schemann, 2005). Fed contractions are continuous and have moderate intensity ranging in 15-20 mm Hg (Kong and Singh, 2008). They can be decomposed as tonic contractions (TCs) (also called sustained contractions) and antral contractions (ACs) (Indireshkumar et al., 2000).

TC is a weak continuous contraction of stomach muscles, which produces positive pressure differences between the stomach cavity and the duodenum. TCs involve all stomach muscles (three layers of smooth muscle: Longitudinal, circular, and oblique layers) to coordinate accommodation of the stomach to varying volumes of gastric contents. TCs are also known as fundic contractions, since the shallow indentations act on the proximal great curvature, they are helpful for moving food from top to bottom of the stomach (Pal et al., 2007). In addition, the fundic pressure gradient is regarded as the driving force for liquid emptying (Indireshkumar et al., 2000).

After gastric contents are transported to the antrum, ACs contribute to the mixing and homogenization of gastric contents. ACs are composed of antral contraction waves (ACWs) and terminal antral contractions (TACs). ACWs initiate at the mid-corpus where pacesetter cells (interstitial cells of Cajal) are located, and travel towards the terminal antrum within 60 s. The mean occlusion rates are 40%-60%. A higher occlusion indicates a higher pressure on the gastric contents. It has been reported that antral pressure increases from 50 mm Hg in the upper region of the antrum to more than 200 mm Hg at pylorus (Savoye-Collet et al., 2003; Sun et al., 1995). The propagation velocity is around 2-3 $mm \cdot s^{-1}$, averages 2.5 $mm \cdot s^{-1}$ and increases from the proximal region to distal region of the stomach. The frequency is around 3 min^{-1}, however, a lower frequency has also been demonstrated after ingesting a liquid meal (Kong and Singh, 2008; Koziolek et al., 2013).

In general, the speed and frequency of ACWs are nearly constant for different food types and viscosities. For instance, it has been reported that the speed of ACWs is 2.8 $mm \cdot s^{-1}$ for liquid food

and 3.1 $mm \cdot s^{-1}$ for solid-containing food; furthermore, the frequency is same (2.9 min^{-1}) for these two types of food (Kunz et al., 1999). Marciani et al. (2001a) reported effects of the food viscosity, they showed that the speed and frequency of ACWs are 1.57 $mm \cdot s^{-1}$ and 2.98 min^{-1} respectively for the food with 0.06 Pa·s of viscosity. These parameters are almost unchanged for food with 29.5 Pa·s of viscosity, the speed is 1.55 $mm \cdot s^{-1}$ and the frequency is 2.92 min^{-1}. However, ACW parameters can be influenced by physical conditions. Ajaj et al. (2004) found that the mean velocity of ACWs decreased down to 1.0 $mm \cdot s^{-1}$ in patients with gastroparesis, while the mean speed was 2.4 $mm \cdot s^{-1}$ for healthy volunteers.

TACs are segmental contractions of the terminal region of the antrum, which occur when ACWs reach the terminal antrum, the contraction widens and deepens, and often occludes the antral lumen (Bilecen et al., 2000; Schulze, 2006). When the pylorus is closed, gastric contents will be forcefully pushed back to the stomach lumen by TACs through the narrow path induced by the contraction. This eject has a nozzle effect which can help to mix and emulsify gastric contents. In addition, it rubs and grinds large food particles.

Gastric motility causes the movement of food during the digestion, however, the relationship between the motility and the gastric force is still unclear. The force (or stress) that acts on solids can be classified as compressive force and shear force. The compressive force is the direct compression on the solids from the gastric wall by movements. The shear force is the hydrodynamic shear when the gastric flow exists. Consequently, it is unknown which is the dominant gastric force.

Regarding the hydraulic pressure: Kwiatek et al. (2009) reported that the mean pressure is 1.6-2.8 mm Hg for liquid food; Desipio et al. (2007) reported that the mean pressure is 12.8 mm Hg for liquid food and 9.9 mm Hg for solid-containing food; the maximum pressure is 60.5 mm Hg for liquid food and 53.6 mm Hg for solid-containing food, which was found by Desipio et al. (2007). Regarding the breaking force on solid foods: Marciani et al. (2001a) and Vassallo et al. (1992) reported that the gastric force to grind solid foods is between 0.1 N and 1 N. Marciani et al.

(2001a) stated that the average force of the stomach to crush solid food is only 0.65 N. Kamba et al. (2001, 2002) found that generated compressive forces can be 1.89 N for hard solids in the antrum.

To summarize, the mechanical breakdown of solids involves compressive forces resulting from movements of the stomach wall, as well as the shear forces generating from the surrounding gastric fluid flow and pressure.

1.3 *In Vivo*, *In Vitro* and *In Silico* Studies on Gastric Digestion

Understanding gastric digestion mechanisms is important for the design and manufacture of novel and healthy foods (Liu et al., 2020). For this reason, gastric digestion has received intensive attentions. The studies of gastric digestion in stomach can be classified as *in vivo*, *in vitro*, or *in silico* studies. These studies have been extensively reviewed (Bornhorst and Paul Singh, 2014; Brandstaeter et al., 2019; Ferrua and Singh, 2015; Kong and Singh, 2008; Koziolek et al., 2016; Le Feunteun et al., 2020).

In vivo studies are those which involve living organisms. Gastric emptying is an important topic of *in vivo* studies; it plays a leading role in digestion, satiety and absorption of nutrient (Smeets et al., 2021). There are various methods for measuring gastric emptying. The common approaches include: ^{13}C-octanoic acid and ^{13}C-acetate breath test, paracetamol absorption test, ultrasonography (Glerup et al., 2007), MRI (Schwizer et al., 1992) and gamma scintigraphy (Abell et al., 2008). It was found that, in the digestive period, the emptying rate of stomach is highly dependent on food's volume, osmolality (the concentration of dissolved particles per kilogram of solution, osmol·kg^{-1}), chemical composition and caloric density (Hunt et al., 1985). A larger meal volume provides a faster gastric emptying at a given calorie load, however, gastric emptying is slowed down by higher calorie amount at a given volume of the meal (Kwiatek et al., 2009). Camps et al. (2016) confirmed that the increase in energy density and viscosity of foods slows down the

gastric emptying process, while the energy load plays a major role, the viscosity is more important in increasing satiety.

In vivo studies provided important first-hand information about gastric emptying. Generally speaking, by providing end-point measurements that are directly applicable to human food consumption, *in vivo* experiments on humans are useful to study many types of food (Mackie et al., 2020). However, *in vivo* experiments can be technically difficult and costly since the complexity of the multi-stage digestion, it sometimes might cause serious ethical problems especially when involving with potentially harmful substances, e.g., xenobiotics and pathogenic microorganisms (Guerra et al., 2012). As a result, it is hard to investigate the details of digestion using this method.

In vitro experiments simulate digestive process outside the body. *In vitro* gastric models are used more and more to be an alternative to *in vivo* analyses to solve problems interested by industries and researchers. There are a broad range of *in vitro* systems available, the models used can be classified as static and dynamic models (Guerra et al., 2012). Static models have been used to evaluate the biochemical environment, but they don't physiologically mimic the real gastric digestion conditions (Li et al., 2019). A standardized protocol of static *in vitro* simulation of gastrointestinal digestion based on an international consensus was developed by Brodkorb et al. (2019).

Static models are practical, cheap and feasible options for evaluating many experimental conditions and a large number of samples. However, more recent *in vitro* experiments adopted dynamic models, which were developed with more realistic conditions incorporated, e.g., gastric morphology, anatomy and peristalsis. There are some review papers which compare different *in vitro* models in different aspects (Dupont et al., 2019; Ji et al., 2021; Li et al., 2020; Sensoy, 2021; Wu and Chen, 2019; Zhong and Langrish, 2020). *In vitro* dynamic systems include TNO gastrointestinal model (TIM) (Bornhorst et al., 2016; Lafond et al., 2015), simulator of the human intestinal microbial ecosystem (SHIME) (Garcia-Villalba et al., 2017; Molly et al., 1993),

engineered stomach and small intestinal (ESIN) system (Guerra et al., 2016), dynamic artificial digestive system (DIDGI) (de La Pomélie et al., 2019; Ménard et al., 2014), simulator of the gastrointestinal tract (SIMGI) (Barroso et al., 2015; Miralles et al., 2018), *in vitro* mechanical gastric system (IMGS) (Barros et al., 2016), dynamic gastric model (DGM) (Vardakou et al., 2011; Wickham et al., 2012), human gastric simulator (HGS) (Kong and Singh, 2010), dynamic gastric simulating model (DGSM) (Do et al., 2016), near real dynamic *in vitro* human stomach (new DIVHS) system (Wang et al., 2019), improved version of DIVHS (DHS-IV) (Shang et al., 2020; Wang et al., 2022), human gastric digestion simulator (GDS) (Kobayashi et al., 2017; Kozu et al., 2017; Kozu et al., 2014b), and artificial gastric digestive system (AGDS) (Liu et al., 2019).

TIM, SHIME, ESIN, DIDGI, SIMGI, and IMGS simulate not only stomach but also the small intestine. Moreover, SHIME and SIMGI simulate the fermentation of the large intestine. While DGM, HGS, DGSM, DIVHS, DHS-IV, DGS, and AGDS emphasize the simulation of the mechanical, dynamic, and chemical conditions of the stomach.

It can be seen from these studies that *in vitro* measurements have good reproducibility without any ethical problems. They may use complex control systems to mimic the physiological functions of the human digestive system as much as possible. A well-designed *in vitro* system can track foods' structural and physicochemical changes during the digestion (Peng et al., 2021). A major challenge for developing *in vitro* gastric models is how to simulate realistic gastric emptying (Peng et al., 2021). This is a difficult task due to the limit of the current experimental designs (Kong and Singh, 2008; Li et al., 2020). As for limitations, e.g., the experimental system does not include interactions with the host, and the mechanisms of mixing, emptying and absorption differ from *in vivo* conditions.

Even through advanced imaging techniques have given a better understanding of the secretory (Sauter et al., 2012) and motor activities (Kwiatek et al., 2006; Pal et al., 2004; Treier et al., 2006) of the stomach wall, computational modelling tools make it possible to have a first insight into the actual conditions that foods experience during digestion (Ferrua and Singh, 2015). *In silico*

methods perform digestion experiments using numerical methods. They can be classified as 0-dimensional (0D) system simulations, computational solid mechanics (CSM) simulations and multi-dimensional computational fluid dynamics (CFD) simulations.

0D system simulations have a low computation cost, they only consider the time dependency, so they are suitable for predicting the global behavior of a digestion process. Kondjoyan et al. (2015) determined the digestibility of myofibrillar proteins by pepsin with *in vitro* experiments and 0D mathematical modelling. The 0D model includes a primary model which predicts *in vitro* digestion kinetics, and a secondary model which accounts for the heat effects based on the protein denaturation mechanisms. They showed that heating time, temperature, enzyme concentration, pH and residence time in the stomach all affect digestibility. Sicard et al. (2018) developed a 0D reaction-diffusion mathematical model to predict the digestion of meat proteins in the human stomach. The pH buffering of meat, pepsin and proton diffusion in bolus particles were taken into account. They showed that the bolus particle size, the variation of gastric pH, and pH buffering capacity of meat influence the protein digestion. Moreover, they found that the mass transfer between gastric fluid and bolus particles has significant effects on digestibility, while the amount of pepsin has little effects.

CSM simulations focus on the food flow-fracture in the stomach, by using a viscoplastic-damage constitutive law. Skamniotis et al. (2020) showed that bolus separation during backward extrusion and/or peristaltic wave intrusion, as well as bolus agglomeration caused by hydrostatic compression near the pylorus, are two competing phenomena that can influence the free surface to volume ratio of the bolus. Before studying food disintegration in the human stomach, the same group developed CSM models for simulating deformation-fracture during cutting in ultra-soft solids. They showed that Eulerian finite element analysis is a versatile approach to model largely different material cutting behaviors (Skamniotis and Charalambides, 2020), and modelled large strain fracture behavior of soft viscous foods to understand and improve the oral breakdown efficiency of foods (Skamniotis et al., 2017).

CFD simulations can provide even more detailed information in terms of gastric digestion, in particular the flow phenomena in the stomach. Pal et al. (2004) developed the first simplified 2-dimensional (2D) CFD model to investigate the flow and mixing in the stomach. They reported two basic fluid motions: Retrograde jets through ACWs and circulatory flow between ACWs were observed in the simulation results, both of them contribute to mixing. Antrum was identified as a zone of mixing created by ACWs, and multiple and narrower ACWs strengthened the mixing. Pal et al. (2007) discovered a new function of ACWs apart from grinding and mixing. They suggested that ACWs can move liquids along a narrow and long pathway from the fundus to the duodenum through the center of the antrum in coordination with fundic contractions. The characteristics of this pathway were found to be related with properties of ACWs. When ACWs are narrower and more occlusive, the pathway will be closer to the lesser curvature and the deeper into the fundus.

In another 2D simulation, Kozu et al. (2010) created a symmetrical computational domain of distal human-stomach. They investigated flow behavior of Newtonian fluids with seven different viscosities (from 7.3×10^{-4} to 4.7×10^{3} Pa·s). The results showed that the fluid viscosity greatly influences velocity profile in the computational region. In a later study with a similar computational domain, the same group (Kozu et al., 2014a) observed that the retropulsive flow was against the direction of peristalsis for liquid contents, i.e., water and starch syrup solutions. The maximum Reynolds number (Re) approached 125 in their simulation. They showed that the viscosity of liquid gastric contents (1×10^{-3}-0.1 Pa·s) hardly affect the maximum flow velocity. Hao et al. (2015) used a 2D stomach model which was partially filled with water-like fluid. They used multiphase flows to study effects of the buoyancy on the gastric emptying and motion of gastro-retentive micro-particles. The influence of particle density and viscosity, as well as gastric juice viscosity were investigated. They found that recirculating flows can mix particles with conventional density (neutrally buoyant) and transport them to the pylorus (the emptying ratio reaches 67% after 180 min). However, the particles with low density remained floating on the surface of the fluid phase and the particles with high density deposited in the bottom of the stomach. As a consequence, the retention time of these particles has been significantly increased.

Alokaily et al. (2019) used a geometrical model of the stomach consisting of an axisymmetric tube of different diameters, with a wall at one end, to represent the gastric antrum and the closed pylorus. They performed a parametric study (i.e., the fluid viscosity, wave speed, wave width, and maximum relative occlusion) on gastric flows (retropulsive jet near the pylorus and the recirculation between consecutive ACWs). They indicated that the mixing efficiency increases as the relative occlusion increases, or as the viscosity or wave width decreases. The retropulsive jet was quantified using its maximum velocity and length along the centerline. Under different wave shape, they found that these quantities are independent of Re when Re is low, and when Re is larger than 1, the peak velocity decreases and the jet length increases with increasing Re.

By using the same geometric model as Alokaily et al. (2019), Dufour et al. (2021) investigated the dispersing characteristics of ACW flow in the distal stomach and determined the effects of ACWs on liquid drops (the dispersed phase fluid). They performed simulations and experiments with different rheological properties, two relative occlusions (0.6 and 0.75), and various ACW speeds (1.0 to 7.5 $mm \cdot s^{-1}$). It has been found that the viscosity ratio (the dispersed phase fluid over the continuous phase fluid) affects the retraction dynamics of a drop's tail. They also found that a drop broke up when a critical capillary number was larger than 0.51 and the drop passed to the wave apex within a critical dimensionless distance of 0.3. Avvari (2021) developed a theoretical model of the pyloric channel, the model was simplified as a 2D tube with sinusoidal motility. It was used to estimate the resistance to gastric emptying and duodenogastric reflux from the pylorus. They indicated that the resistance of pyloric channel is related to the flow behavior index (a parameter which indicates the degree of non-Newtonian characteristics of the fluid), pressure gradient and channel diameter.

Although 0D and 2D numerical simulations contribute to the understanding of digestion in the stomach, they still cannot completely represent the complex geometry and function of the human stomach. Moreover, the asymmetric nature of the human stomach has to be taken into account, especially when gravity effects on the lower part of the stomach are considered. Therefore, it is necessary to model the stomach with a 3D geometry.

Following the initial work done by Singh (2007), Singh and Singh (2010) developed a 3D gastric model and analyzed the dynamics of different Newtonian fluids. The geometrical model was an average-sized human stomach, and the motility pattern was represented by a series of ACWs. They predicted the retropulsive and recirculating motions within the stomach antrum, and indicated that the dynamics is significantly affected by the motor activity of the ACWs and viscosity of the gastric fluid. The flow dynamics of gastric contents with different viscosities was further investigated in a later study from the same research group (Ferrua and Singh, 2010). Their numerical results showed that the retropulsive velocities become weaker when the viscosity is reduced, while the pressure increased. They also indicated that gastric contents with high viscosity are hard to be mixed. By using this simplified model, Ferrua and Singh (2011) investigated flow behaviors of gastric liquids with different rheological properties, and analyzed their effects on the flow field, pressure gradients and motion of discrete food particles. Ferrua et al. (2011) showed that a change in the rheological properties of gastric fluid can significantly influence the formation and strength of eddy structures. A higher retropulsive velocity was achieved when the viscosity was increased. Xue et al. (2012) (from the same group) studied the effects of food particles by using the Euler-Euler multiphase model. They investigated the effects of the density difference (between the particle and the fluid) and the ratio of loaded particle on gastric flow. The results showed that the small (5%) density difference and the increase (from 10% to 30%) in the ratio of loaded particle have significant impact on the flow field. Ferrua et al. (2014) studied the ability of the human stomach to advect and transport gastric contents with different rheological properties. The flow behavior of two Newtonian fluids and a pseudoplastic fluid were characterized. Results showed that the chaotic gastric advection is always relatively weak and the gastric rheology has minor effects on the flow advective properties.

Harrison et al. (2018) investigated the mixing and emptying behavior for aqueous liquid contents in the first three minutes inside the stomach using a coupled biomechanical-smoothed particle hydrodynamics (B-SPH) model. The model showed the ability of B-SPH method in simulating complex stomach behavior. They found that the gastric emptying rate increases with a

smaller period in between ACWs and it has a nonlinear relationship with the viscosity of the gastric content. Moreover, they found that the changes of period between ACWs have minor influence on the degree of gastric mixing.

Imai et al. (2013) simulated the flow in the stomach during the gastric mixing process with an anatomically realistic geometry (Pullan et al., 2004). A free-surface flow modeling was adopted so it is possible to analyze the effects of posture on gastric mixing. The fill level was high in the upright, prone, and right lateral positions, and the antral recirculation could mix the filled contents well. However, most of gastric contents were located outside antral recirculation by the supine and left lateral positions, which led to a poor mixing. In a later study, Berry et al. (2016) updated the model with peristaltic waves of inhomogeneous velocity from the corpus to the pylorus derived from MRI images of a human stomach. The model showed that the accelerating TAC can enhance the gastric mixing, the level of gastric mixing increased almost linearly with the maximum contraction velocity. In addition, TAC acceleration can increase particle strain and trituration. By using the same geometry, Miyagawa et al. (2016) simulated free surface gastric flow with moving boundaries. They identified a flow separation behind the contraction at $Re = 30$, and this flow separation increased the mixing efficiency. Afterwards, with the same geometrical model, Ishida et al. (2019) showed that impaired coordination between antral contraction and pyloric closure can result in delayed gastric emptying, bile reflux and rapid gastric emptying. They found that when the pylorus was unable to close, the emptying rate increased from 3-8 $ml \cdot min^{-1}$ to 10-30 $ml \cdot min^{-1}$, and the retrograde flow from the duodenum to the antrum happened in the process of antral relaxation. Rapid emptying occurred when the pylorus started opening during TACs.

Kamaltdinov's group has focused on the mathematical model of antroduodenal portion of the gastrointestinal tract extended from a preliminary 2D simulation (Trusov et al., 2013). Firstly, they constructed a 3D computational domain of the antroduodenal region, and evaluated nodes dislocation of computational grids when peristaltic waves passed through the gastric antrum as well as the motor activity of the pyloric sphincter (Kamaltdinov, 2014). In a later research, Trusov et al. (2016) studied multiphase flow with chemical absorption and gastric secretions within the

first 15 minutes of digestion. They observed that the increased acidity leads to a faster disintegration of food particles and the delayed emptying of heavy food particles.

Based on previous work (Trusov et al., 2016), Kamaltdinov et al. (2017a) further examined the acidity in the antroduodenal section of the gastrointestinal tract, to identify abnormal zones when drinking beverages with various pH values. The model introduced damages of three functions, i.e., motility, secretion and absorption, to five regions of the gastrointestinal tract, i.e., stomach body, antrum, duodenum, pancreas and liver, by solving additional ordinary differential sub-models that describe the level of damage. They showed an anomalous increase of acidity in the opening zone of the pylorus and the cap zone of the duodenum when a drink has pH value of 2.3. A later paper focused on the mathematic model development of investigating the mixture flow in the antroduodenum (Kamaltdinov et al., 2017b). They found that a drink with pH level equal to 2.3 can potentially damage the mucous layer of the gastrointestinal tract, especially when disorders of the alkaline secretion take place. More recent researches about the multiphase flow model of the antroduodenum can be found in their conference papers (Kamaltdinov et al., 2018; Kamaltdinov et al., 2020; Kamaltdinov et al., 2021).

(Acharya et al., 2021) used the immersed boundary method to simulate the peristalsis of the stomach by systematically activating muscle fibers embedded in a 3D stomach and gravity driven bolus transporting into the stomach due to density differences between ingested contents and gastric fluids. The interaction between a solid pill and gastric flow was investigated by Seo and Mittal (2022), the immersed boundary method was used to account for the fluid-structure interaction of the drug and the fluid in the human stomach. Their CFD results showed that the retropulsive jet and flow recirculation induced by ACWs have significant effects on the pill motion and the mixing of the dissolved drug (modelled as the scalar species). In addition, they also found that the dissolution was increased by the gastric flow, especially when relative motions between the gastric flow and the pill exist.

It might be noted that the food-emptying is assumed to be only related to hydrodynamics in many studies (Harrison et al., 2018; Imai et al., 2013; Ishida et al., 2019). However, the real food-emptying process is a complex physiological process which is related to food properties (e.g., size of particles, hardness, composition, viscosity, osmolality and energy density) and stomach conditions (e.g., volume, secretion and motility). The assumption of this thesis is that, before the mechanism of food-emptying is fully understood, it is more realistic to specify the emptying rate rather than calculate it from the numerical results.

A difficulty of CFD simulation is that the gastric digestion is an extremely complicated process related to chemical reaction of heterogeneous chyme, whose composition can be influenced by the physical form of the consumed food (Bornhorst et al., 2013). So far, there are still very few CFD studies which have taken the mixing of food species with different properties and the chemical reaction into account (Trusov et al., 2016). In addition, no numerical studies took all modes of muscle contractions of the stomach into account. To my knowledge, the TCs, which determine the gastric emptying rate, haven't been well simulated in previous numerical studies (Ferrua and Singh, 2010; Ferrua et al., 2011). The simulation of gastric motility, the effects of wrinkles at the stomach inner-surface as well as the mixing of foods and gastric juice are challenging tasks to be carried out.

1.4 Thesis Objectives, Structure and Research Tools

The introduction above shows that gastric digestion in human-stomach is an extremely complicated process. *In vivo*, *in vitro* and *in silico* methods play different roles in understanding this process. The general purpose of this thesis is to obtain a better understanding of the connection between food properties and physicochemical digestion of the food in human stomach. The specific objectives are as follows:

(1) Develop a near-real numerical model for simulating gastric digestion induced by the motility of the stomach wall and enzymatic reactions;

(2) Predict and validate the gastric flow and disintegration with available data in literature, qualitatively and quantitatively elaborate flow structures, mixing, digestion and emptying;
(3) Illustrate the mechanism of the formation of the Magenstrasse (stomach road) for fast liquid emptying;
(4) Incorporate the protein digestion kinetics and diffusion physics into the fluid flow model;
(5) Evaluate factors (e.g., heat treatment on proteins, H^+ secretion rate and gastric motility) that influence the protein digestion.

To achieve these goals, a CFD model which can account for different modes of gastric motility and the effect of the stomach-inner-wrinkles was developed. CFD simulations of mixing, digestions, and emptying of different gastric contents were performed. The solver is based on *PimpleDyMFoam* of OpenFOAM® 18.06. Significant modifications were made to model the dynamics of gastric contents with different properties. OpenFOAM® is a C++ object-oriented and open-source library for CFD and structural analysis (Jasak et al., 2007). It is becoming increasingly popular among both in academic research and in industrial applications. OpenFOAM® represents open-source field operation and manipulation, which can be used to solve partial differential equations (PDEs) and ordinary differential equations (ODEs). Complex physical models in continuum mechanics can be implemented by mimicking the form of PDEs in software. The library provides finite volume and finite element discretization in the form of operators, and supports with polyhedral meshes as well as parallel computing. Related auxiliary tools from pre-processing, mesh manipulation, data acquisition, etc., are incorporated into the library.

The structure of the thesis is as follows. Chapter 1 introduces the research background and reviews literature regarding the gastric digestion. In chapter 2, the human-stomach model and governing equations are stated. Simulation results of the PhD thesis are composed of the following parts:

(1) In chapter 3, the gastric flow of three types of liquid foods is analyzed using the numerical model to gain insights of hydrodynamic effects induced by peristalsis of the stomach wall.

The mixing of hydrogen ions (H^+) in the liquid contents under the effects of TACs is also analyzed.

(2) In chapter 4, the mechanism of the Magenstrasse formation is discussed. The gastric motility, the high viscosity of food boluses, and the food matrix made of heavy and deposited food particles are found to be the main reasons for its formation.

(3) In chapter 5, the model is further developed for analyzing meat-protein digestion. Solid food digestion is observed using this model, the digestion rate and the emptying rate are calculated, and the role of gastric motility, H^+ secretion rate and the heating effects on the meat samples are also analyzed.

Finally, in chapter 6, all results obtained in the above chapters are summarized and future works are described.

1.5 List of Scientific Publications

Li CY*, Jin Y (2020). A CFD Model for Investigating the Dynamics of Liquid Gastric Contents in Human-Stomach Induced by Gastric Motility. *Journal of Food Engineering*, 110461. DOI: 10.1016/j.jfoodeng.2020.110461

Li CY, Xiao J, Chen XD, Jin Y* (2021). Mixing and emptying of gastric contents in human-stomach: A numerical study. *Journal of Biomechanics*, 110293. DOI: 10.1016/j.jbiomech.2021.110293

Li CY, Gasow S, Jin Y, Xiao J*, Chen XD* (2021). Simulation based investigation of 2D soft-elastic reactors for better mixing performance. *Engineering Applications of Computational Fluid Mechanics*, 15(1), 1229-1242. DOI: 10.1080/19942060.2021.1955746

Li CY, Jin Y* (2022). Digestion of Meat Proteins in a Human-Stomach: A CFD Simulation Study. *Innovative Food Science and Emerging Technologies*, under review.

CHAPTER 2

Mathematical Models, Numerical Methods and Computational Meshes

2.1 Geometrical Model

Due to the significant variability in shape and size of the human-stomach, a simplified 3D model of the human stomach is used in this study, see Fig. 2.1. The geometry is constructed with a series of circular rings with different diameters connected to the profile line and perpendicular to the imaginary centerline (indicated in yellow). O, P and W are points that indicate the origin, the center of the first circle and the center of the last circle, respectively. The geometrical model is constructed similarly as the one studied by Ferrua and Singh (2010). It also has a similar characteristic dimension as a real stomach, and the volume is 1.17 L, which represents a postprandial state (the period after a meal) of human stomach. The inlet of the stomach is neglected with the assumption that the food will not flow back to the esophagus during the digestion process. It has been expected that the digestion process can be qualitatively studied using this stomach model. The main geometric parameters of stomachs in this thesis and in typical studies in the literatures are shown in Table 2.1. It can be seen that my stomach-geometry is within a reasonable range, which confirms the capability of the model to reproduce the shape and dimensions of a human-stomach.

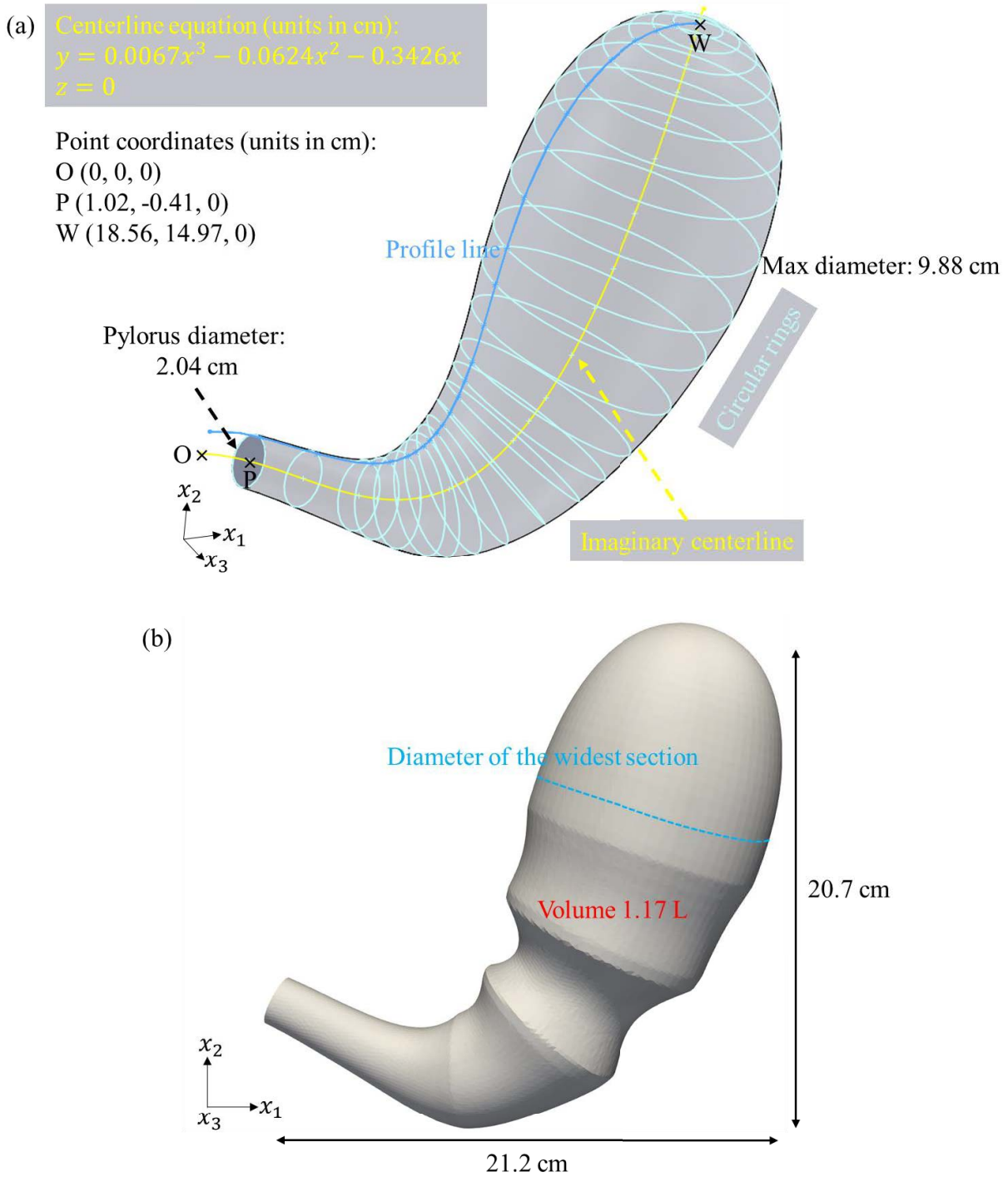

Fig. 2.1. (a) Schematic description of the 3D human stomach model developed in this thesis. (b) The J-shaped stomach (indicated in a state of ACWs occur) has 21.2 cm in width (x_1-direction) and 20.7 cm in height (x_2-direction). The maximum transverse diameter is 9.88 cm (roughly 10.0 cm in humans (Schulze, 2006)).

Table 2.1. Parameters of stomach-geometries in different studies.

Total volume (L)	Antrum diameter ($\times 10^{-3}$ m)	Pylorus diameter ($\times 10^{-3}$ m)	Type of study	Reference
0.65	50	9	*in silico*	(Ishida et al., 2019)
0.9	NA	12	*in silico*	(Ferrua and Singh, 2010)
1.2	NA	23	*in silico*	(Harrison et al., 2018)
0.3	NA	NA	*in vivo*	(Gopirajah et al., 2016)
~0.5	20-60	20	*in vitro*	(Wang et al., 2019)
1.17	21-56	20.4	*in silico*	This thesis

"NA" means that the data are not available.

2.2 Governing Equations

The gastric contents are supposed to be composed of water and food boluses in the early stage of digestion. Food boluses are a collection of solid food particles mixed with amylase-containing saliva (Kong and Singh, 2008). The statistical effects of the food particles on the continuous field can be accounted for by macroscopic properties, e.g., density, diffusion coefficient, and (apparent) viscosity. So N types of food boluses can be treated as fluids of N species. The mass fractions are c_1, c_2, …, c_N, respectively. After food boluses are well mixed with gastric juice, the mixture is called the chyme. The collection of small food particles suspended in the chyme can still be treated as a fluid, while large food particles usually deposit in the distal stomach, behaving like a porous matrix. This porous matrix hereby is called the food matrix, whereas the microstructure of food matrix discussed in Kong and Singh (2008) is not the focus in this thesis. The food matrix is

relatively stable in the stomach due to the gastric sieving which prevents the large particles from passing through the pylorus.

It has been assumed that the variation of food density is small. This assumption is in accordance with the density values used in Kozu et al. (2014a) and Xue et al. (2012). Thus, the main gastric contents can be treated as an incompressible fluid, while the effect of density variation on momentum transport is accounted for with the Boussinesq approximation. The governing equations describe the conservation of mass, momentum, and species. They read:

$$\rho_0 \frac{\partial u_i}{\partial x_i} = \dot{s}_m, \tag{2.1}$$

$$\frac{\partial u_i}{\partial t} + \frac{\partial (u_j u_i)}{\partial x_j} = -\frac{\partial p}{\partial x_i} + \frac{\partial \tau_{ij}}{\partial x_j} + \phi \frac{\rho_m - \rho_0}{\rho_0} g_i + \dot{s}_{ui}, \tag{2.2}$$

$$\frac{\partial c_\alpha}{\partial t} + \frac{\partial (u_i c_\alpha)}{\partial x_i} = D_\alpha \frac{\partial^2 c_\alpha}{\partial x_i^2} + \dot{s}_{c\alpha}, \tag{2.3}$$

where the velocity components u_i, pressure p and species concentration c_α are the main variables to be solved. ρ_0, ρ_m, D_α, ϕ, g_i and $\tau_{ij} = 2\nu_m s_{ij}$ are the reference density (same as the liquid density ρ_l), mixture density, diffusivity, porosity, gravity acceleration rate and viscous stress tensor, respectively. $s_{ij} = \frac{1}{2}\left(\frac{\partial u_i}{\partial x_j} + \frac{\partial u_j}{\partial x_i}\right)$ is the strain rate. $\dot{s}_m$, $\dot{s}_{ui}$ and $\dot{s}_{c\alpha}$ are the source terms.

The source term $\dot{s}_m$ in the mass conservation Eq. (2.1) is calculated as

$$\dot{s}_m = \dot{s}_G + \dot{s}_W + \dot{s}_P, \tag{2.4}$$

where $\dot{s}_G$, $\dot{s}_W$ and $\dot{s}_P$ denote the sources of mass due to secretion of gastric juice, motility of stomach inner-wrinkles and disintegration of large particles in the food matrix into small particles, respectively. The juice is secreted from the upper part of porous medium zone, where the distance from the wall is smaller than 3 mm, Fig. 2.2b shows a cross-section view of the gastric juice secretion region. Chen et al. (2016) suggested that these wrinkles might have non-negligible effects on grinding food particles and mixing them with the gastric juice. The region where the distance is smaller than 5 mm from the wall is set as a porous medium, which is used to model the effect of wrinkles at the stomach inner surface.

The effect of density variation on the momentum equation is accounted for with the Boussinesq approximation, expressed as $\phi \frac{\rho_m - \rho_0}{\rho_0} g_i$ in Eq. (2.2). The Boussinesq approximation assumes gravity is strong sufficiently so the difference in inertia is negligible. The source term $\dot{s}_{ui}$ is calculated as

$$\dot{s}_{ui} = \phi \dot{s}_{pi} + \frac{\dot{s}_m u_i}{\rho_0}. \tag{2.5}$$

The drag force by the porous matrix (including wrinkles and the food matrix) $\dot{s}_{pi}$ is calculated as

$$\dot{s}_{pi} = \phi \frac{\nu_m}{K} (u_i - u_{si}), \tag{2.6}$$

where u_{si} is the velocity of solids the porous matrix, assuming it to be equal to the velocity of the dynamic mesh. $K = \frac{D_p^2 \phi^3}{180(1-\phi)^2}$ is the permeability, D_p is set to 1.6 mm (Huh et al., 2003) and 0.4 mm (Villanueva-Carvajal et al., 2013) to represent the effective diameter of wrinkles and the food matrix respectively, they are estimated as the characteristic length scale of the stomach wrinkles and the food matrix.

α in Eq. (2.3) denotes the species in the gastric contents, which can be n^{th} food species (n, n = 1, 2, …, N), hydrogen ions (H) or enzymes (E). c_n, c_H and c_E denote the mass concentration of n^{th} food species (non-dimensional), mole concentration of hydrogen ions and concentration of total enzymes. Hydrogen ions and enzymes have negligible mass, so the density and viscosity of the mixture are calculated as

$$\rho_m = \sum_0^N c_n \rho_n, \tag{2.7}$$

$$\nu_m = \sum_0^N c_n \nu_n. \tag{2.8}$$

ρ_0 is the density of water, which is also used as the reference density. ν_0 is the kinematic viscosity of the water. The source terms for c_n, c_H and c_E are calculated as

$$\dot{s}_{cn} = \frac{\dot{s}_W c_n + \dot{s}_P}{\rho_0}, \tag{2.9}$$

$$\dot{s}_{cH} = \frac{\dot{s}_W c_H + \dot{s}_G c_{HG}}{\rho_0}, \tag{2.10}$$

$$\dot{s}_{cE} = \frac{\dot{s}_W c_E + \dot{s}_G c_{EG}}{\rho_0}. \tag{2.11}$$

2.3 Muscle Contractions of the Stomach

Table 2.2 shows the characteristic parameters of muscle contractions used in different studies. It can be seen that the TC was neglected in most of simulations in the past. However, it is hard to specify the rate of gastric emptying without the TC accounted for. The muscle contractions, including ACs and TCs, are modelled by a dynamic mesh in this thesis. The motility of ACs is demonstrated in Fig. 2.2a. For each mesh points at the stomach surface, I find the closest point at the centerline (O-P-E-S-I in Fig. 2.2a). An arc on the centerline with the center $\boldsymbol{x_0}$ and the length h_{ACW} starts to move from point S to point E every 20 seconds. The arc center reaches point E in 60 seconds, which is the life cycle of an ACW. During this period, the mesh points at stomach surface which correspond to the point $\boldsymbol{x_1}$ in the arc move with the Eq. (2.12):

$$\boldsymbol{d}_{AC}(\boldsymbol{x_1}) = \boldsymbol{n}\, cos\left(\frac{\pi}{2}\left[\!\left[\frac{2l_{01}}{h_{ACW}}\right]\!\right]_{-1,1}\right)(t_{ACW} + t_{TAC}), \tag{2.12}$$

$$t_{ACW} = A_{ACW} sin\left(\pi\left[\!\left[\frac{t - t_0^{ACW}}{T_{ACW}^{lc}}\right]\!\right]_{0,1}\right), \tag{2.13}$$

$$t_{TAC} = A_{TAC} sin\left(\pi\left[\!\left[\frac{t - t_0^{TAC}}{T_{TAC}^{lc}}\right]\!\right]_{0,1}\right). \tag{2.14}$$

Here $\boldsymbol{d}_{AC}$ is the displacement of the points at the surface. $\boldsymbol{n} = \frac{\boldsymbol{D}_{sc}}{|\boldsymbol{D}_{sc}|}$ is the direction vector, $\boldsymbol{D}_{sc}$ denotes the distance vector pointing from a point at the stomach surface to the closest point at the centerline. A_{ACW} (1.0 cm in the simulation) is the amplitude of the ACW. A_{TAC} (1.0 cm in the simulation) is the amplitude of the TAC. As shown in Fig. 2.2b, the TAC is demonstrated. T_{ACW}^{lc} and T_{TAC}^{lc} indicate the life cycle of an ACW and a TAC, in my simulations, they are 60 s and 4s respectively. l_{01} is arc length from point $\boldsymbol{x_0}$ to point $\boldsymbol{x_1}$. h_{ACW} (3.8 cm in my cases) is width of an ACW represented by the length on the centerline. For a variable x, the function $[\![x]\!]_{a,b}$ is defined as

$$[\![x]\!]_{a,b} = \begin{cases} x & a \le x \le b \\ 0 & otherwise \end{cases}, \tag{2.15}$$

where t_0^{ACW} and t_0^{TAC} are the start time of an ACW and a TAC, respectively.

Table 2.2. Characteristic parameters of muscle contractions in numerical studies. u, T, r, and h denote the velocity, generation period, maximum contraction rate, and width of different modes of muscle contractions, respectively.

TCs	ACs						Reference
	ACWs				TACs		
	u_{ACW} (× 10^{-3} m·s^{-1})	T_{ACW} (s)	r_{ACW}	h_{ACW} (× 10^{-3} m)	r_{TAC}	T_{TAC} (s)	
No	2.5	20	40%	18	80%	20	(Ishida et al., 2019)
No	2.4	20	65%	20	NA		(Xue et al., 2012)
No	1.25/2.5/5.0	NA	40%	60	NA		(Kozu et al., 2014a)
No	2.5	20	90%	12.6/18/23.4	NA		(Pal et al., 2007; Pal et al., 2004)
No	2.2	20	90%	NA	NA		(Harrison et al., 2018)
Yes	2.166	20	26.4%	38	43.7%	20	This thesis

"NA" means that the data are not available.

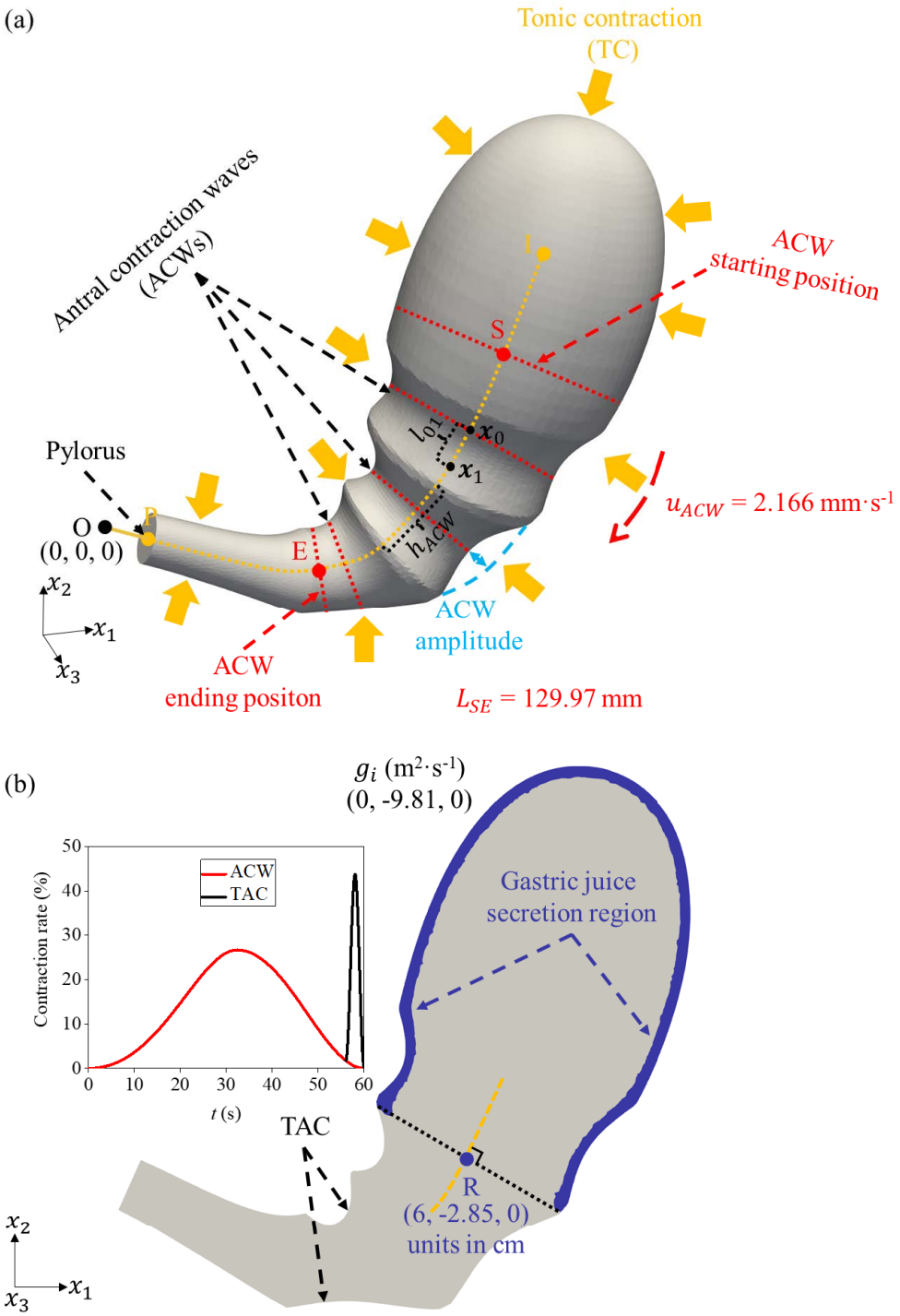

Fig. 2.2. Schematic description of the 3D human-stomach. Movements of stomach-muscles are indicated schematically. (a) 3D view, (b) cross-sectional view. R is a point on the centerline, the region colored in blue indicates the gastric juice secretion. The gravity g_i has the magnitude 9.81 m^2·s^{-1} and points to the negative x_2-direction. The contraction rate is the degree of occlusion.

The TC is modeled by the contraction of the stomach inner surface towards the centerline, see orange arrows in Fig. 2.2a. The contraction velocity $\mathbf{u}_{TC}$ of the TC has the direction determined by its location at the stomach surface and the closest point at the centerline (O-P-E-S-I in Fig. 2.2a). The magnitude of $\mathbf{u}_{TC}$, $|\mathbf{u}_{TC}|$, is given according to the emptying rate of the stomach. Since the gastric contents are assumed to be incompressible, the mass of the gastric contents can be expressed as

$$G(t) = \int_V \rho_0 \phi dV. \tag{2.16}$$

If an objective mass of the gastric contents $G_o(t)$ as a function of time t is given, $|\mathbf{u}_{TC}|$ is adjusted using a PID controller so that $G(t)$ approaches $G_o(t)$, expressed as

$$|\mathbf{u}_{TC}| = K_p e(t) + K_i \int_0^t e(t')dt' + K_d \frac{de(t)}{dt}, \tag{2.17}$$

where K_p, K_i, and K_d are PID coefficients. t' is the variable of integration (values are from time 0 to the present time t). $e(t) = G_o(t) - G(t)$ is the error of $G(t)$. However, $e(t)$ is not exactly 0 due to the time lag between G and G_o. In order to make the value of $G(t)$ identical to the objective function of mass $G_o(t)$, after the mesh is deformed, the porosity of the stomach wrinkles ϕ_W is updated as

$$\phi_W = (G_o(t)/\rho_0 - V_t + V_W)/V_W, \tag{2.18}$$

where V_t and V_W are the total volume of stomach and the volume of the stomach wrinkles, respectively. Besides keeping the mass conservation, the variation of ϕ_W is also used to simulate the motility of wrinkles (expansion/shrinking).

2.4 Numerical Methods

The finite volume method (FVM) is used to solve the governing equations. The CFD solver is developed based on the open source CFD program OpenFOAM® 18.06. The solutions are advanced in time, with the second-order implicit backward method. To compute the derivatives of

the velocity, the variables at the interfaces of the grid cells are obtained using linear interpolation. The linear interpolation of the interfacial values leads to a second-order central difference scheme for spatial discretization. The pressure at the new time level is determined by the Poisson equation. The velocity is corrected with the pressure-implicit with splitting of operators (PISO) pressure velocity coupling scheme.

The Courant number Co for the current implicit solver can be larger than 1. However, the time step must be sufficiently small to capture high-frequency transient fluctuations. In practice, the maximum local Courant number Co_{max} is set to the value 0.2 to capture the transient motions which have small time scales.

2.5 Computational Meshes in the Thesis

The dynamic mesh method in OpenFOAM® can be used to simulate the flow problem with the change of the shape of the computational domain caused by the moving boundary (Baniabedalruhman, 2015; Li et al., 2021). Dynamic mesh handling includes cases of deforming mesh and topological changes; the former keeps the number and connectivity of mesh cells unchanged, while the later has varied mesh size and connectivity during the simulation (Jasak, 2009).

When dynamic meshes are considered, the integral form of the conservation equation for a general tensorial property φ, over an arbitrary control volume (CV) V with a moving boundary, it reads (Jasak and Tukovic, 2006):

$$\frac{d}{dt}\int_V \rho\varphi dV + \int_S \rho\varphi\left(u_j - u_{gj}\right)n_j dS = \int_S \Gamma \frac{\partial\varphi}{\partial x_j} n_j dS + \int_V S_\varphi dV, \tag{2.19}$$

where ρ is the fluid density, n_j is the outward pointing unit normal vector on the boundary surface, u_j is the fluid velocity, u_{gj} is the mesh velocity of the moving mesh, Γ is the diffusion coefficient and S_φ is the source term of φ. Here, S represents the boundary of the CV. Due to the moving boundary, one additional equation has to be satisfied simultaneously to obtain mass

conservation. This equation relates the change of the CV to the velocity u_{gj}, which is space conservation law (SCL) (Demirdžić and Perić, 1988):

$$\frac{d}{dt}\int_V dV - \int_S u_{gj} n_j dS = 0. \tag{2.20}$$

A CV is one cell in Fig. 2.3, CVs don't overlap and fully fill the computational domain. The topology of the CV is a general polyhedron, and bounded by flat faces. The change of the computational domain due to TCs and ACs is modeled using the deforming mesh techniques in the simulations, there are no topological changes involved. In moving boundary problems of this thesis, the boundary and domain shapes change with time. The boundary movement is prescribed based on Eq. (2.12), and internal points also move to accommodate changes of the domain shape and preserve the mesh validity and quality. Due to the complexity of the stomach geometry, the mesh generation is a challenging task. In the simulations, unstructured meshes are generated by ANSYS ICEM 19.2, see Fig. 2.3, mesh 1 is used to illustrate the features (mesh 2 is finer but has a similar pattern of the cell distribution).

Four prism layers have been created from triangulated surface mesh, the majority volume of the interior is filled with hexahedral cells, there are tetrahedral cells as transition between them, and pyramids are used to make conformal between tetrahedral and hexahedral quad faces. The overall number of cells for each type is shown in Table 2.3.

Table 2.3. Cell numbers of different types in the mesh of Fig. 2.3.

Type	Hexahedra	Prisms	Pyramids	Tetrahedra
Number	101383	209112	19144	272908

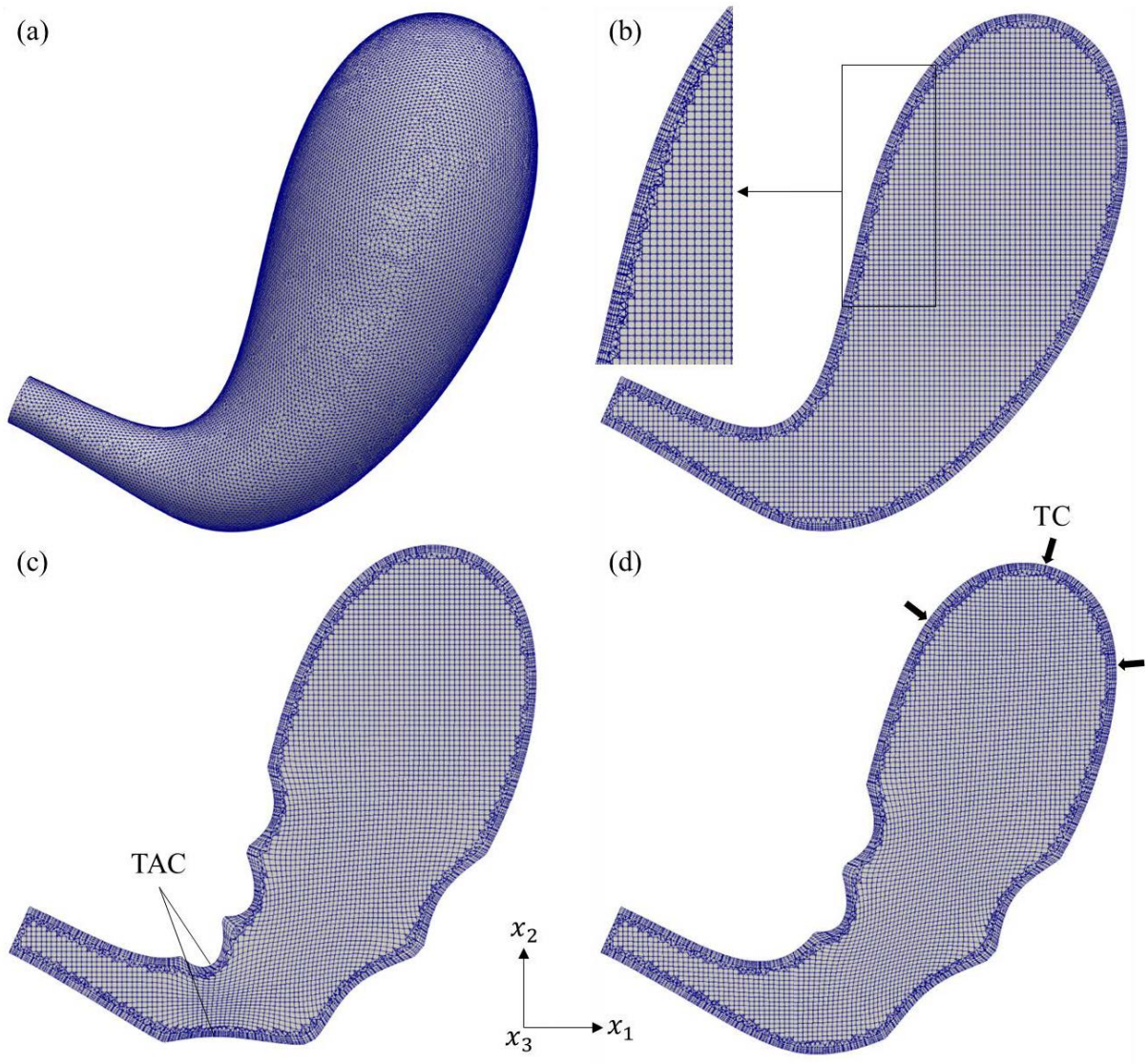

Fig. 2.3. View of a computational mesh, which has approximately 6×10^5 cells. (a) Surface mesh, (b) cross-sectional view of the initial mesh and zoomed view of the left part, (c) the mesh in the cross-section when a (terminal antral contraction) TAC is at the most occluded state, (d) the mesh in the cross-plane after tonic contractions (TCs), and the stomach volume is around 63% of its initial volume.

The mesh validity should meet topological and geometrical requirements. Topological validity includes: Two different points are not allowed to be in an exactly identical position, any point is at least in one face; a boundary face is only addressed by a cell and a boundary patch, an internal face can never be shared by more than two cells; two cells cannot share more than one face; all the

edges in a cell are exactly used by two faces of the cell in question, the mesh cells cannot overlap each other. Geometrical validity includes: The cells have to fill the computational domain; every cell must be convex, and the cell center is inside the cell; all cells are geometrically closed. The topology (i.e., patch, face zone and cell zone) and geometry have been well checked for the meshes used in the thesis.

The mesh quality preservation is only related to the geometrical validations. When the requirements of convexity and orthogonality tests are satisfied, the initial valid mesh is still valid if there are no face and cells inverted when the mesh moves. The commonly used mesh quality metrics are orthogonality, skewness and aspect ratio. Cell non-orthogonality is defined as the angle between the face normal vector S_j and the vector connecting the center of two adjacent grids d_j, i.e., the line connecting two adjacent cell-centers is not aligned with the face normal, see Fig. 2.4a. The grid orthogonality influences the face center (f) gradient and gives more diffusion to the solution. The angle should be small to reduce the truncation error of the diffusion term. Cell skewness (see Fig. 2.4b) indicates the deviation between d_j and f, this deviation vector is δ_j. f' represents the intersection point of d_j and f. The degree of skewness is defined as $\frac{|\delta_j|}{|d_j|}$. If $|\delta_j|$ is not equal to zero, namely f and f' are not equal (i.e., the line connecting two adjacent cell-centers does not pass through the face-center), the cell is skewed. Skewness affects the interpolation from the cell center to the face center, and it also increases the diffusion of the solution. Cell aspect ratio is the ratio of the length to its width of a cell, i.e., $\frac{\Delta y}{\Delta x}$, see Fig. 2.4c. High aspect ratio can cause smear gradients.

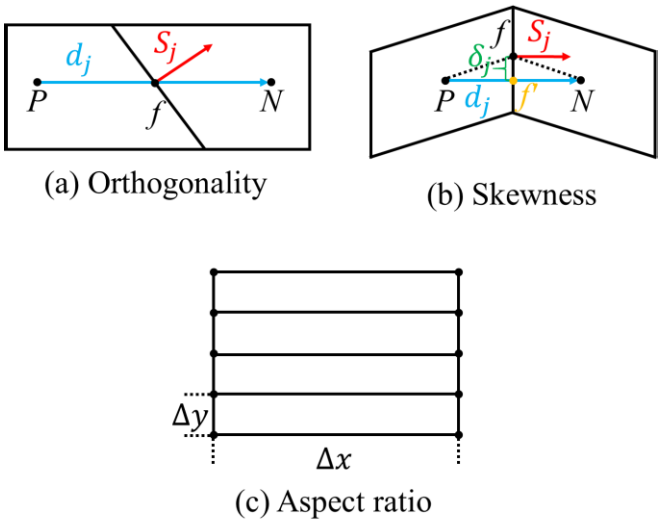

Fig. 2.4. Schematic description of grid quality metrics.

The checking results of the initial mesh are listed in Table 2.4. In OpenFOAM®, the maximum face non-orthogonality angle less than 70 ° is a safe value. Generally, the maximum skewness up to 0.95 is acceptable, and the threshold in OpenFOAM® is 4. The maximum aspect ratio should be kept below 35, and the threshold in OpenFOAM® is 1000. It can be seen that the mesh quality meets the calculation needs well, and there are no cells significantly distorted even with a remarkable decrease of the geometry volume during the calculation, see Fig. 2.3d. Therefore, good mesh quality is guaranteed during the calculation, thus to enable high accuracy computations.

Table 2.4. Results of quality checking of mesh 1.

Quality metrics	Non-orthogonality	Skewness	Aspect ratio
Maximum value	60.1193 °	0.826663	7.78599

The irregular boundary motion is solution-dependent, which is among the most complex level of dynamic mesh features. The boundary motion needs to be considered as the boundary condition on the mesh motion equation. The internal point motion is determined by solving the motion equation (Jasak and Tukovic, 2006). There are three choices, the pseudo-solid equation (Johnson

and Tezduyar, 1994), the Laplace equation (Löhner and Yang, 1996), and the radial basic function interpolation (De Boer et al., 2007). The available solvers can be found in the source library of OpenFOAM®.

In CFD simulations of the thesis, the Laplace equation is used to solve the problem of the moving stomach-wall. The Laplace equation for motion displacement (d_j):

$$\xi \frac{\partial^2 d_j}{\partial x_i \partial x_i} = 0, \tag{2.21}$$

where ξ is the diffusion coefficient. ξ can be determined by different diffusivity models (Alokaily, 2017). The diffusivity of the field based on the inverse of the distance from the stomach-wall is used in the simulation. With this option, ξ is proportional to the inverse distance to the moving stomach-wall. I found this method can keep good mesh qualities in the simulations. After solving Eq. (2.21), all mesh points will be updated to new positions based on the calculated displacement, $x_j^{new} = d_j + x_j^{old}$.

CHAPTER 3

Hydrodynamics of Liquid Contents and Species Transport

Knowledge of dynamics of gastric contents is essential for understanding and simulating the breakdown of food structures and subsequent nutrient release during digestion. Before going to the study on the complex mixture of food, I focus on the gastric dynamics of a few real liquid foods.

3.1 Description of Test Cases

The developed CFD model is used to simulate the emptying and mixing processes for three types of liquid foods. They are the water, commercial orange juice, and whole milk. The source of mass due to disintegration of large particles $\dot{s}_P$ (Eq. 2.4) and the source of enzymes $\dot{s}_{cE}$ (Eq. 2.11) are set to zero. Since only one food species and water are considered in the gastric contents, the density and viscosity of the mixture are $\rho_m = c_F\rho_F + (1 - c_F)\rho_0$ and $\nu_m = c_F\nu_F + (1 - c_F)\nu_0$, respectively. Here F indicates that food species.

The properties of liquid foods are shown in Table 3.1. The density, viscosity and pH of the commercial juice are found in Islam et al. (2017). The density (Adams et al., 2019), viscosity (POPESCU and ANGEL, 2019), and pH (Ortiz Araque et al., 2018) of the whole milk are found in literatures. The temperature of foods in human stomach is assumed to be 310 K. The diffusion coefficient D_F for water is found in the literature (Holz et al., 2000). The values of D_F for other foods are estimated by the Stokes–Einstein equation:

$$D = \frac{k_B T_a}{6\pi\mu R}, \tag{3.1}$$

where k_B is the Boltzmann's constant, T_a is the absolute temperature, μ is the dynamic viscosity, R is the radius of the spherical particle. The median particle size for a commercial orange juice is about 98.5 μm in radius (Islam et al., 2017). The largest particles in milk are fat globules (Bylund, 2003), which has a radius in the range of 0.05-5 μm, with an average radius around 2 μm (Wiking et al., 2004). The diffusion coefficient of hydrogen ions in water is 9.31 × 10^{-9} $m^2 \cdot s^{-1}$ (Abrahamsson et al., 2005). The diffusion coefficients of hydrogen ions for other foods are scaled down by the ratio of their viscosities to water. The energy amount of water, orange juice, and milk are 0 kcal per 100 g, 45 kcal per 100 g (Stobdan et al., 2010), and 62 kcal per 100 ml (Walter et al., 2020) respectively.

Table 3.1. The physical properties of liquids used in the CFD simulations.

Food	ρ_F ($kg \cdot m^{-3}$)	ν_F ($\times 10^{-6}$ $m^2 \cdot s^{-1}$)	D_F ($\times 10^{-12}$ $m^2 \cdot s^{-1}$)	D_H ($\times 10^{-9}$ $m^2 \cdot s^{-1}$)	Energy amount ($kcal \cdot g^{-1}$)	pH
Water	1000	1	3090	9.31	0	7
Orange juice	1020	3.04	0.759	3.1	0.45	3.65
Whole milk	1026	1.95	58.3	4.66	0.608	6.8

Assuming uniformly distributed hydrogen ions in the initial conditions, their concentrations are 1.0 × 10^{-7} $mol \cdot L^{-1}$, 2.239 × 10^{-4} $mol \cdot L^{-1}$, and 1.585 × 10^{-7} $mol \cdot L^{-1}$ for water, commercial orange juice, and whole milk respectively. The corresponding pH values are 7, 3.65, and 6.8 respectively. Gastric juice is released with the constant secretion rate 2.7 × 10^{-4} $L \cdot s^{-1}$ and H^+ concentration 2.5 × 10^{-2} $mol \cdot L^{-1}$ (pH ≈ 1.6). The gastric juice is assumed to have the same density as water.

Kong and Singh (2008) suggested that the gastric emptying is controlled to have about 2 to 4 kcal·min^{-1} (8.4 to 16.8 kJ·min^{-1}) caloric contents delivered to the duodenum through a negative feedback mechanism mediated by the duodenal receptors. Faas et al. (2002) indicated that meals with a similar energy content empty from the stomach at similar rates regardless of their composition and consistency. Based on this consideration, a 0D model for calculating the gastric emptying rate has been developed, see Appendix. This 0D model is not directly used in my CFD simulations. However, the idea of specifying the flow rate of caloric contents at the pylorus is adopted. In the thesis, I assume that the energy content leaves the stomach and enters the duodenum with a constant rate (3 kcal·min^{-1}). The corresponding gastric emptying rate r_{emp} and period for half-emptying T_{he} are shown in Table 3.2.

Table 3.2. Computational parameters for food emptying and mixing processes.

Food	r_{emp} (× 10^{-8} m^3·s^{-1})	T_{he} (min)
Water	26.99	30
Orange juice	10.89	74.34
Whole milk	8.065	100.42

Fig. 3.1 shows the calculated pH values at the outlet of the stomach for different mesh resolutions and different water-emptying rates. Two unstructured meshes are used in this chapter, mesh 1 (illustrated in section 2.5) has about 6 × 10^5 cells, while mesh 2 has about 2.3 × 10^6 cells. 24 processors are used in the MPI-parallel calculations. It takes about 10 h (using mesh 1) or 100 h (using mesh 2) to calculate a water-emptying process of 200 s. It can be seen that the numerical results are only mildly changed when the mesh resolution is improved. According to the mesh-convergence study, mesh 1 is used in this chapter. It is hard to find reliable and repeatable experimental results for validating the CFD results. However, the CFD results have been

qualitatively compared with the results in previous studies. They will be shown in the discussion below.

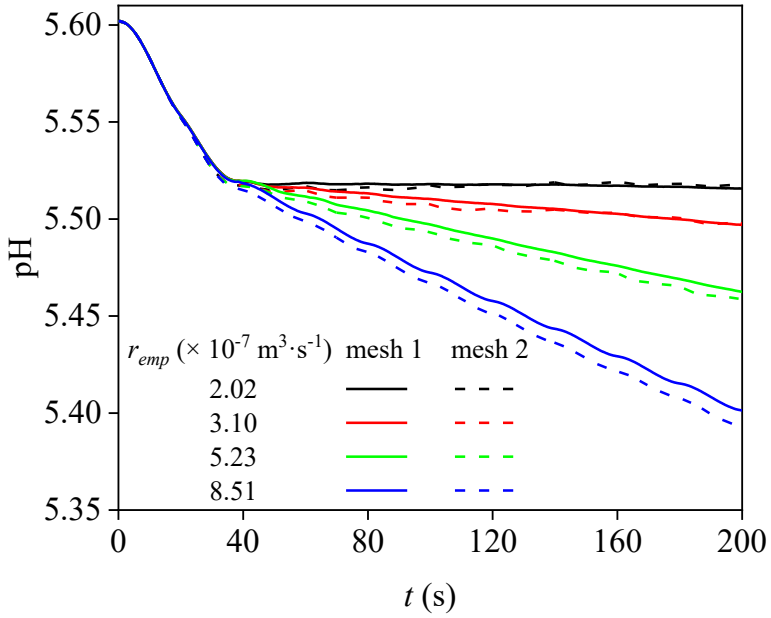

Fig. 3.1. pH values at outlet for different water-emptying rates and mesh resolutions, without TACs. Mesh 1 and mesh 2 have approximately 6×10^5 and 2.3×10^6 cells, respectively.

3.2 Effects of Terminal Antral Contractions on Gastric Dynamics

Fig. 3.2 compares the vortical structures identified by the iso-surfaces of $Q = 0.001$ s^{-1} for the water emptying process from 56 s to 60 s with an interval of 1 s. The TAC occurs every 20 s after 56 s, and it lasts for 4 s each time. Q is the invariants of the velocity gradient tensor, which is defined as $-\frac{1}{2}\frac{\partial u_i}{\partial x_j}\frac{\partial u_j}{\partial x_i}$ for an incompressible flow. Hunt et al. (1988) suggested that the vortical structures can be identified by positive Q. The 3D vortex structures are colored with the velocity component in the vertical direction to indicate their dynamics. At the starting time of the TAC, both cases have same flow fields, see Fig. 3.2 at t = 56 s. However, it can be seen that TACs have

obviously increased the maximum velocity at the later time. The ACW starts at the middle body of the stomach and moves downwards. In the regions of contraction, the fluid is forced to move away from both ends of an ACW. Flow speeds close to the contraction region are fast. The flow speeds are relatively small in the top region of stomach, where no vortices are identified, see Fig. 3.2a. The contraction of TACs creates retrograde “jets”, see Fig. 3.2b at 57 s and 58 s, this retropulsive jet-like fluid flow was also found in other research works by Pal et al. (2004), Ferrua et al. (2011) and Schulze (2006). It should be noted that, in the previous studies, the retropulsive jet-like fluid flow was captured when the pylorus is closed. The numerical results in this section show that this type of flows also occurs when the pylorus is open.

TACs can generate strong flow separations and thereby enhancing the mixing of gastric contents. In Fig. 3.2b at 57 s, due to the intensive contraction of TACs, the fluid is mainly pushed in two directions, one is towards the pylorus, and the other is towards the fundus. In Fig. 3.2b (at 58 s), the TAC approaches its most occluded state, the upward flow and downward flow coexist. As the contraction relaxes, we can see the gastric contents sink towards the terminal antrum, see Fig. 3.2b at 59 s. The contraction and relaxation can enlarge the high-speed region, they also stimulate small vortical structures in the fundus region, which intensify the recirculation in the stomach.

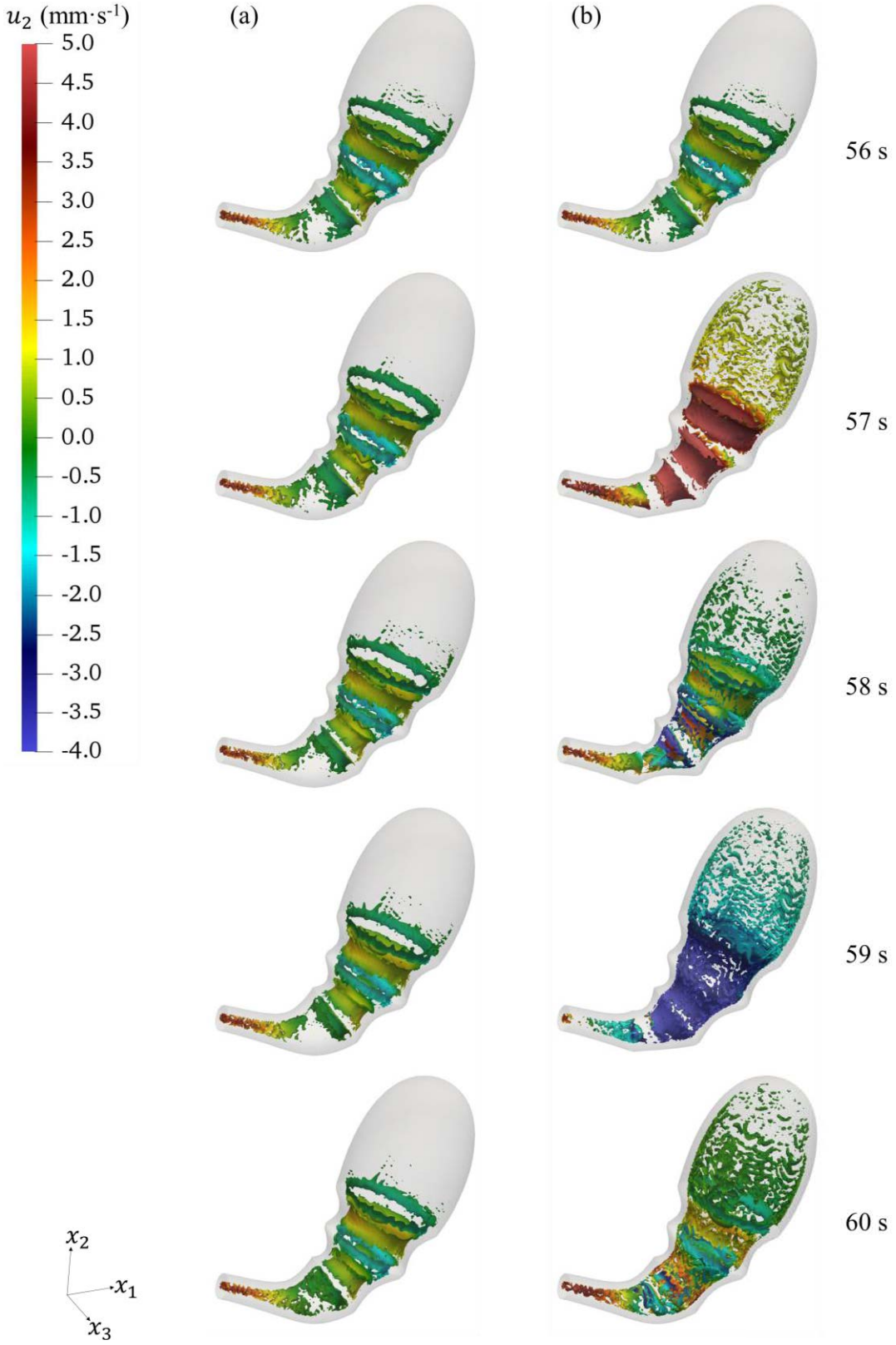

Fig. 3.2. Effects of TACs on the flow structures identified by the Q-criterion colored with u_2. (a) Emptying of water, without TACs; (b) emptying of water, with TACs.

The calculated maximum local velocity $|\mathbf{u}|_{max}$ for the water-emptying during a period of the TAC (56-60 s) is compared with the results of other CFD studies. The value of $|\mathbf{u}|_{max}$ is the lowest (~11.1 mm·s^{-1}) when the TAC starts, while the highest value is around 29.4 mm·s^{-1}. My numerical results cannot be compared quantitatively with the results of other studies due to the difference of stomach-geometries and muscle movements. However, as seen in Table 3.3, the velocity from my numerical results varies in a similar range as those in other studies, which are 7.5-78 mm·s^{-1}.

Table 3.3. Maximum local velocity $|\mathbf{u}|_{max}$ in the study of this chapter and other references. $\mu_0 = \rho_0 \nu_0$ is the dynamic viscosity.

ρ_0 (kg·m^{-3})	μ_0 (× 10^{-3} Pa·s)	$\|\mathbf{u}\|_{max}$ (× 10^{-3} m·s^{-1})	Reference
1000	1	7.5	(Pal et al., 2007; Pal et al., 2004)
1000	1	78	(Ferrua and Singh, 2010)
997	0.91	9	(Kozu et al., 2014a)
1000	1	77.4	(Alokaily et al., 2019)
1000	1	11.1-29.4	This thesis

The impact of TACs on gastric dynamics is further quantified in the current study. Fig. 3.3 shows the change of volume averaged kinetic energy in the stomach for the water-emptying process. The volume averaged kinetic energy is defined as

$$Ke = \frac{1}{2}\frac{\int_V u_i u_i dV}{\int_V dV}. \tag{3.2}$$

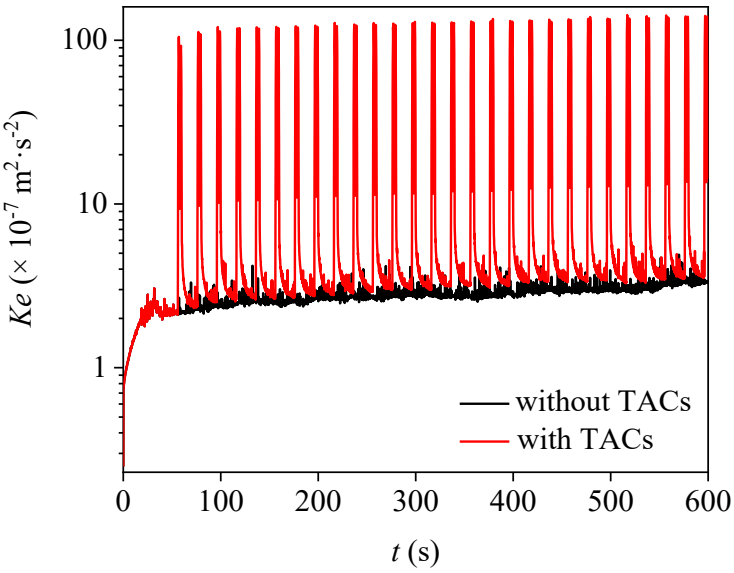

Fig. 3.3. Effects of TACs on the volume averaged kinetic energy for the water-emptying process.

As can be seen in Fig. 3.3, the periodically generated TACs cause periodic oscillations of the averaged kinetic energy. With a constant propagating velocity profile, Pal et al. (2004) reported that the TAC nearly doubled the retropulsive flow velocity, which is in line with my results, see Fig. 3.4. The maximum retropulsive velocity caused by TACs is around 20 mm·s^{-1}, while the maximum velocity at the same time without TACs is about 10 mm·s^{-1}. The maximum velocity for the case without TACs locates at the region close to the pylorus due to the narrow exit (see Fig. 3.4a); the maximum velocity for case with TACs is in retropulsive-jet like motions (see Fig. 3.4b). The TACs not only increase the maximum velocity in the stomach, but also introduce more chaotic flows in the upper part of the stomach, the averaged kinetic energy can give information on overall impacts of TACs. My results show that TACs can increase the averaged kinetic energy by dozens of times.

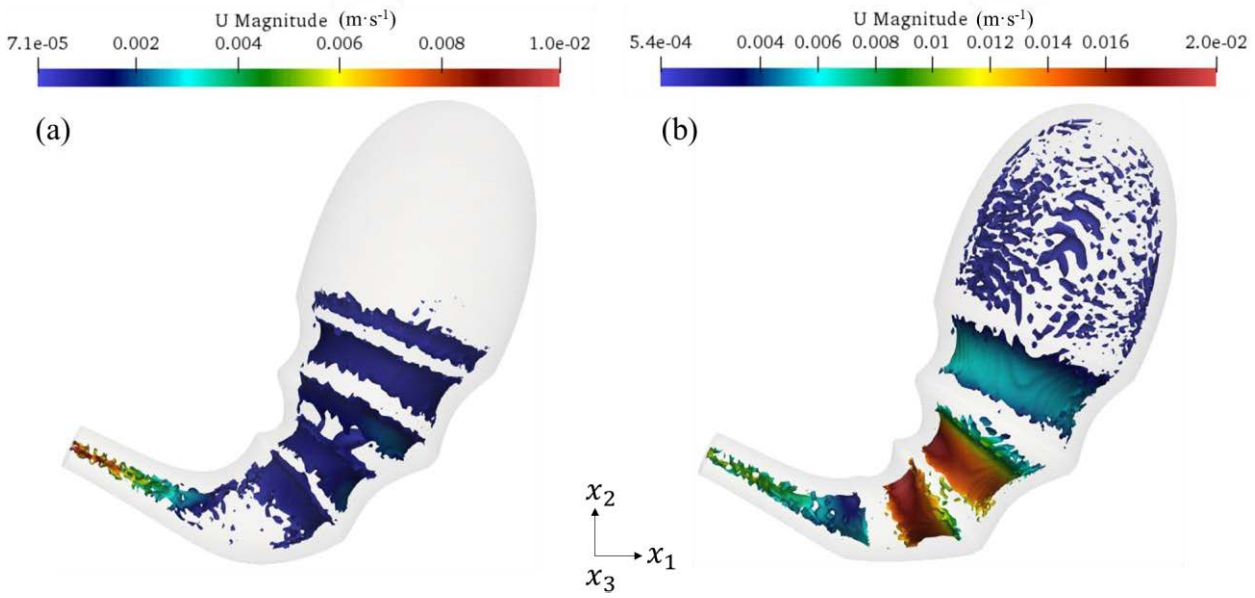

Fig. 3.4. Q-criterion iso-surface showing vortex structures colored by velocity magnitude in x_2-direction at 57 s for the water-emptying process. (a) Without TACs, (b) with TACs.

3.3 Effects of Food Properties on Gastric Dynamics

The flow field developed inside the stomach can be significantly influenced by the physical properties of gastric contents. To investigate this effect, the flow fields in the stomach model for three Newtonian liquids are analyzed. Fig.3.5 shows the vortical structures of three emptying processes, the color is coded according to the velocity magnitude in x_2-direction. As can be seen from the water-emptying process, there are fewer vortices, especially on the top region where no vortices exist, see Fig. 3.5a. The small vortical structures populate in the pyloric canal region for all cases. They are also found in the upper region for the emptying cases of orange juice and milk. The large vortical structures are found in the stomach for different emptying scenarios, they are dominant for the mass transfer. The visible region of vortex structures expands slightly with time for the water-emptying case, while it shrinks for other cases. The large structures break into small ones, some small structures are further dissipated. The dissipation process is more obvious for foods with higher viscosity.

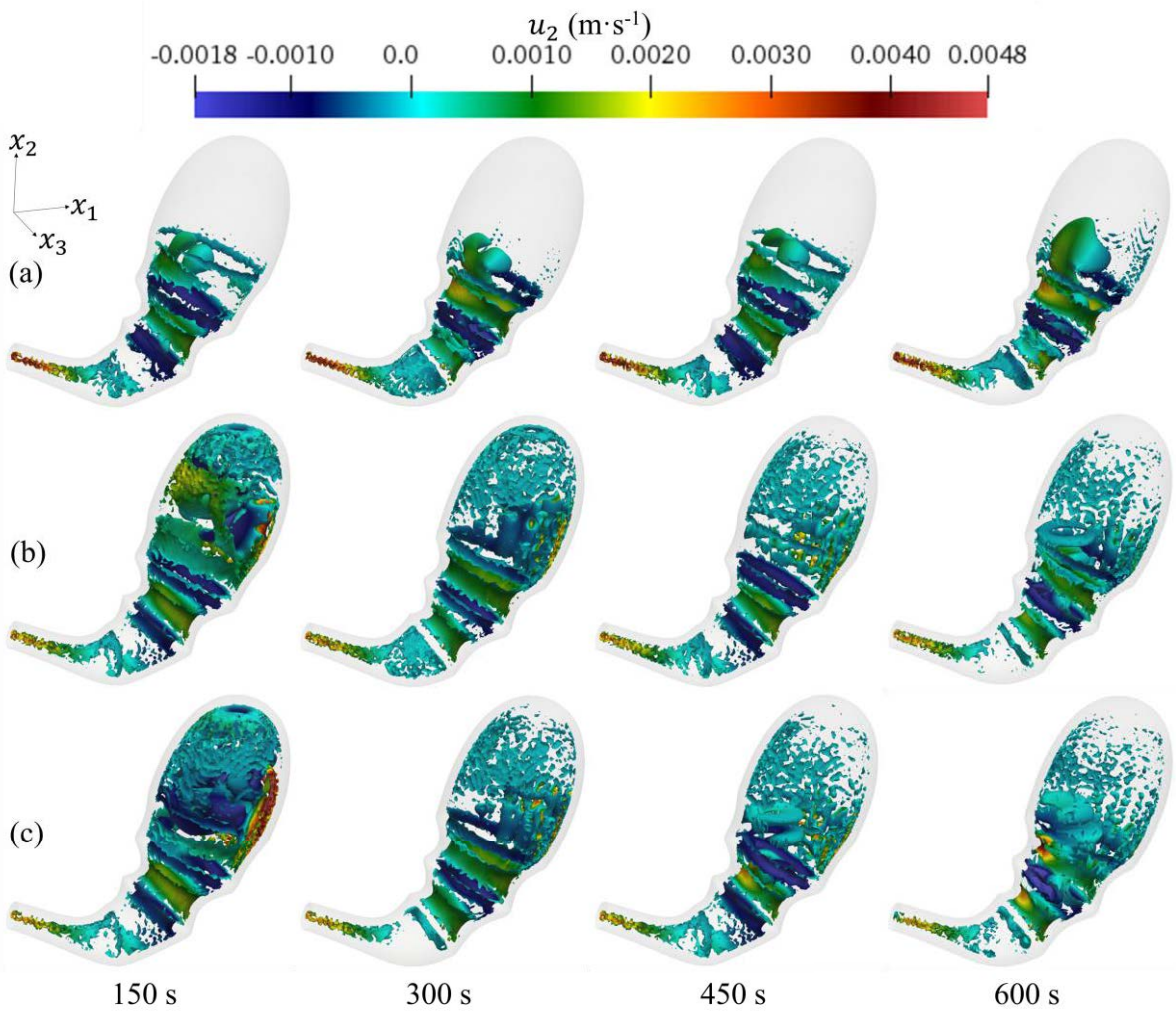

Fig. 3.5. Snapshots of Q-criterion contours colored by the velocity component in x_2-direction for the emptying of water (a), orange juice (b), and whole milk (c) at different time instants, without TACs.

Fig. 3.6 compares the averaged kinetic energy of three foods over time. As an overall trend, it can be seen that the kinetic energy increases slightly in the case of water. While in the other two cases: The kinetic energy increases firstly, then decreases, and finally oscillates with a stable amplitude. The changes of averaged kinetic energy are less intensive after 300 s, indicating that the mixing becomes fully developed. During the mixing and emptying process, the test case of water has the largest values of kinetic energy while the test case of orange juice has the smallest

values, suggesting that the averaged kinetic energy becomes higher with the decrease of the viscosity.

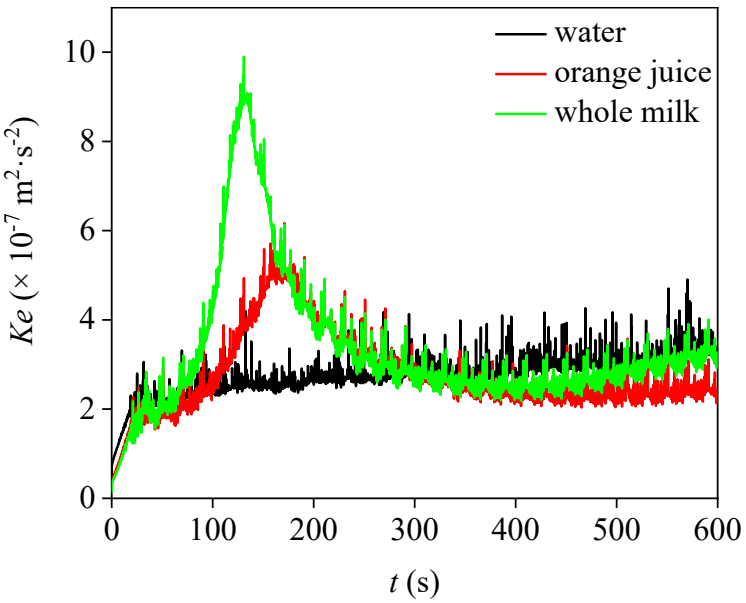

Fig. 3.6. Volume averaged kinetic energy for the mixing and emptying of water, orange juice, and whole milk, without TACs.

3.4 Mixing of Foods and the Gastric Juice

The gastric pH varies among different regions of the stomach due to the inhomogeneous distribution of hydrogen ions. The studies by Abuhelwa et al. (2016) and Mennah-Govela et al. (2020) show that meal caloric content, protein content, initial pH, and interactions between food properties and composition played an important role in determining the food buffering capacity and thus the gastric pH distribution. To better understand the transport of hydrogen ions and dynamics of pH distribution in stomach, the mixing of foods and gastric juice is studied by using my CFD model.

Fig. 3.7 shows the pH distributions for the water-emptying process at various time instants. The gastric acid secretion region has the lowest pH value, and the low pH regions are enlarged in both cases as the mixing progresses. The mixing is less efficient in the upper region than in the lower region, where ACWs generate continuously. ACWs introduce more intensive fluid flows in the lower region, see Fig. 3.5a, which will bring stronger convections of hydrogen ions in this region. The mixing patterns for both cases are similar, while the pH is more uniformly distributed when TACs are considered, showing that TACs can enhance the mixing efficiency for gastric juices. TACs can push hydrogen ions back to the upper region of the stomach, which makes the pH lower, see Fig. 3.7b at 600 s, this is beneficial for the digestion.

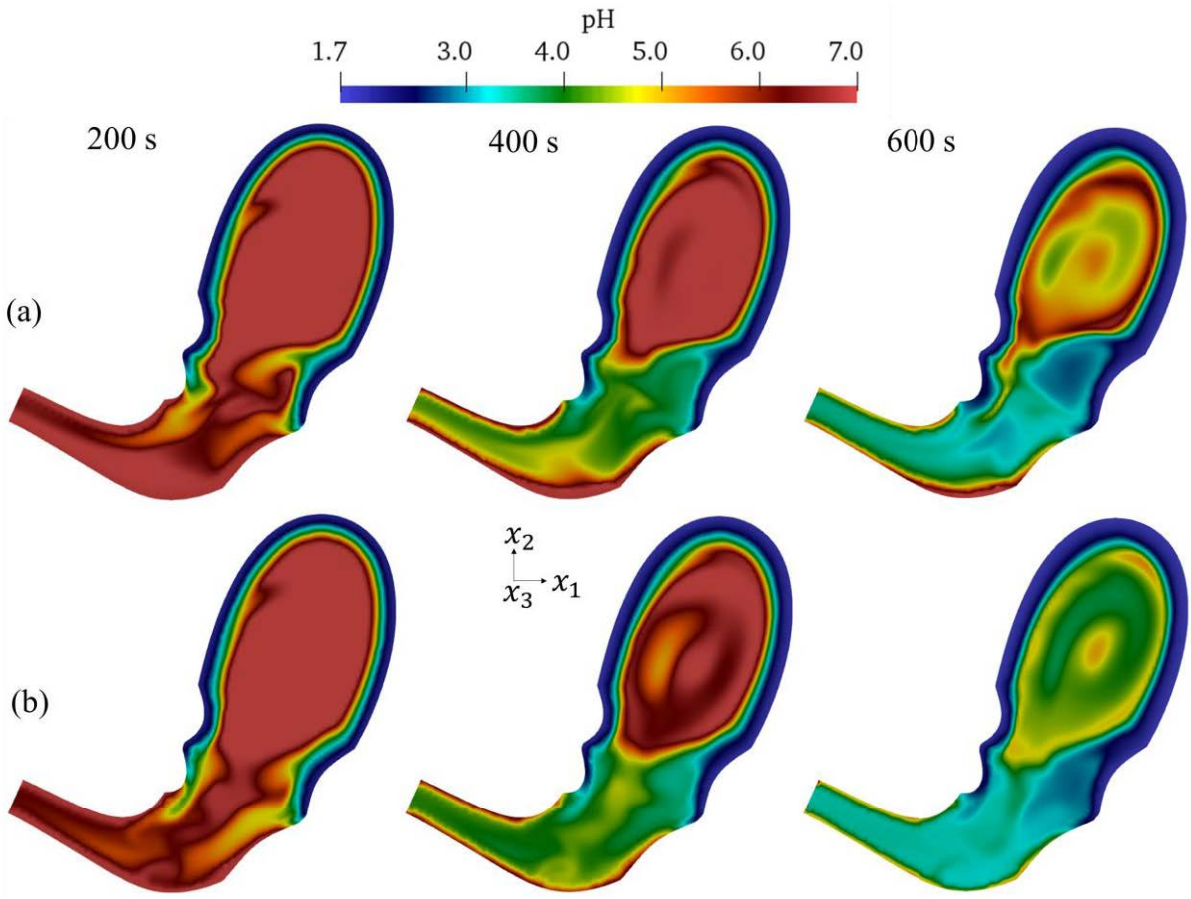

Fig. 3.7. Effects of the TAC on the distribution of pH, showing on the cross-section. (a) Emptying of water, without the TAC; (b) emptying of water, with the TAC.

A mixing rate for hydrogen ions can be defined to quantify the extent of the mixing in the stomach, it indicates the difference of H^+ concentrations in the stomach lumen with the secreted gastric juice, which is calculated as

$$r_{mix} = 1 - \frac{M_t}{M_0}. \tag{3.3}$$

The mixing index at time t is calculated as

$$M_t = \frac{\int_V (c_H(t) - c_{HG})^2 dV}{c_{HG}^2 \int_V dV}. \tag{3.4}$$

Here $c_H(t)$ and c_{HG} are the local H^+ concentration in the lumen and the H^+ concentration in the gastric juice, respectively. r_{mix} is 1 when hydrogen ions are uniformly distributed and have the same concentration as that of the gastric juice. Furthermore, the volume averaged pH value in the stomach is defined as

$$\overline{\mathrm{pH}} = \frac{-\int_V \log_{10}(c_H(t)) dV}{\int_V dV}. \tag{3.5}$$

According to the numerical results shown in Fig. 3.8a, the mixing rate is not evidently influenced by TACs. However, slightly higher mixing rate can still be observed when TACs are accounted for since it slows down the emptying of hydrogen ions. The slight change of the H^+ concentration might result in significant change of the pH. From Fig. 3.8b, we can clearly see that TACs reduce the averaged pH value in the stomach.

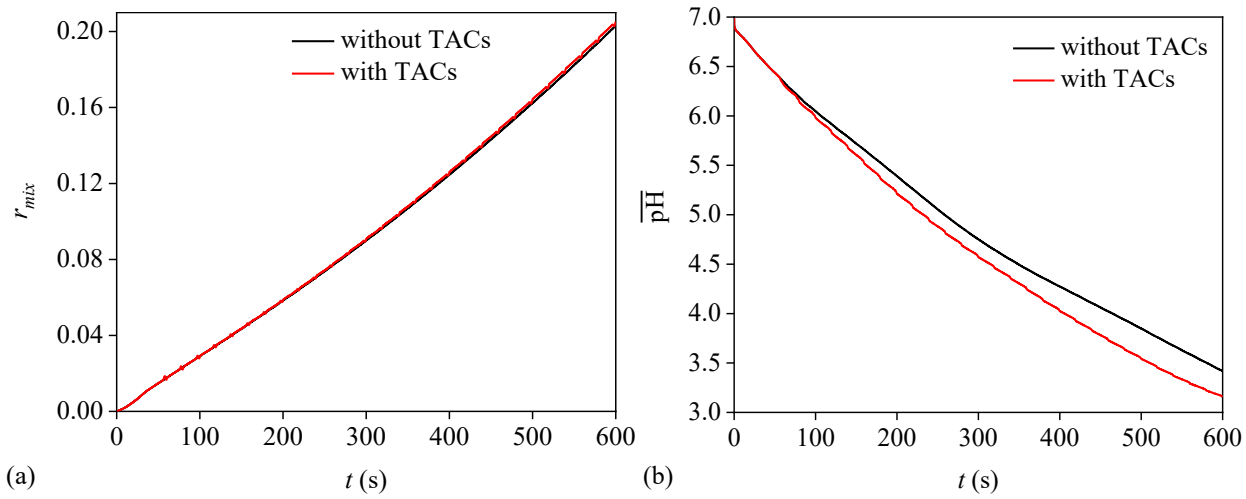

Fig. 3.8. Effects of TACs on the mixing rate r_{mix} (a) and the averaged pH ($\overline{\text{pH}}$) in the stomach (b) for the water-emptying process.

Based on the numerical results, the pH distribution for different foods are compared, see Fig. 3.9. It can be found that low pH region enlarges uniformly from the gastric juice secretion region to the inner lumen of stomach for the water, while it enlarges from top to bottom of the stomach for the orange juice and milk. The gastric juice has the same properties as water, while the orange juice and milk have higher density and viscosity than the gastric juice. Due to the higher density of foods (than the gastric juice), the food settles down and the gastric juice floats to the top. The accumulation of gastric juice on the top will further force the heavier food to discharge downward and reduce the viscosity of the upper region. From a kinematic point, higher viscosity could hinder the transport of hydrogen ions towards the pylorus, thus hydrogen ions are more efficiently transported in the top region where viscosity is lower compared with that of the lower region for cases of orange juice and milk.

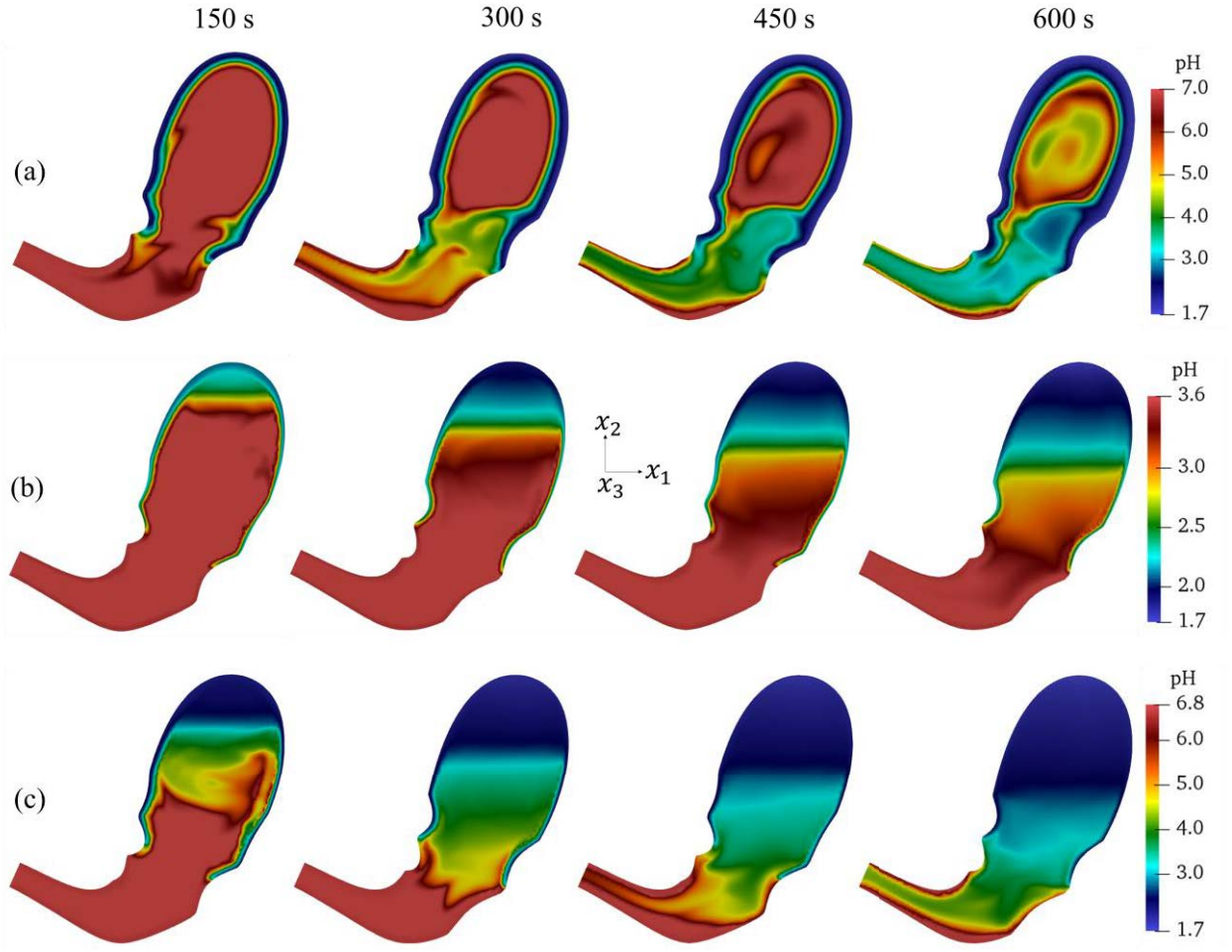

Fig. 3.9. Distributions of pH on the cross-sectional plane for the mixing and emptying of water (a), orange juice (b), and whole milk (c), without TACs.

Fig. 3.10a shows the histories of r_{mix} for the water, orange juice and milk. The value of r_{mix} increases slowly with time in all cases. According to a non-linear extrapolation, it will take about 50 minutes by estimation for the pH to become uniformly distributed (reaching an acidic state with the pH value of 1.6). From a perspective of mixing, lower initial pH, higher H^+ diffusion coefficient, lower viscosity and smaller emptying rate might favor the mixing of the gastric juice and liquid foods, thereby leading to higher values of r_{mix}. Among these factors, the emptying rate is expected to play a key role in determining the mixing rate, since a lower emptying rate can provide longer mixing time. Fig. 3.10b shows how the averaged pH values in the stomach evolve with time. For

the three types of liquid foods under consideration, the pH for milk decreases the fastest with time due to its slowest emptying rate.

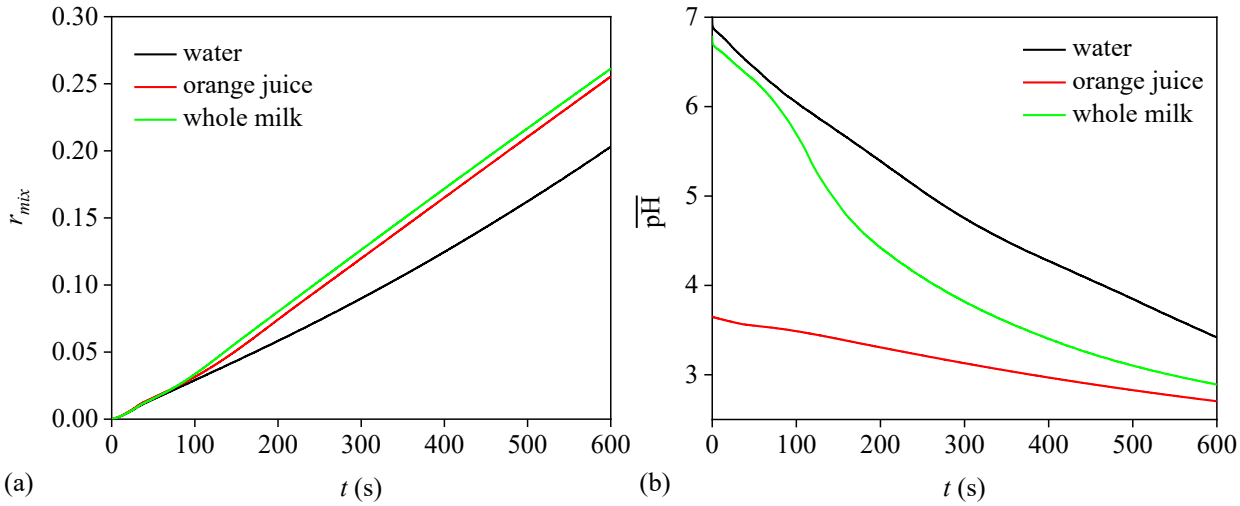

Fig. 3.10. The mixing rate r_{mix} (a) and the averaged pH ($\overline{\text{pH}}$) in the stomach (b) for emptying processes of water, orange juice, and whole milk, without TACs.

3.5 Conclusion

The objective of the study in this chapter is to better understand the effects of gastric motility on the dynamics of gastric contents in human stomach, including the mixing of gastric juices and gastric contents. To reach this purpose, the flows in a human stomach with an opened pylorus are simulated.

Three types of liquid foods with different properties are studied, the emptying rates are determined according to their calorie amount. The numerical results show that TACs can significantly increase the averaged kinetic energy in the stomach, and the maximum velocity is nearly doubled compared to the case without TACs. When a TAC contracts the terminal antrum, the gastric contents are forced away from the pylorus sphincter, creating a retropulsive jet. The

numerical results confirm the phenomenon observed in previous studies (Ferrua et al., 2011; Pal et al., 2004; Schulze, 2006). The TACs not only increase the maximum velocity in the stomach, but also make the flow more chaotic. Small vortical structures can be observed close to the pylorus and in the upper region of the stomach after the TAC starts.

The numerical results show that the mixing patterns vary among foods. Initial pH, H^+ diffusion coefficient, density, viscosity and emptying rate might affect the mixing of the gastric juice and liquid foods. hydrogen ions are transported from the top region to the bottom region when the food is heavier than the gastric juice. By contrast, if the food has the same density as the gastric juice, hydrogen ions are transported from the acid-secretion region to the inner lumen of the stomach. The retropulsive jet induced by the TAC pushes hydrogen ions back to the upper part of the stomach, leading to the slower emptying of hydrogen ions. It also enhances the mixing of hydrogen ions and the gastric contents. These characteristics are favorable for the digestion in the stomach.

CHAPTER 4

‘‘Magenstrasse’’ for Gastric Mixing and Emptying

Mixing and emptying of gastric contents are the most important functions of stomach. The corresponding process is related to hydrodynamics, mass transfer, chemical reactions, etc. People believe that the gastric motility of stomach plays an important role in this process. The gastric motility might help to grind the large food particles, enhance gastric mixing and thus affect the emptying rate (Bornhorst, 2017; Bornhorst and Paul Singh, 2014; Camilleri et al., 1986). Despite of these general knowledge, however, the mechanism for gastric mixing and emptying is still not fully understood due to its high complexity.

An important phenomenon related to gastric mixing and emptying is the Magenstrasse (stomach road), which describes the fast emptying of ingested liquids from the fed stomach (or postprandial stomach, denoting the stomach after eating, see Grimm et al. (2017)). Based on a numerical study, Pal et al. (2007) indicated that the ACWs induce the Magenstrasse along a narrow and long pathway close to the lesser curvature of the stomach, which is the stomach region with shorter curvature (Podolsky et al., 2015). It might funnel liquid gastric contents from the farthest reaches of fundus directly to the intestine within 10 min. The *in vitro* experiments by Chen et al. (2016) and Wang et al. (2019) also confirmed that liquid gastric contents are emptied much faster than solid gastric contents.

The *in vivo* experiments by Koziolek et al. (2016) and Grimm et al. (2017) showed that the Magenstrasse plays an important role in the administration of drugs through the fed stomach. The drugs (tablets, capsules, liquids) released off the Magenstrasse may take several hours to enter the

duodenum, at low concentrations; when released on the Magenstrasse, the drug can enter the duodenum within 10 minutes, at high concentrations (Pal et al., 2007). However, the long pathway close to the lesser curvature suggested by Pal et al. (2007) was not found in the *in vivo* experiments. Instead, the water is found to flow around the chyme in the lumen along the entire stomach wall. The possible reason is that the gastric contents have a broad range of viscosity values. This observation is in accordance with the early experiment made by Scheunert (1912), who demonstrated that the water can flow around the gastric contents and thus reach the intestine faster. Ferrua and Singh (2015) also stated that, only water-like fluids are emptied in the long pathway close to the lesser curvature. This long pathway is even not found when tomato juice is emptied, although its properties are only mildly different from those of water. Therefore, the Magenstrasse is not a pure hydrodynamic problem, while the mixing of gastric contents with different properties should be investigated to understand its mechanism.

The purpose of this chapter is to better understand the mixing and emptying of gastric contents in human-stomach, particularly the physics of the Magenstrasse. To achieve this goal, the mixing and emptying process is simulated numerically. The mechanism for the Magenstrasse is studied based on the numerical results.

4.1 Description of Test Cases

The species properties used in this chapter are shown in Table 4.1. The properties of water and hydrogen ions have the physical values. The properties of food boluses are given tentatively in this study but they are within the range of properties for the real foods. $\dot{s}_P$ and $\dot{s}_{cE}$ are equal to zero, there are no enzyme secretions and chemical digestions, see Eq. (2.4) and Eq. (2.11).

Table 4.1. The properties of species in the study of this chapter. FB means food bolus. ρ, D and ν are density, diffusion coefficient and kinematic viscosity, respectively.

Species	Color in Fig. 4.4	ρ (kg·m^{-3})	D (m^2·s^{-1})	ν (m^2·s^{-1})
Water	-	1000	-	1.0×10^{-6}
H^+	-	-	9.31×10^{-9}	-
FB1	Lavender	1000	6.6×10^{-9}	3.0×10^{-5}
FB2	Blue	1050	5.7×10^{-9}	7.0×10^{-5}
FB3	Green	1100	2.98×10^{-9}	9.0×10^{-5}
FB4	Red	1150	1.67×10^{-9}	1.0×10^{-4}
FB5	Black	1175	1.23×10^{-9}	2.0×10^{-4}

The test cases in this chapter can be classified as three groups, see Table 4.2. The emptying of water is studied in the test cases of group G1. Before the water-emptying process starts, the stomach is assumed to be filled with water. The initial velocity is 0. The initial H^+ concentration is 2.5×10^{-6} mol·L^{-1} (pH ≈ 5.6) (Kong and Singh, 2008). Gastric juice is released in the porous medium zone (wrinkles) with the constant secretion rate (2.7×10^{-4} L·s^{-1}) (Versantvoort et al., 2004) and H^+ concentration ($c_{HG} = 2.5 \times 10^{-2}$ mol·L^{-1}, pH ≈ 1.6) (Kong and Singh, 2008). For the water-emptying process, the muscle contraction is dominated by TCs and ACWs (Ehrlein and Schemann, 2005). TAC doesn't occur in this process, while ACWs are released every 20 s (Harrison et al., 2018). The outlet (pylorus) is kept open during the water-emptying process. Fig. 4.1 shows the history for the mass of gastric contents. Since constant values of emptying rate r_{emp} are used in the study, the objective mass of gastric contents (G_o) changes linearly with time. The calculated mass of gastric contents G is almost identical to G_o. In the simulation, the stomach is shrunk to about 65% of its original volume due to emptying of the gastric contents. Further

shrinking of the stomach is not studied since the mesh-quality is downgraded as the stomach-volume is further reduced.

Table 4.2. Test cases in this chapter.

Group	Species	r_{emp} (× 10^{-4} kg·s^{-1})	Pylorus	Description
G1	Water, H^+	2.02-8.51	Open	Water-emptying
G2	Water, FB1-5	0	Closed	Water-food-mixing
G3	Water, FB1	2.02	Open	Water-food-emptying

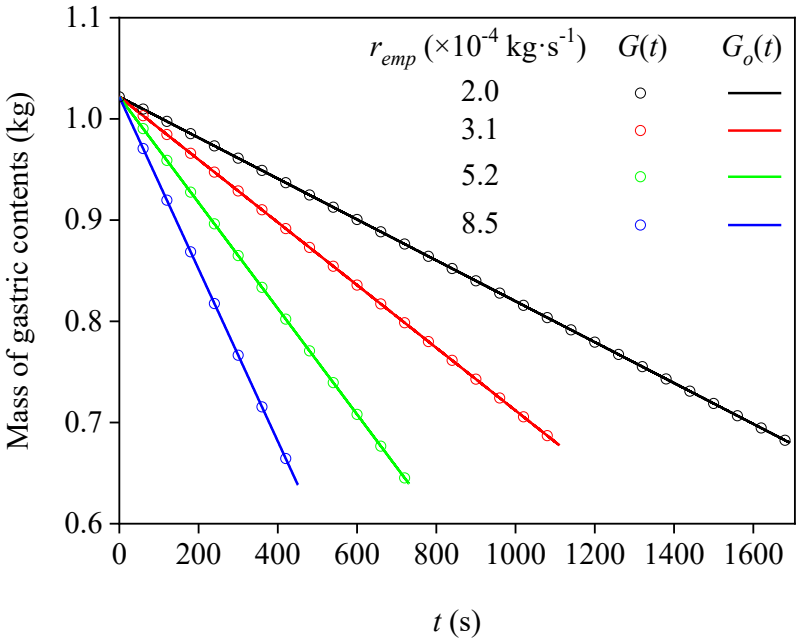

Fig. 4.1. Mass of gastric contents versus time for different emptying rates. Symbols: Calculated values $G(t)$. Lines: Objective values $G_o(t)$.

The mixing of food boluses and water is studied in the cases of group G2. The outlet is set to be closed when the food-mixing process is simulated. The increase of mass due to secretion of gastric juice is neglected. Besides TC and ACWs, TAC plays also an important role during the

food-mixing process, so it is accounted for in the simulation. The TAC occurs every 20 s after 56 s, while it lasts for 4 s (King et al., 1984) each time (e.g., 56-60s, 76-80s, …).

The emptying of the food and water mixture (chyme) is studied in the cases of group G3. The boundary and initial conditions in these cases are the same as those in group G2, except that the pylorus is kept open. The food matrix with ϕ_F = 0.4 and D_p = 0.4 mm (Villanueva-Carvajal et al., 2013) is considered in group G3.

Two unstructured meshes are used in this chapter. They have about 6×10^5 cells (mesh 1) and 2.3×10^6 cells (mesh 2), respectively. According to the mesh-convergence study (discussed in section 4.2), mesh 1 is used in the analysis.

4.2 Fast Emptying along the Lesser Curvature of Stomach

I first studied the water-emptying process in the stomach. Fig. 4.2 shows the evolution of the pH-distribution with time, and the pattern of pH-distribution is not qualitatively changed as the value of r_{emp} increases. The pH value is lower in the porous medium zone due to the secretion of gastric juice. It might be observed that hydrogen ions close to the lesser curvature are more rapidly transported than the ones close to the greater curvature. A similar phenomenon was also found by Grimm et al. (2017). Hydrogen ions already reach the pylorus before 600 s. This phenomenon was also captured by Pal et al. (2007) in their numerical study, which indicates that the Magenstrasse can funnel liquid gastric contents from the farthest reaches of fundus directly to the intestine within 10 min. As a result, more hydrogen ions secreted at the lesser curvature of stomach will be brought out of the stomach.

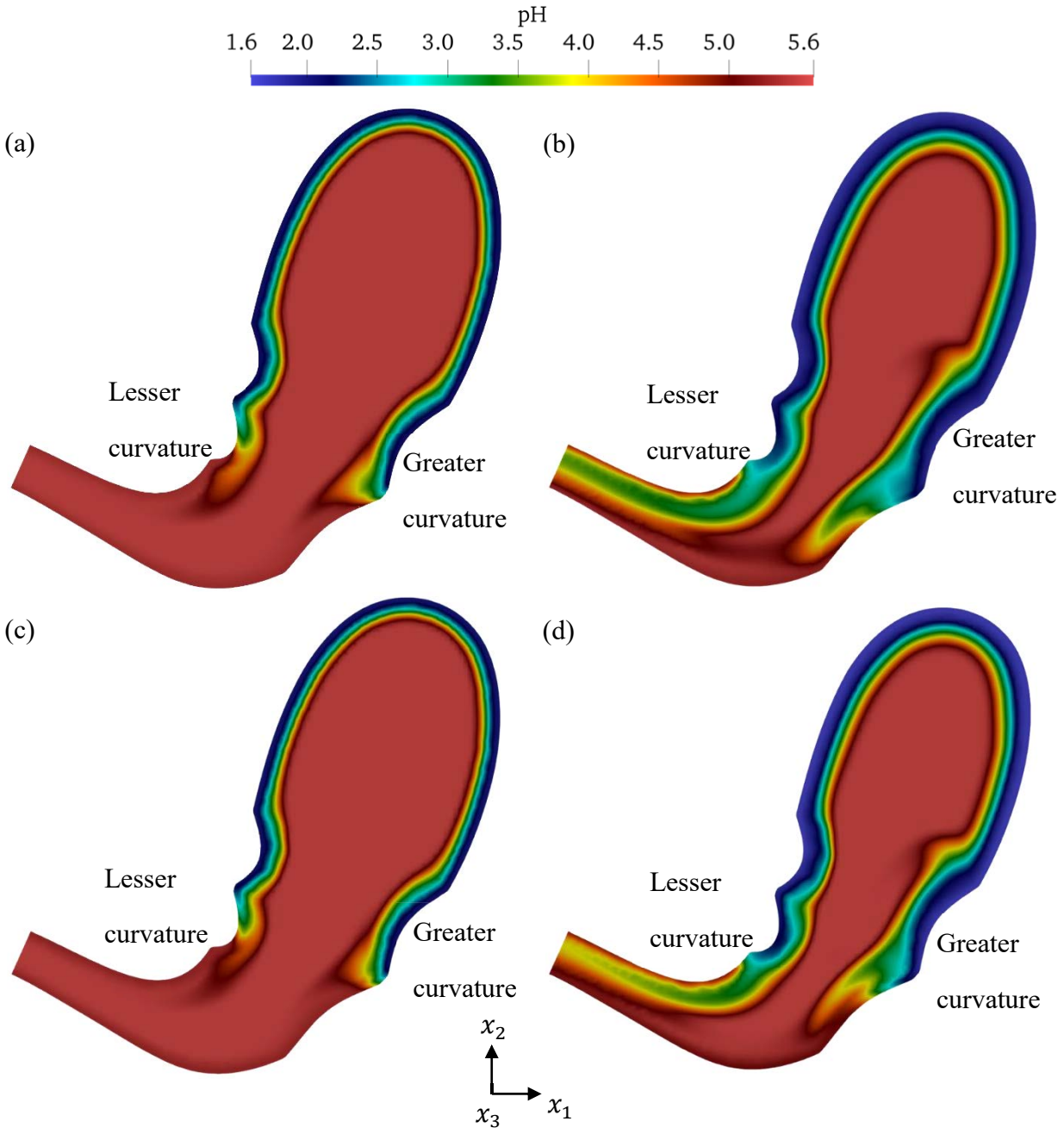

Fig. 4.2. Evolution of the pH-distribution in a cross section of the stomach, G1. r_{emp} = 2.02 × 10^{-4} kg·s^{-1}, (a) t = 200 s, (b) t = 600 s; r_{emp} = 5. 23 × 10^{-4} kg·s^{-1}, (c) t = 200 s, (d) t = 600 s.

Fig. 4.3a shows the relationship between the volume averaged pH value ($\overline{\text{pH}}$) in the stomach and the mass of emptied gastric contents $G_{emp} = r_{emp} \cdot t$, where r_{emp} is the emptying rate. It

can be seen that $\overline{\mathrm{pH}}$ becomes slightly higher as a higher-resolution mesh is used, however, the numerical results are not qualitatively changed. So, mesh 1 is used in this chapter. Fig. 4.3b shows the pH values for the emptied gastric contents. Fig. 4.3b shows that the gastric contents have a lower pH value as the emptying rate decreases, leading to a lower pH value inside the stomach and also at the outlet.

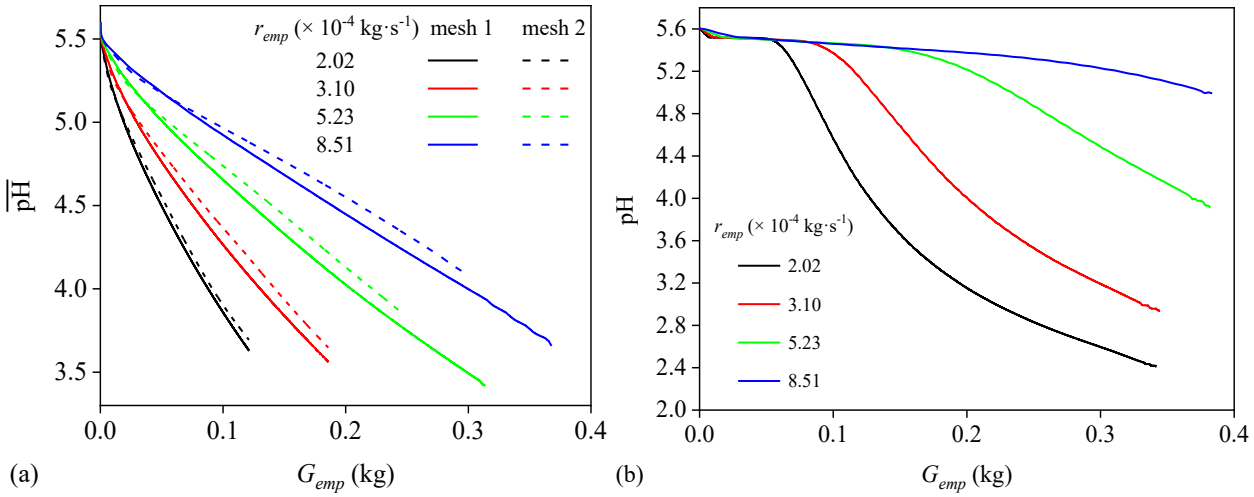

Fig. 4.3. G1: (a) Volume averaged pH value ($\overline{\mathrm{pH}}$) in the stomach and (b) pH value at the outlet versus mass of emptied gastric contents G_{emp} for different emptying rates.

4.3 Mixing of Food Boluses and Water

The *in vivo* experiments by Koziolek et al. (2016) and Grimm et al. (2017) didn't show the exclusive Magenstrasse at the lesser curvature of stomach. The possible reason is that real food boluses have much more complicated properties than water. The mixing of food boluses and water is studied in the cases of group G2. Fig. 4.4a shows the initial distribution of food boluses, which are surrounded by water. Shortly after the mixing process starts (after a few seconds), the food mixture becomes multi-layered, see Fig. 4.4b. The heavy food boluses concentrate in the distal stomach. This is in accordance with the study by Schulze (2006), who stated that food is segmented

in different layers inside the stomach. Chen et al. (2016) also showed in their *in vitro* experiment that the food particles heavier than water fell down onto the greater curvature.

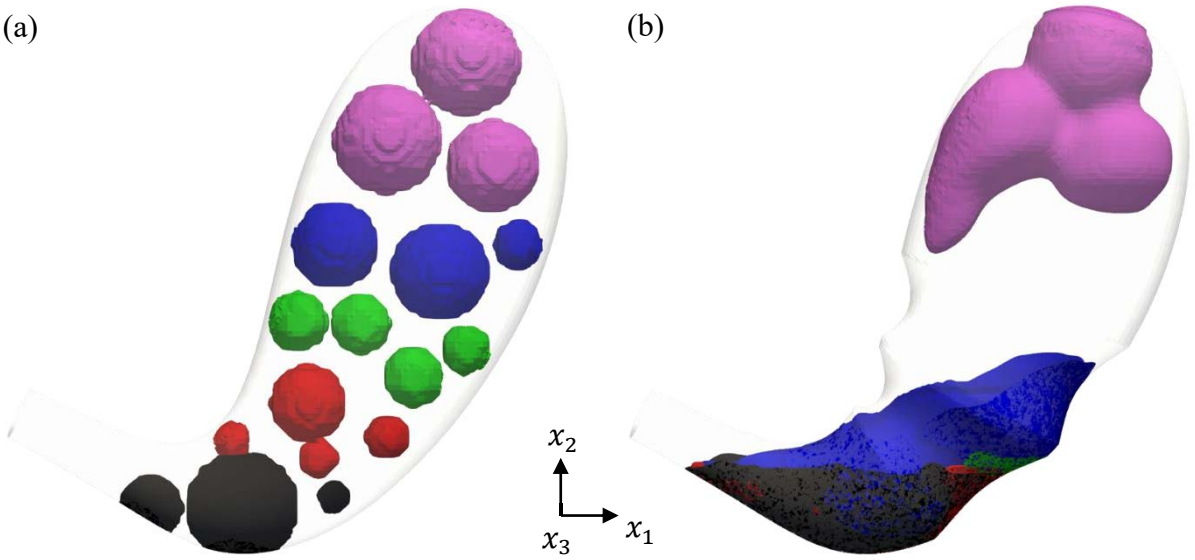

Fig. 4.4. Distribution of different food species in the stomach. The food species are shown in their colors indicated in Table 4.1 when their mass fraction $c_n \geq 0.1$, the group is G2. (a) t = 0 s, (b) t = 600 s.

An important phenomenon with respect to the food mixing is the "retropulsive jet-like motion", which is induced by the muscle contraction. The numerical simulation of the stomach with an opened pylorus has already indicated the existence of the "retropulsive jet-like motion", see Fig. 3.2. Hereby, its mechanism in a closed stomach with food species of different viscosity and density values is investigated.

Fig. 4.5 shows the vortical structures identified by the iso-surfaces of Q = 0.01 s^{-1} in a period of TAC, which starts at 56 s and ends at 60 s. The vortical structures are colored with the vertical velocity component (u_2) to indicate the direction of their motions. It can be seen that the food is forced back to the stomach by the TAC at 57 s. It sinks towards the terminal antrum at 59 s.

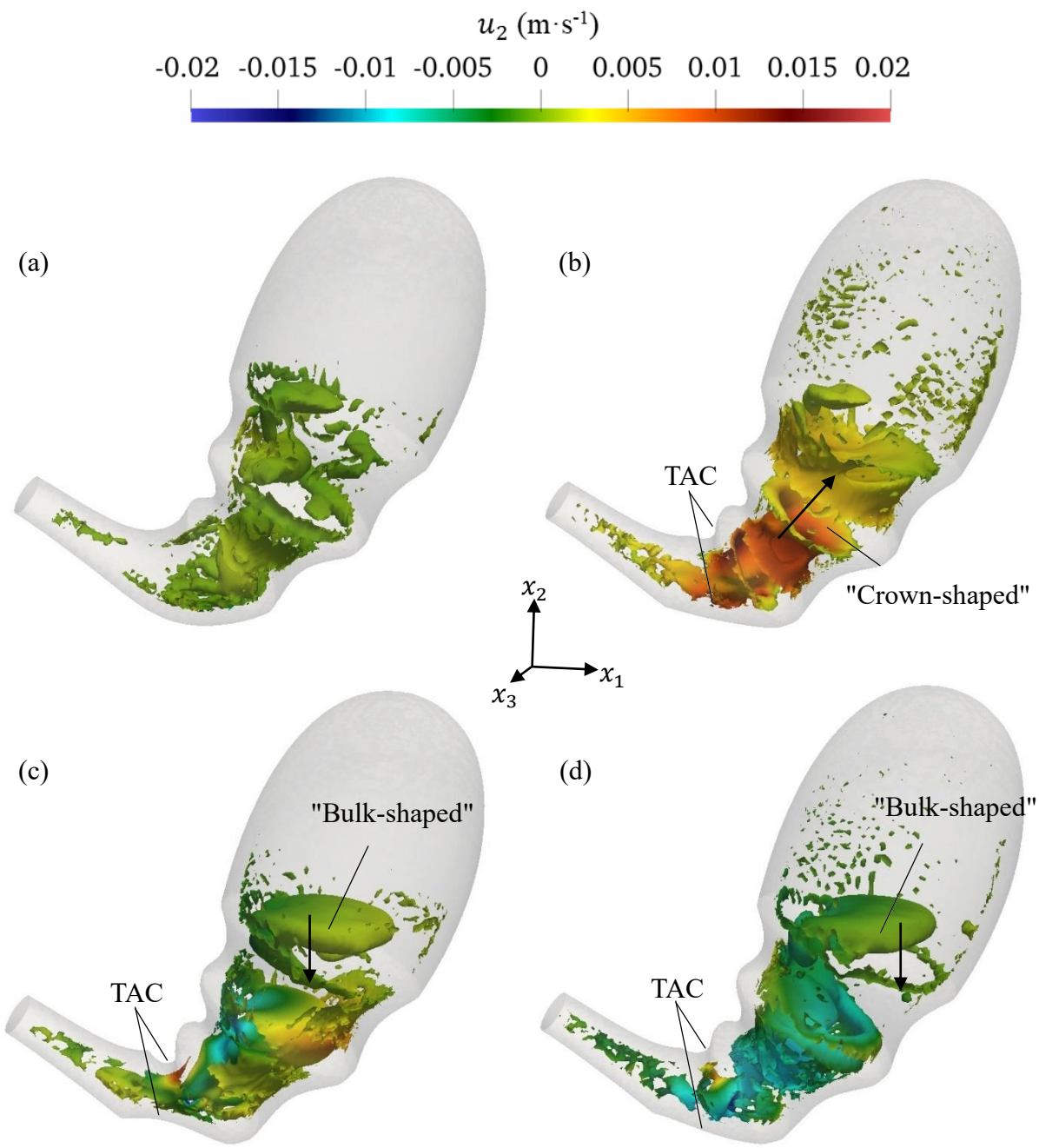

Fig. 4.5. Vortical structures identified by Q = 0.01 s^{-1} during a period of the TAC, G2. The vortical structures are colored by the vertical velocity u_2. (a) t = 56 s; (b) t = 57 s; (c) t = 58 s; (d) t = 59 s.

The similar “retropulsive jet-like motion” was also captured in previous studies (Ferrua et al., 2011; Ishida et al., 2019; Pal et al., 2004; Schulze, 2006). The transient flows are shown with

velocity vectors in these studies. In this chapter, the coherent structures of the "retropulsive jet-like motion" are more clearly identified using the iso-surfaces of Q: Two shapes of large vortical structures are found in Fig. 4.5. "Crown-shaped" structures which have a high upward velocity can be observed when the gastric contents are ejected, see Fig. 4.5b. "Bulk-shaped" structures fall slowly when the TAC relaxes, see Fig. 4.5c. Compared with flows shown in Fig. 3.2, it can be noticed that the "retropulsive jet-like motion" is considerably enhanced when the pylorus is closed.

Besides the large vortical structures, we can also see small vortices close to the porous medium zone (modeled wrinkles). Chen et al. (2016) and Wang et al. (2019) stated that that the wrinkles help to grind the large food particles. The mechanism might be related to these vortices which result in the velocity variation in small length scales and thus the shear stress to cut the large food particles.

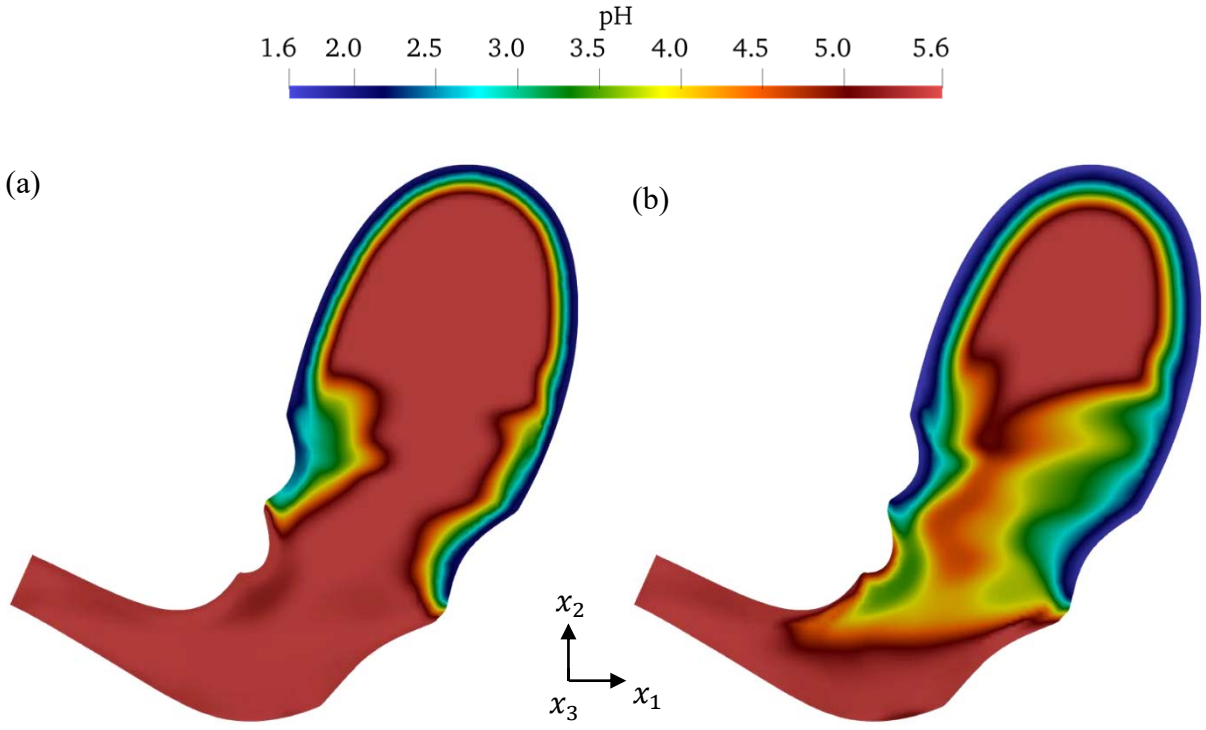

Fig. 4.6. Distribution of pH values, G2. (a) t = 200 s; (b) t = 600 s.

Fig. 4.6 shows the distribution of pH values, the food inside the stomach will influence H^+ distributions. Unlike the water-emptying process, see Fig. 4.2, it is hard for hydrogen ions to access the pylorus when there are heavy food boluses. The main reason is that the heavy food boluses close to the bottom of stomach have high viscosity thus the convection is weak, and this can hinder the transport of hydrogen ions. Hydrogen ions cannot be efficiently transported to the pylorus by diffusion. It can be also seen that, compared with the water-emptying process, the hydrogen ions are more efficiently transported to the central region of the stomach in the food-mixing process.

A mixing rate can be defined to quantify the extent of the food-mixing. For food species n, it is calculated as

$$m_{r,n} = 1 - \frac{\int_V (c_n - \bar{c}_n)^2 dV}{\int_V (c_{n0} - \bar{c}_{n0})^2 dV}, \tag{4.1}$$

where $\bar{c}_n = \frac{1}{V}\int_V c_n dV$ is the mean mass fraction of species n. c_{n0} and $\bar{c}_{n0}$ are the local and mean mass fraction of species n for the initial field, respectively. The mixing of a single food species and water is studied.

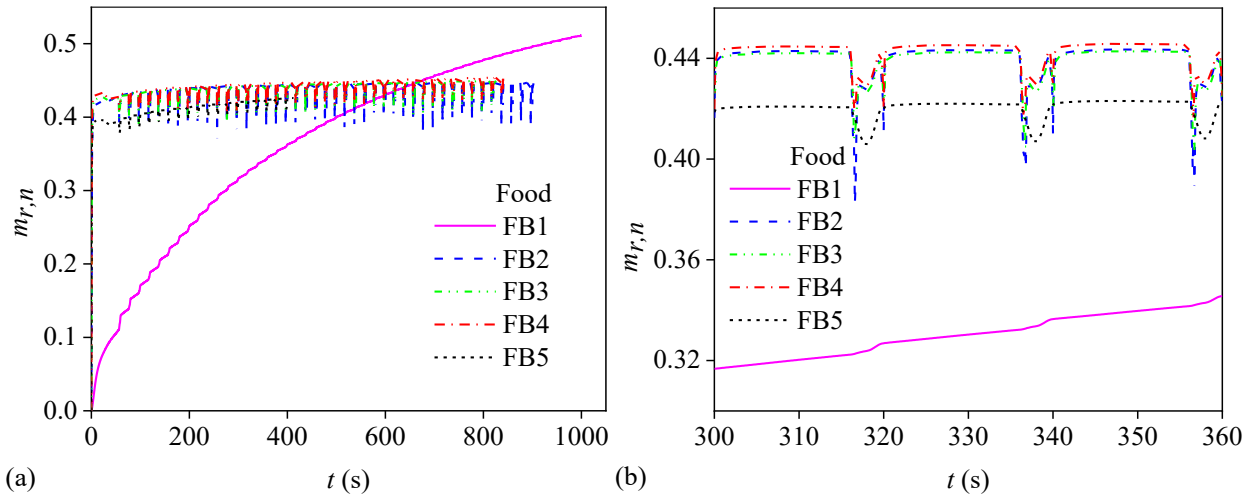

Fig. 4.7. The histories of $m_{r,n}$ for the mixing of different food species with water, G2. (a) The results for the whole calculated period; (b) the results for the period 300-360 s.

Fig. 4.7a shows that the value of $m_{r,n}$ increases monotonically with time when the food boluses have the same density as water (see the curve for FB1). The histories of $m_{r,n}$ for food boluses FB2-5 are similar: The value of $m_{r,n}$ increases to ~0.43 shortly after the mixing starts. Then, the value of $m_{r,n}$ changes slowly due to the low efficiency of mixing. Fig. 4.7b shows the zoomed results during the period 300-360 s. A perturbation of $m_{r,n}$ occurs during each TAC period, however, the TAC doesn't enhance the mixing of heavy foods.

4.4 Effects of the Food Matrix

In the test cases of food emptying (G3), the pylorus is kept open while the gastric contents are composed of water and food boluses FB1. The food boluses FB1 represent the small suspended solid particles which have the same density as water. Although the food boluses have higher viscosity than water, the water is not emptied faster than foods, see Fig. 4.8a. Therefore, gastric motility of stomach and high viscosity of foods are not sufficient for the formation of the Magenstrasse. Its mechanism needs to be more deeply investigated.

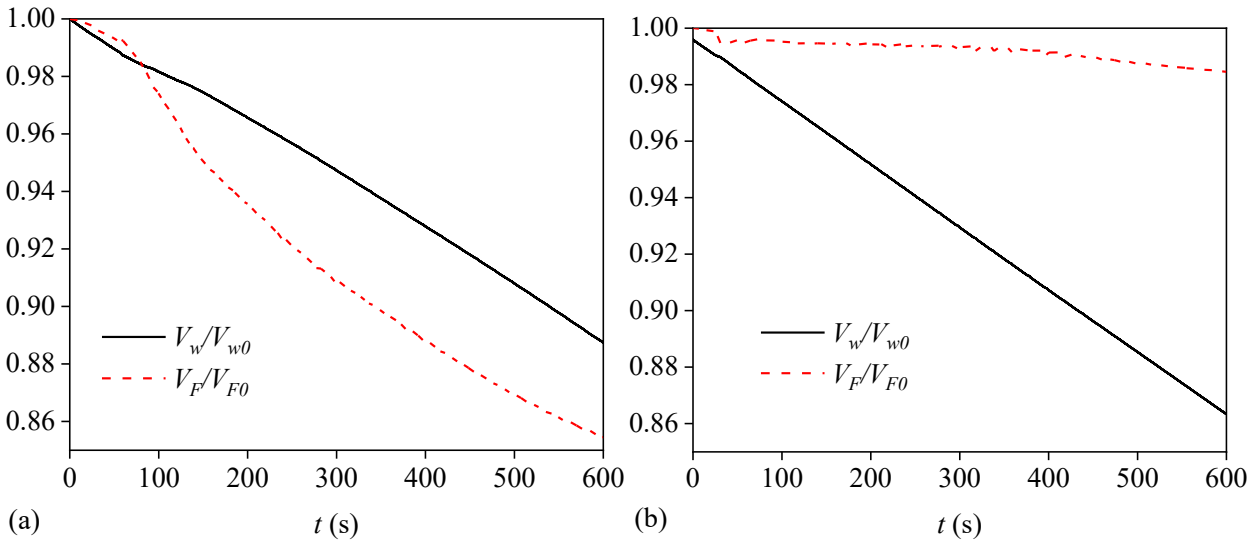

Fig. 4.8. Relative volumes of water V_w/V_{w0} and food boluses V_F/V_{F0} versus time, G3. (a) Without food matrix; (b) with food matrix.

My numerical results of food mixing (G2) show that the heavy food boluses will drop to the distal stomach shortly after ingestion, generating a food matrix. The flow resistance in the food matrix is determined by the Darcy's law. In the zone of food matrix as well as the zone of wrinkles, the flow resistance to the small food particles is much larger than the one to water, since the former has much higher viscosity. This may explain why small food particles are emptied more slowly than water.

It might be also noted that the length scale of large solid food particles is close to the length scale of stomach wrinkles. Thus, the region of wrinkles close to the stomach inner-surface cannot be perfectly filled with solid food particles. On the other hand, the food matrix is expected to have a smaller permeability than the stomach wrinkles while food particles are stickier (resulting in higher viscosity). Therefore, the region close to the stomach inner-surface has lower flow-resistance than the food matrix. This may explain why Koziolek et al. (2016) observed that the water ingested after a meal will flow around the chyme along the entire stomach wall.

Based on this understanding, I have calculated another test case in which a food matrix occupies part of the distal stomach. The porous matrix is assumed to move together with the dynamic mesh. Fast emptying of water doesn't occur when the food matrix is not considered (Fig. 4.8a). By contrast, the water is emptied faster than the food boluses due to the food matrix (Fig. 4.8b). The effect of the food matrix on the food mass fraction is shown in Fig. 4.9a and b, indicating that the food matrix slows down the transport of the light food boluses to the pylorus. The effect of the food matrix on the velocity magnitude of water $c_0|\mathbf{u}|$ is shown in Fig. 4.9c and d. Due to the food matrix, the water flows close to the inner surface of stomach, leading to the Magenstrasse. The numerical results show that the motility of stomach, the high viscosity of food boluses, and the food matrix made of heavy food particles are the main reasons for the formation of the Magenstrasse.

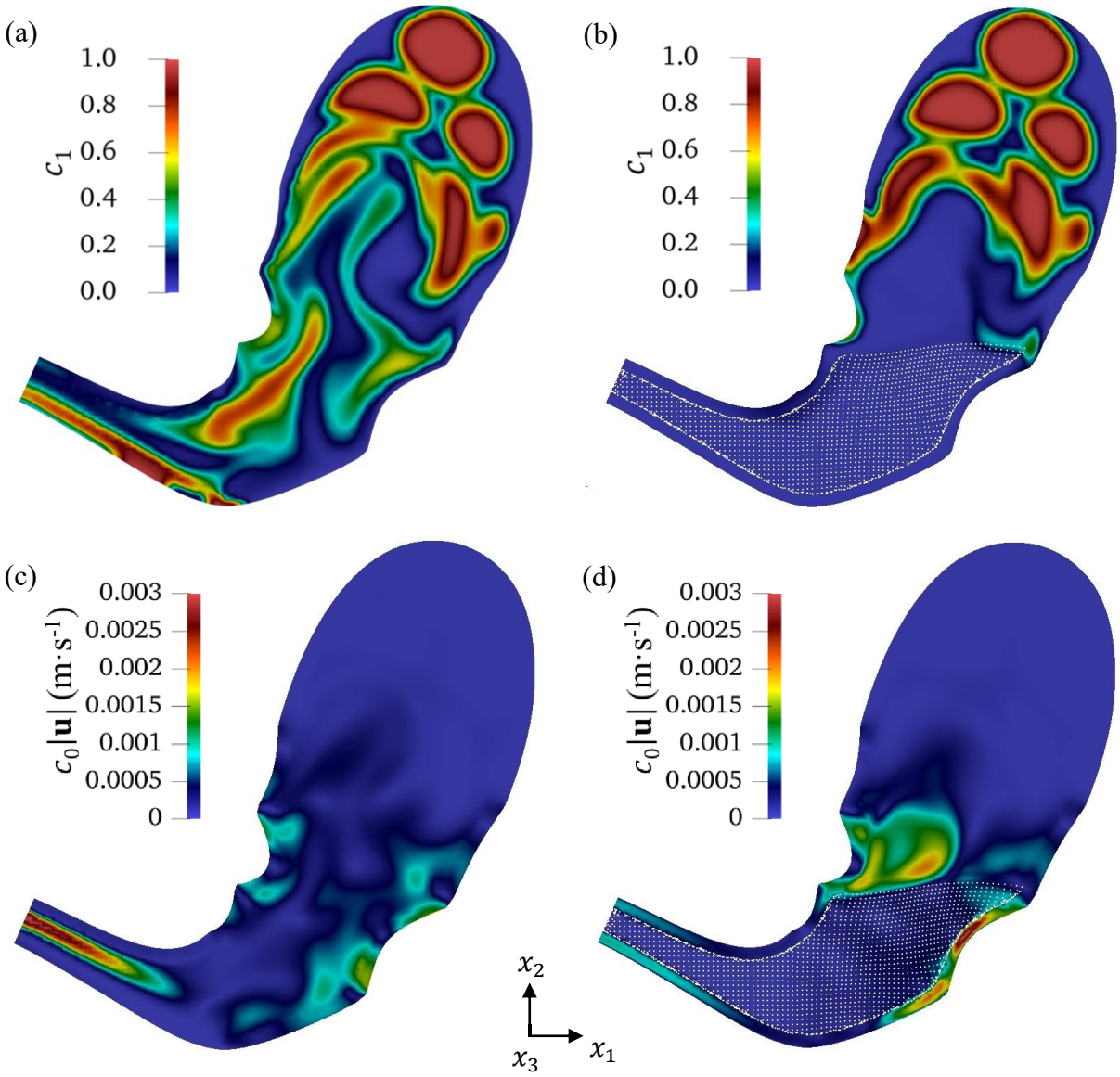

Fig. 4.9. Instantaneous food mass fraction and water-velocity fields in the stomach, G3, t = 250 s. (a) c_1, without food matrix; (b) c_1, with food matrix; (c) $c_0|\mathbf{u}|$, without food matrix; (d) $c_0|\mathbf{u}|$, with food matrix.

4.5 Conclusion

The mixing and emptying of gastric contents in human stomach is investigated based on the CFD simulation to understand the mechanism of the Magenstrasse. The numerical results in this chapter confirm a fast pathway close to the lesser curvature of stomach for hydrogen ions to be

transported to the pylorus when water is emptied, this is in accordance with the study by Pal et al. (2007). However, this phenomenon doesn't occur when the gastric contents are made of food species with different properties.

When the gastric contents are mixed, TACs force the gastric contents back into the proximal antrum, leading to the retropulsive jet-like motion. Two types of large vortices, "crown-shaped" and "bulk-shaped", are found in the central region of stomach during the retropulsive flow. Besides these large vortices, small vortical structures close to the wrinkles of stomach inner-surface can be also found. TACs enhance the mixing of water and light food boluses, however, it has limited effects on heavy food boluses, leading to multi-layers of different food species. This phenomenon is consistent with the results of *in vivo* experiments, while it hasn't been captured in previous numerical studies.

Our numerical results support that the Magenstrasse is due to the gastric motility, high viscosity of food boluses, and the food matrix made of heavy food particles. The food matrix and stomach wrinkles have larger flow resistance to light food boluses (due to their higher viscosity) than to water. In addition, since the large solid food particles cannot perfectly fill the stomach wrinkles, the flow resistance close to the stomach inner-surface is lower than the one in the food matrix. As a result, the water is emptied rapidly close to the stomach inner-surface and around the chyme, leading to the Magenstrasse. The observation in previous *in vivo* experiments might be explained by this mechanism.

CHAPTER 5

Digestion of Meat Proteins

The disintegration rate of food particles in the human stomach is relevant to physicochemical properties and structure of the food, and the degree of physical forces as well as the environment of chemical reactions present in the stomach (Kong and Singh, 2008). In the stomach, pepsin is the main digestive enzyme, which is produced by gastric chief cells (Podolsky et al., 2015). With the help of pepsin, food-proteins are broken down into smaller pieces (e.g., peptide fragments and amino acids). Pepsin is the most active in acidic conditions between pH 1.5 to 2.5 and inactive when at pH greater or equal to 6.5, but it is fully denatured until pH 8.0 (Piper and Fenton, 1965).

The purpose of this chapter is to better understand the physics of the meat-protein digestion and emptying in stomach using a CFD method. For this purpose, the CFD model is further improved so the chemical reaction in stomach can be simulated. The disintegration of large food particles is modeled using a reaction-diffusion-convection model. Based on the numerical results, I will investigate how gastric digestion and emptying are affected by the treatment temperature of meat and stomach function.

5.1 Modeling for the Disintegration of Large Food Particles

The numerical results from section 4.3 suggested that the food species with different density values are distributed in different layers in stomach. Large particles cannot pass through the pylorus due to gastric sieving. Thus, a stable food matrix made of heavy food particles is generated in the distal stomach. The food matrix plays an important role in the formation of Magenstrasse

(stomach road), which describes the fast emptying of ingested liquids from the fed stomach (or postprandial stomach). So, the food matrix is further modeled as a porous medium in my CFD model. So, only liquid gastric contents and small food particles which can be emptied are treated as fluid. They are assumed to be an incompressible Newtonian fluid.

The concentrations of hydrogen ions and enzymes in the food matrix are c_{HM} and c_{EM}, respectively. Then the amounts of hydrogen ions and enzymes transported from the liquid to the food matrix are

$$\frac{dm_H}{dt} = (c_H - c_{HM})k_H A_s,\ \frac{dm_E}{dt} = (c_E - c_{EM})k_E A_s, \tag{5.1}$$

where A_s is the surface area of food particles in each mesh cell. m_H and m_E are amounts of hydrogen ions and enzymes in each mesh cell. c_{HM} and c_{EM} are updated by

$$c_{HM} = \frac{m_H}{V_{cell}},\ c_{EM} = \frac{m_E}{V_{cell}}, \tag{5.2}$$

where V_{cell} is the volume of a mesh cell. The mass transfer coefficients k_H and k_E are calculated from the local Sherwood numbers (Sh):

$$k_H = Sh_H \frac{D_H}{d_p},\ k_E = Sh_E \frac{D_E}{d_p}, \tag{5.3}$$

where D_H and D_E are the diffusivity of hydrogen ions and enzymes, respectively. The Sherwood numbers are calculated as

$$Sh_H = 2.0 + 0.6Re^{1/2}Sc_H^{1/3},\ Sh_E = 2.0 + 0.6Re^{1/2}Sc_E^{1/3}, \tag{5.4}$$

with the Reynolds number (Re) and Schmidt numbers (Sc) defined as

$$Re = \frac{|u_i - u_{si}|d_p}{\nu},\ Sc_H = \frac{\nu_m}{D_H},\ Sc_E = \frac{\nu_m}{D_E}, \tag{5.5}$$

where d_p is the diameter of food particles in each mesh cell. According to Sicard et al. (2018), the concentration of active enzymes in the food matrix c_E^{pH} is calculated as

$$c_E^{\mathrm{pH}} = \frac{c_E}{1 + \frac{10^{-\mathrm{pH}}}{K_{a1}} + \frac{K_{a2}}{10^{-\mathrm{pH}}}}, \tag{5.6}$$

where $\mathrm{pH} = -\log_{10}(c_H)$, which is used to specify the acidity of the aqueous solution. K_{a1} and K_{a2} are kinetic rate constants of the absorption reaction on cleavage sites. L is the pseudo reaction rate.

The ratio of digested protein in the food matrix c_P is calculated as

$$\frac{1}{l_f}\frac{dc_P}{dt} + c_P = c_{Emax}^{\mathrm{pH}} \frac{c_E^{\mathrm{pH}}}{c_E^{\mathrm{pH}}+L}, \tag{5.7}$$

l_f is kinetic rate constant for the formation of peptides and amino acids from protein cleavage. c_{Emax}^{pH} is a constant representing the fraction of active enzyme which can access the cleavage sites available on the protein. c_E^{pH} is the concentration of active enzymes.

The source term due to digestion of proteins in the food matrix $\dot{s}_P$ is calculated as

$$\dot{s}_P = \rho_P \frac{dc_P}{dt}, \tag{5.7}$$

where ρ_P is the density of the protein, 1220 kg·m^{-3} (Quillin and Matthews, 2000) is used in the simulation.

5.2 Description of Test Cases

A scenario that solids and liquids are consumed simultaneously is investigated in this chapter. Initially, there are liquid, small food particles and large deposited particles, see Fig. 5.1. Small meat particles are suspended solid particles, which have the same density as the liquid and a higher viscosity (see ρ_l, ν_F and ν_l in Table 5.1). They are assumed to be a collection of unlinked food particles that will separate quickly and get mixed with the gastric fluid (Jalabert-Malbos et al., 2007). Thus, the small meat particles are simulated as a passive scalar, see Eq. (2.3). Since only one food species and water are considered in the gastric contents, the density and viscosity of the mixture are $\rho_m = c_F\rho_F + (1-c_F)\rho_l$ and $\nu_m = c_F\nu_F + (1-c_F)\nu_l$, respectively. Here F indicates small meat particles.

It has been shown that the large and heavy meat boluses drop to the distal stomach after ingestion and form the food matrix immediately. An *in vivo* study also showed that solids locate initially in the proximal stomach and move to the distal stomach in a later time (Collins et al., 1991). Thus, the food matrix (see Fig. 5.1, the dark brown region) is modeled as a porous medium, with the porosity (ϕ_F) 0.0343 (McDonald and Sun, 2001). The presence of solid meal in the distal

stomach will act as a flow resistance to the liquids and small solid particles. The large solid particles in the food matrix will be broken down by chemical reactions, generating small meat particles, which are also modeled as a fluid. In this way, gastric liquids are increasing in viscosity as they mix with the tiny particles resulting from the disintegration of solids, which is consistent with the observation from an *in vivo* experiment (Marciani et al., 2001a). The main properties used in the study of this chapter is shown in Table 5.1.

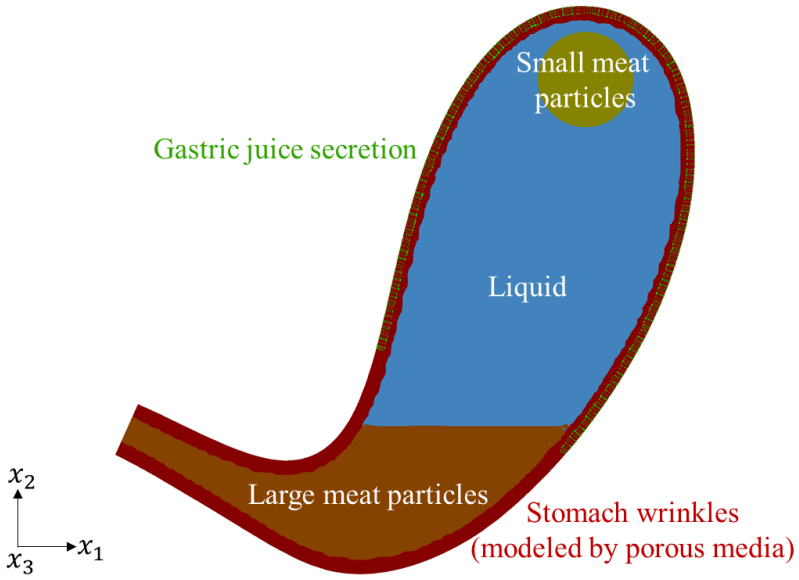

Fig. 5.1. Schematic description of initial distributions of gastric contents on a cross-section. The dark brown region represents large meat particles which are located in the distal stomach, forming the food matrix. The blue region indicates the liquid gastric contents. Small meat particles (light brown region) are assumed to occupy a spherical region with the diameter 3 cm.

Table 5.1. The properties of gastric contents. D_F is estimated according to Erickson (2009), and some other parameters are from Sicard et al. (2018).

Species	Property	Value
Liquid	ρ_l (kg·m^{-3})	1.0×10^{3}
	ν_l (m^2·s^{-1})	1.0×10^{-6}
Food (small particles)	D_F (m^2·s^{-1})	5.0×10^{-11}
	ν_F (m^2·s^{-1})	1.0×10^{-5}
Food (large particles)	L (-)	2.45
	pK_{a1} (-)	1.6
	pK_{a2} (-)	2.5
	l_f (s^{-1})	4.1667×10^{-4}
H^+	D_H (m^2·s^{-1})	3.3×10^{-9}
Enzyme (pepsin)	D_E (m^2·s^{-1})	1.4×10^{-10}

Kong and Singh (2008) stated that a human-stomach with a normal function usually controls the caloric emptying rate to be within the range 2-4 kcal·min^{-1}. This is in accordance with the study by Faas et al. (2002), who suggested that gastric contents with similar calories can produce a similar emptying-rate no matter the composition and consistency. I assume an averaged emptying-rate of 3 kcal·min^{-1}, and initially, the solid and liquid gastric contents contain the energy amounts 380.44 kcal and 248.45 kcal, respectively. The eating can increase pH to the range of 4.5-5.8 (Kong and Singh, 2008), an initial pH of 5.6 is assumed to indicate a postprandial state.

The test cases in this chapter can be classified into four groups, see Table 5.2. The first group (G1) compares heating effects, the temperature determines c_{Emax}^{pH}. The second group (G2) studies the effects of TACs. The third group (G3) investigates the effects of motion amplitude. The fourth group (G4) explores the effects of H^+ secretion rate. The test cases have been carried on with the

same boundary an initial condition, the OpenFOAM® built-in boundary conditions and initial field are listed in Table 5.3.

Table 5.2. Test cases in this chapter. A_{ACW} is the amplitude of ACWs, A_{TAC} is the amplitude of TACs. $\dot{m}_H$ is the secretion rate of hydrogen ions.

Case ID		Gastric motility		H^+ secretion	Heating effects	
		A_{ACW} (m)	A_{TAC} (m)	$\dot{m}_H$ ($\times 10^{-6}$ mol·s^{-1})	T_h (°C)	c_{Emax}^{pH} (-)
G1	S0	0.01	0.01	6.75	20 (raw)	0.093
	S1	0.01	0.01	6.75	50	0.113
	S2	0.01	0.01	6.75	70	0.137
	S3	0.01	0.01	6.75	90	0.145
G2		0.01	0 (no TAC)	6.75	70	0.137
G3		0.005	0.005	6.75	70	0.137
G4		0.01	0.01	3.375	70	0.137

Table 5.3. Boundary and initial conditions used in the current numerical model.

* The alternative pressure, $p' = p - \rho g_i h_i$.

** The initial distribution of small meat particles (c_F) is not uniform, c_F is 1 in the spherical region and 0 outside (see Fig. 5.1).

Field	Wall	Outlet	Initial value
u_i (m·s^{-1})	movingWallVelocity	pressureInletOutletVelocity	0
p' (m^2·s^{-2}) *	fixedFluxPressure	totalPressure	0
c_E (U·mg^{-1})	zeroGradient	inletOutlet	0
c_H (mol·L^{-1})	zeroGradient	inletOutlet	2.5×10^{-6}
c_F (-)	zeroGradient	inletOutlet	Non-uniform **

5.3 Verification and Validation

The test cases described in section 5.2 are calculated using two mesh resolutions, they have about 6.0×10^5 mesh elements (mesh 1) and 2.3×10^6 mesh elements (mesh 2). The numerical results of the mixing rate r_{mix} and the volume-averaged kinetic energy Ke in the stomach calculated from two mesh resolutions are compared to perform the mesh-convergence study. r_{mix} is defined for the mixing in Eq. (3.3), which is $r_{mix} = \left(1 - \frac{M_t}{M_0}\right)$, where $M_t = \frac{\int_V (c_H(t) - c_{HG})^2 dV}{c_{HG}^2 \int_V dV}$. M_0 is the initial value of M_t, $c_H(t)$ is the local H^+ concentration in the stomach at time t. The volume-averaged kinetic energy in the stomach is defined in Eq. (3.2), i.e., $Ke = \frac{1}{2}\frac{\int_V u_i u_i dV}{\int_V dV}$.

Based on the numerical results (see Fig. 5.2), mesh 1 is used for later analysis. The effects of heating treatment, gastric motility (including TACs and ACWs) and secretion rate of hydrogen ions on the digestion process are analyzed.

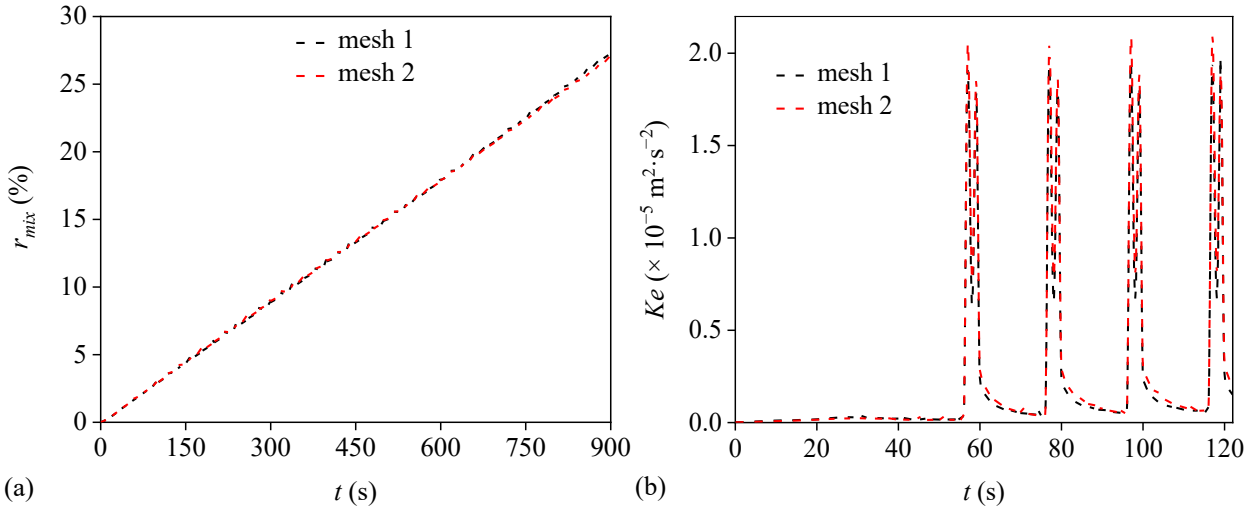

Fig. 5.2. Test case G1-S2 is used to show the mesh sensitivity. 28 processors are used in the MPI-parallel calculations, which takes about 42.3 h by using mesh 1 or 228.6 h by using mesh 2 to calculate a process of 900 s.

It's hard to find realistic and repeatable digestion data to quantitatively validate the CFD results due to the complexity of the problem. Instead, I have qualitatively compared my numerical results with those of previous studies. The details can be found in Table 5.4.

Table 5.4. The comparison of my CFD results with published researches.

Physical quantity	This thesis	Published works
Maximum kinetic energy ($\frac{1}{2}u_i u_i$, $\times 10^{-4}$ m^2·s^{-2})	~3.4-83.3	~0.41 (Kozu et al., 2014a)
		~19.2 (Xue et al., 2012)
		~63.1 (Alokaily et al., 2019)
		~70. 8 (Ferrua and Singh, 2010)
Time to reach acidity (min)	~53-93 for pH < 2	~60 for pH < 3 (Malagelada et al., 1976)
		120 for pH ≈ 2.3 (Wang et al., 2019)
		~120-240 for pH < 2 (Malagelada et al., 1979)

5.4 Effects of Heating Treatment

The cooking affects the digestibility of proteins by unfolding and aggregation of proteins (Bax et al., 2012). The denaturation of protein can increase the number of cleavage sites (Kondjoyan et al., 2015). In my model, the effect of protein denaturing is taken into account by using different values of c_{Emax}^{pH}, see Table 5.2. Fig. 5.3 shows that the digestion rate (r_{dig}), defined as the ratio of digested mass of large particles to its initial value:

$$r_{dig} = 1 - \frac{V_{pl}}{V_{pl0}}, \tag{5.8}$$

where V_{pl} is the volume of the food matrix made of large particles, and V_{pl0} is its initial volume. The value of r_{dig} is close to zero in the first few minutes, and overall, the digestibility is low in the simulated time. It can be seen that the value of r_{dig} is higher as the food is heated with a higher temperature.

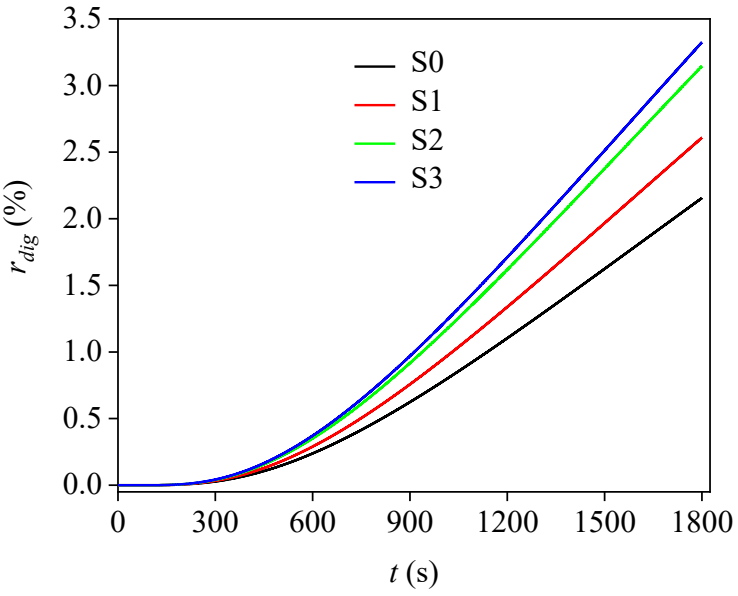

Fig. 5.3. Digestion rates r_{dig} of meat-proteins with different heat treatments versus time t.

According to Burton et al. (2005), the gastric retention rate (r_{gr}) for solids (r_{grs}) and liquid (r_{grl}) are defined as

$$r_{grs} = \frac{V_s}{V_{s0}},\ r_{grl} = \frac{V_l}{V_{l0}}, \tag{5.9}$$

where V_s is the volume of solid food particles, including the small-particle volume V_{ps} and large-particle volume V_{pl}. V_{s0} is the initial volume. V_l is the volume of liquids (including secreted gastric juices during the digestion) in the stomach and V_{l0} is its initial volume. As can be seen in Fig. 5.4, liquids are emptied much faster than solids from the stomach; only a little solid contents can be found in the emptied digesta during the first 30 minutes. This phenomenon is called lag phase. It is also observed in *in vivo* and *in vitro* experiments for emptying of solid and semisolid foods in human-stomach (Camilleri et al., 1985; Peng et al., 2021). The period of lag phase varies individually, which can be a half hour or one hour (Burton et al., 2005). The liquid is emptied almost linear with time. The food matrix made of large meat particles undergoes both mechanical (by ACWs and TACs) and chemical (by enzymes) processes, which help to grind and break down the large particles into smaller ones. These processes take rather long time, so the large particles are emptied much more slowly than liquids.

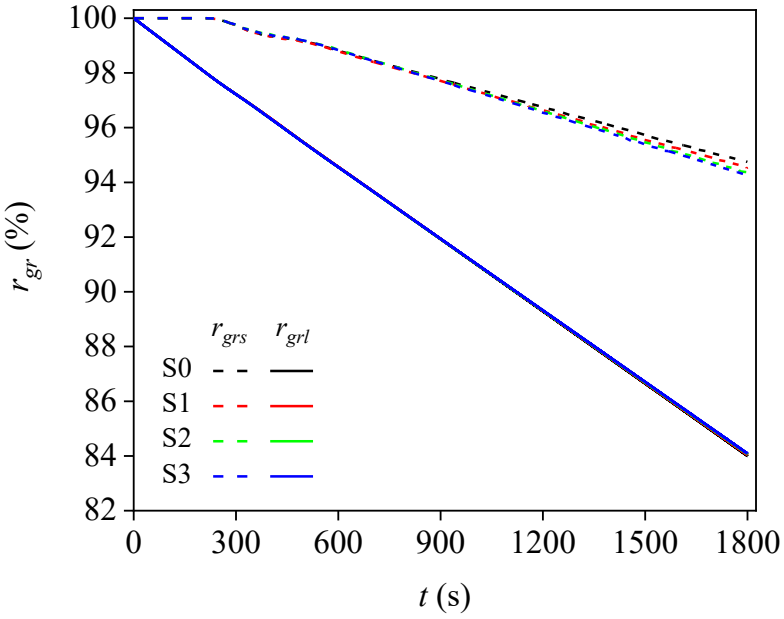

Fig. 5.4. Gastric emptying curves for solid and liquid contents.

Fig.5.5 shows the fraction of large particles (heated at different temperatures and modeled as a food matrix) at 1800 s. It can be seen that large particles are only marginally disintegrated; which infers a slow emptying rate of solid foods. The heating temperature doesn't change the pattern of disintegration. However, the meat treated at a higher temperature is faster disintegrated. At t = 1800 s, large food particles are mainly disintegrated in the region close to the stomach inner-wrinkles. The reason is that hydrogen ions or enzymes cannot penetrate deeply into the food matrix due to its high flow resistance.

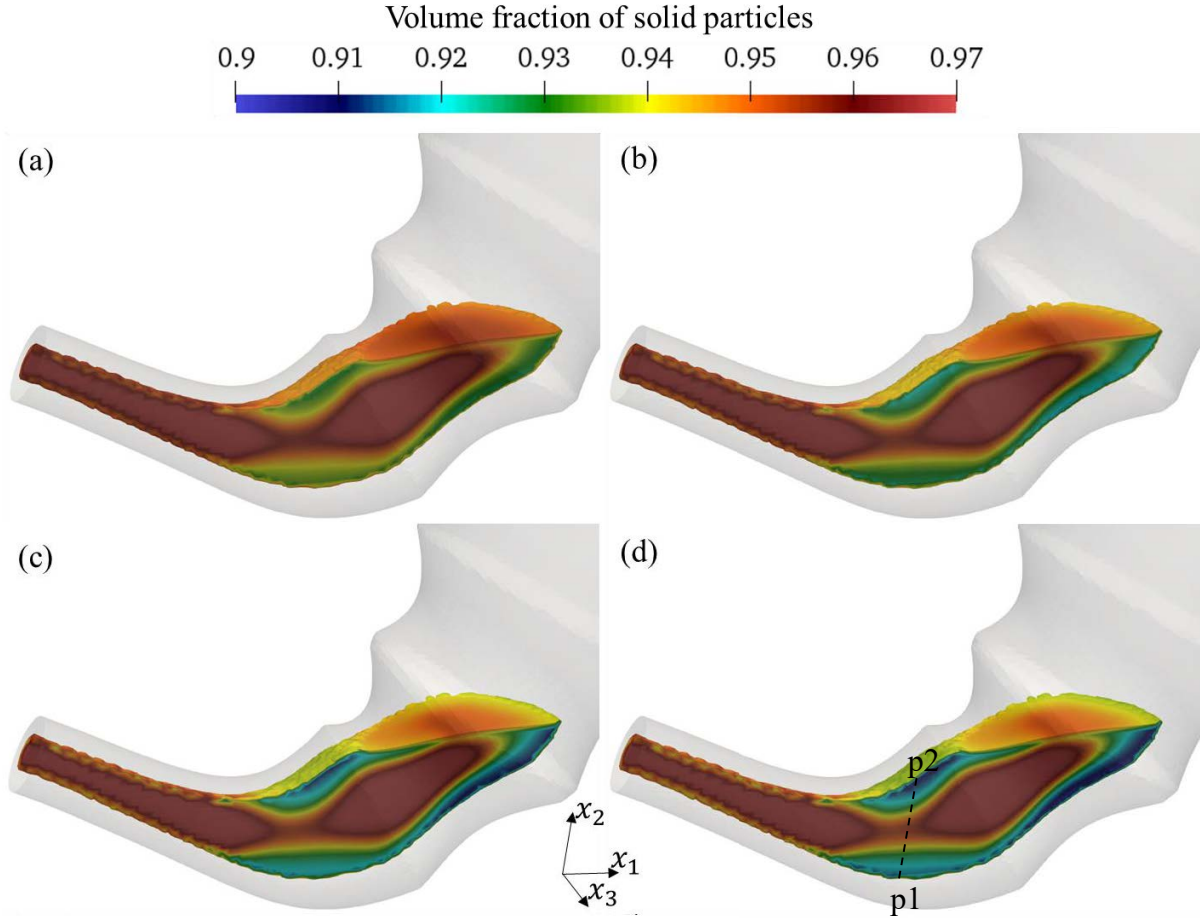

Fig. 5.5. The volume fraction of solid particles in the food matrix (a half is shown) at t = 1800 s. (a), (b), (c) and (d) indicate S0, S1, S2 and S3 respectively. The coordinates of p1 and p2 (unit in meters) are (0.0871, 0.0504, 0) and (0.0871, 0.0846, 0) respectively.

As can be more clearly seen in Fig. 5.6, which is about the fraction of large particles in the line p1-p2 indicated in Fig. 5.5d. This suggests that, when the gastric emptying rate is predicted using a 0D model, the size of food matrix instead of the size of food particles should be used as the characteristic length scale of mass transfer (for hydrogen ions or enzymes). My CFD results also show that more large-particles are disintegrated in the distal stomach close to where TACs originate. This infers the significant effects of TACs on the disintegration of large particles.

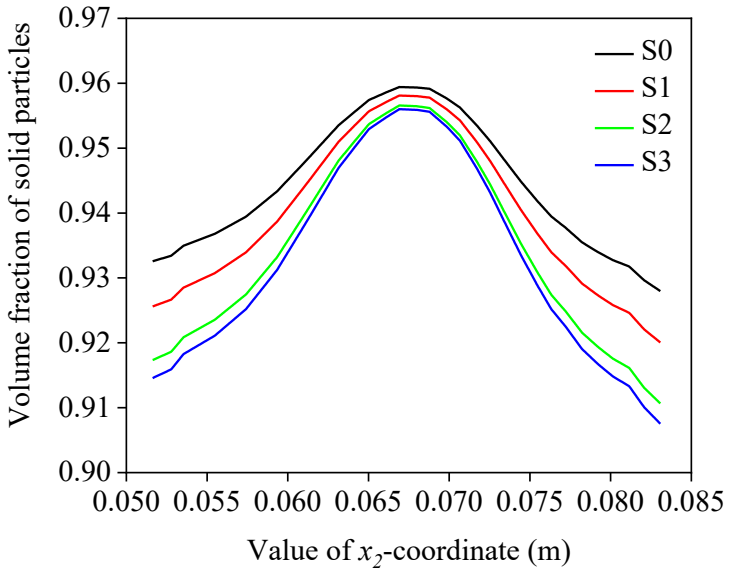

Fig. 5.6. The volume fraction of solid particles plotted along the line at the same location at t = 1800 s for four meat samples. The line is indicated in Fig. 5.5d.

5.5 Effects of Gastric Motility

The stomach can present less motility in the case of gastric disorders. For example, diabetic gastroparesis results in a decreased motility in fundus and antrum, reduced or absent MMC, gastric dysrhythmias, and pylorospasms (De Block et al., 2006). This considerably weakens the digestion function of stomach. In this section, the effects of TACs on the gastric digestion is first investigated. Then, the digestion process with reduced gastric motility amplitudes, as a typical case resulted

from the diseases and medication of stomach, will be studied. The solid gastric contents are made of meat proteins cooked at 70°C (heat treatment S2).

I first compare the digestion rates r_{dig} and the solid-gastric-particle retention rates r_{grs} for the digestion processes with and without TACs. Fig. 5.7 shows evidently that solid gastric contents are emptied faster when the TAC is taken into account.

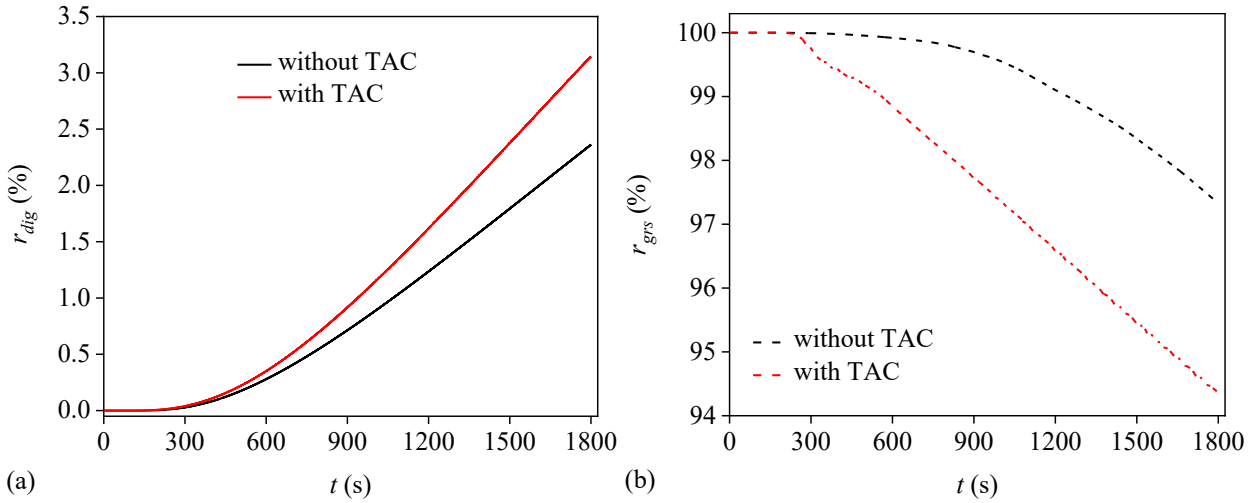

Fig. 5.7. Influences of TACs on gastric digestion rate r_{dig} (a) and retention rate for solids r_{grs} (b).

The effects of TACs on the hydrodynamic in the stomach can be observed from the vortical structures identified with the iso-surfaces of Q. Fig. 5.8 shows the vortical structures at several typical time instants of a TAC period which lasts for 4 seconds. A strong retropulsive jet-like flow can be seen at 57 s when TACs are considered. This phenomenon is consistent with the previous studies, see Pal et al. (2004). The backward flow becomes much weaker in the case without TACs. In addition, the TAC induces strong flow instabilities in the proximal stomach, characterized by the small vortices. It can be expected that TACs enhance mixing of the hydrogen ions and enzymes considerably and thus accelerate the digestion of solid particles in the stomach. This can explain the results in Fig. 5.7 that the emptying rate is much higher when the TACs are taken into account.

Fig. 5.8. Vortical structures identified with Q = 0.001 s^{-1}, colored with the vertical velocity component u_2.

Fig. 5.9 shows pH and enzyme distributions at t = 1800 s. Low pH values and High concentration of enzymes can be found near the gastric wall, where the hydrogen ions and enzymes are secreted together with the gastric juice. Due to the flow resistance by the food matrix made of large food particles, the concentrations of hydrogen ions and enzymes are low near the central region of the chyme (food matrix). More hydrogen ions and enzymes are transported along the inner-wall and flow around the chyme. This is similar to the emptying of water-particle mixture, in which water flows close to the inner stomach-surface, forming the Magenstrasse (Koziolek et al., 2014).

It can be seen that hydrogen ions and enzymes are much better mixed when TACs are considered in the simulation, causing lower pH and higher concentration of enzymes in the proximal stomach, see Fig. 5.9c and d. This is in line with the results shown in Fig. 5.8 that TACs stimulate strong retropulsive backward flows in the antrum and small vortices in the proximal stomach, which benefit the mixing. It also interprets the results in Fig. 5.7 that TACs lead to a faster emptying rate of large solid particles.

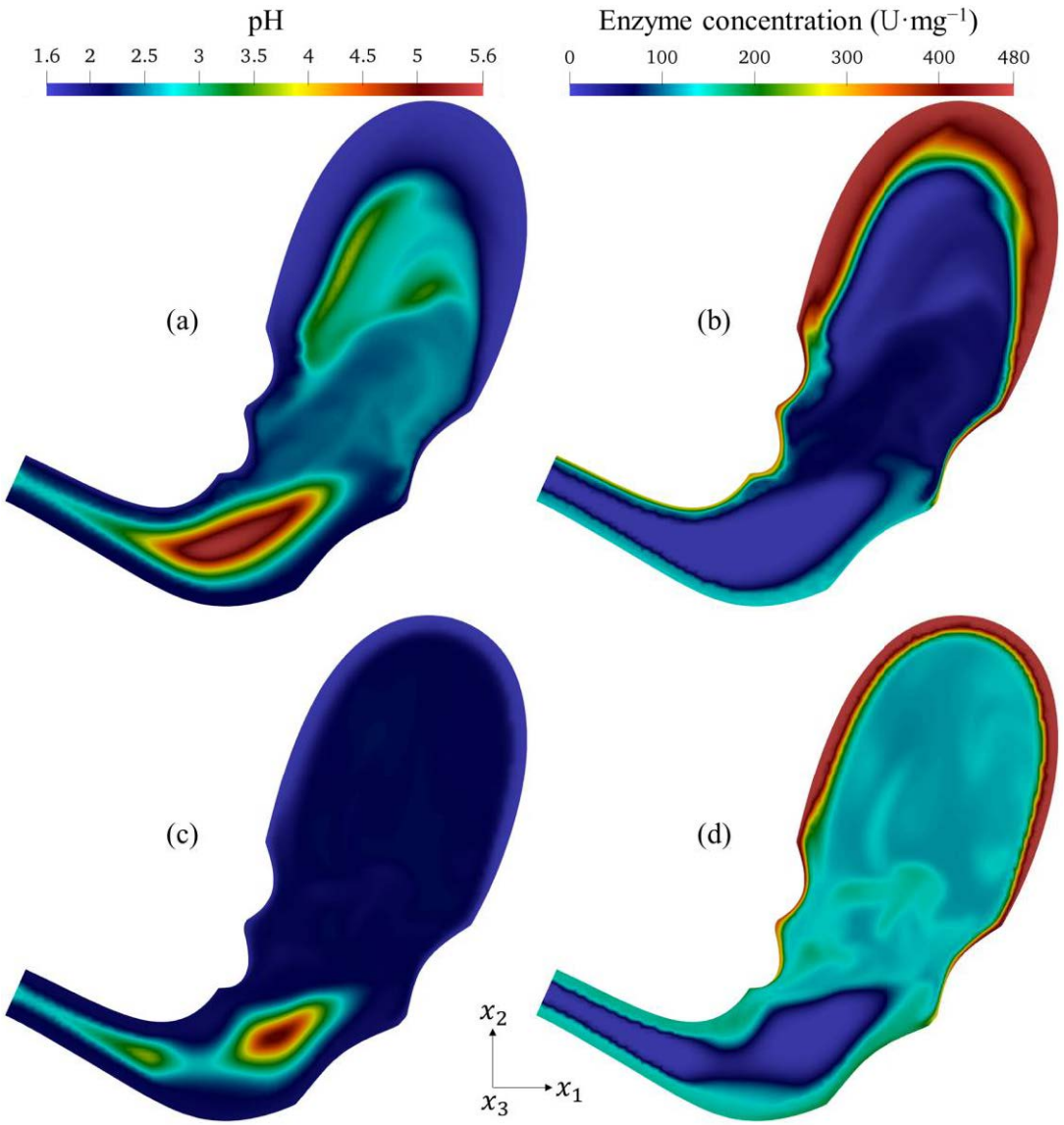

Fig. 5.9. Distributions of pH and enzyme concentration on the cross-section at t = 1800 s. Without TACs: (a) pH, (b) enzyme; with TACs: (c) pH, (d) enzyme.

To make a more systematic study of the effects of gastric motility, the digestion process with the half-amplitude of ACWs and TACs have been calculated. It can be seen in Fig. 5.10, when the amplitude of gastric motility is reduced by a half, the maximum kinetic energy is reduced from 1.92×10^{-5} $m^2 \cdot s^{-2}$ to 0.47×10^{-5} $m^2 \cdot s^{-2}$; the mixing rate r_{mix} at 1800 s is reduced from 53% to 48%; the digestion rate of large particles r_{dig} is reduced from 3.15% to 1.75%; the solid-particle retention rate r_{grs} at t = 1800 s is increased from 94.4% to 97.6%. The significant effects of ACs

indicated by my numerical results are in accordance with the studies by Cardoso-Júnior et al. (2007) and Collins et al. (1996), who stated that ACs are the key factor which determines the emptying rate.

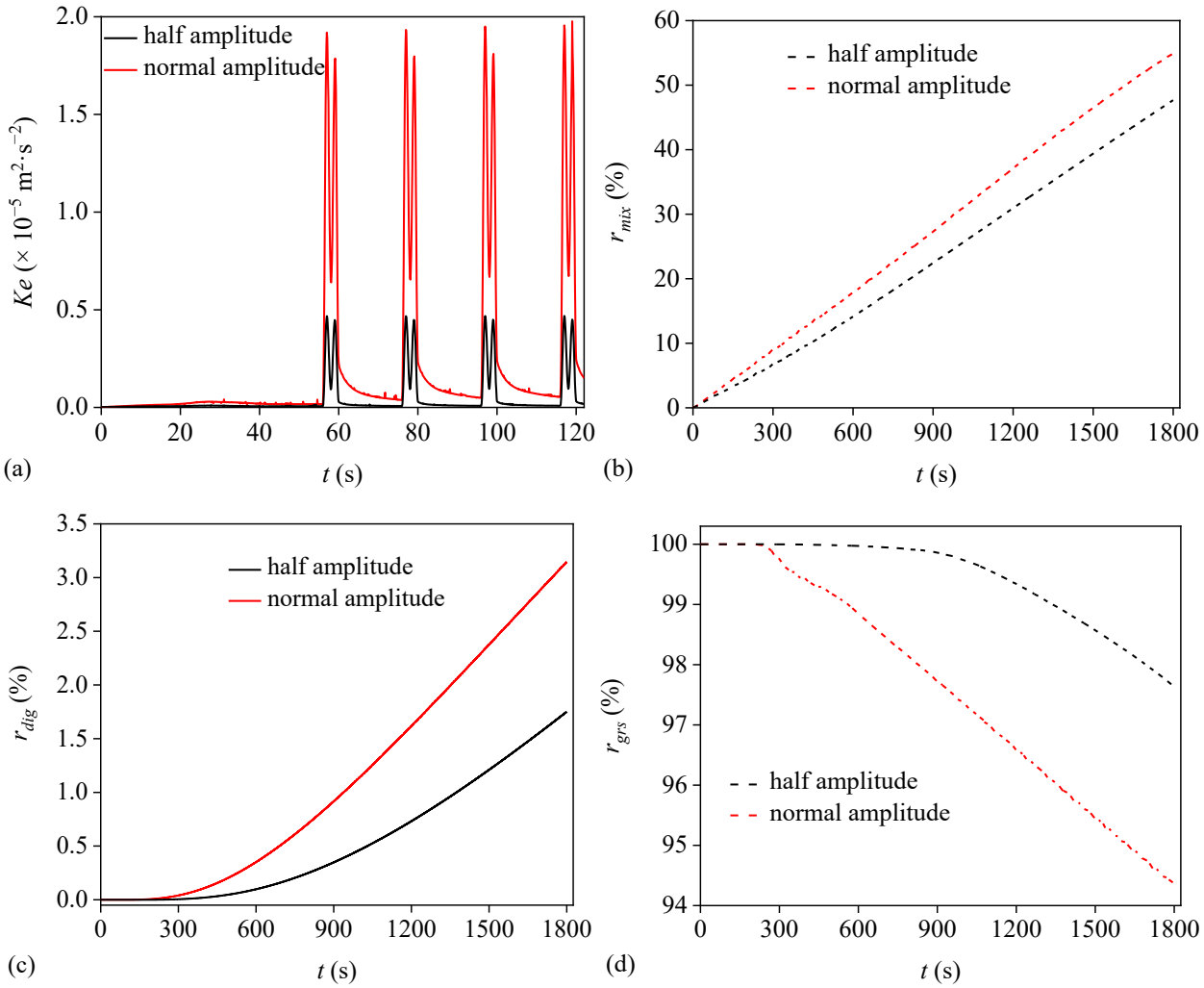

Fig. 5.10. Effects of the amplitude of the gastric motility on averaged kinetic energy Ke (a), mixing rate r_{mix} (b), digestion rate r_{dig} (c) and gastric retention rate for solids r_{grs} (d).

5.6 Effects of H^+ Secretion

Another type of gastric disorders is related to the weakened acid secretion, which often occurs for people with atrophic gastritis (Katelaris et al., 1993). This effect is studied based on my numerical results.

Fig. 5.11 shows that, when the secretion rate of hydrogen ions is reduced by a half, the digestion rate r_{dig} at t = 1800 s is reduced from 3.1% to 2.8%, while the mixing rate r_{mix} reduces from 55% to 32%. According to this trend, a normal stomach needs around one hour to approach the acidic state, this is in accordance with the study by Malagelada et al. (1976), who observed a peak of gastric pH after food intake and followed by a drop to pH < 3 after an hour. By contrast, an abnormal stomach with a half H^+-secretion rate needs around 1.53 hours to approach the acidic state.

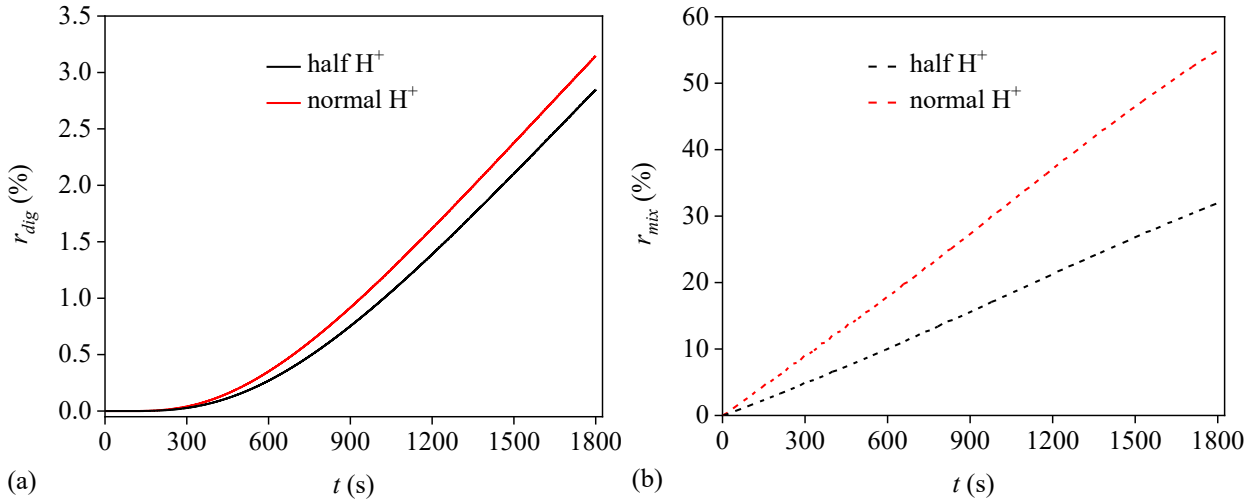

Fig. 5.11. The effects of H^+ secretion on (a) digestion rate r_{dig} and (b) mixing rate r_{mix}.

Transport of hydrogen ions affects the digestion of large particles through its effects on the pepsin activity. As can be expected, the pH in the stomach becomes higher when the secretion rate of hydrogen ions is reduced by a half. This is more obvious in the proximal stomach which is occupied by liquid gastric contents. Due to the flow resistance by the food matrix, the pH value in

the central region of the large food particles are higher. The reduction of hydrogen ions results in higher pH value and thus slower disintegration rate. This is in accordance with the study by Parkman et al. (1998), who indicated that the suppression of the secretion of the gastric juice slows down the delivery of gastric contents.

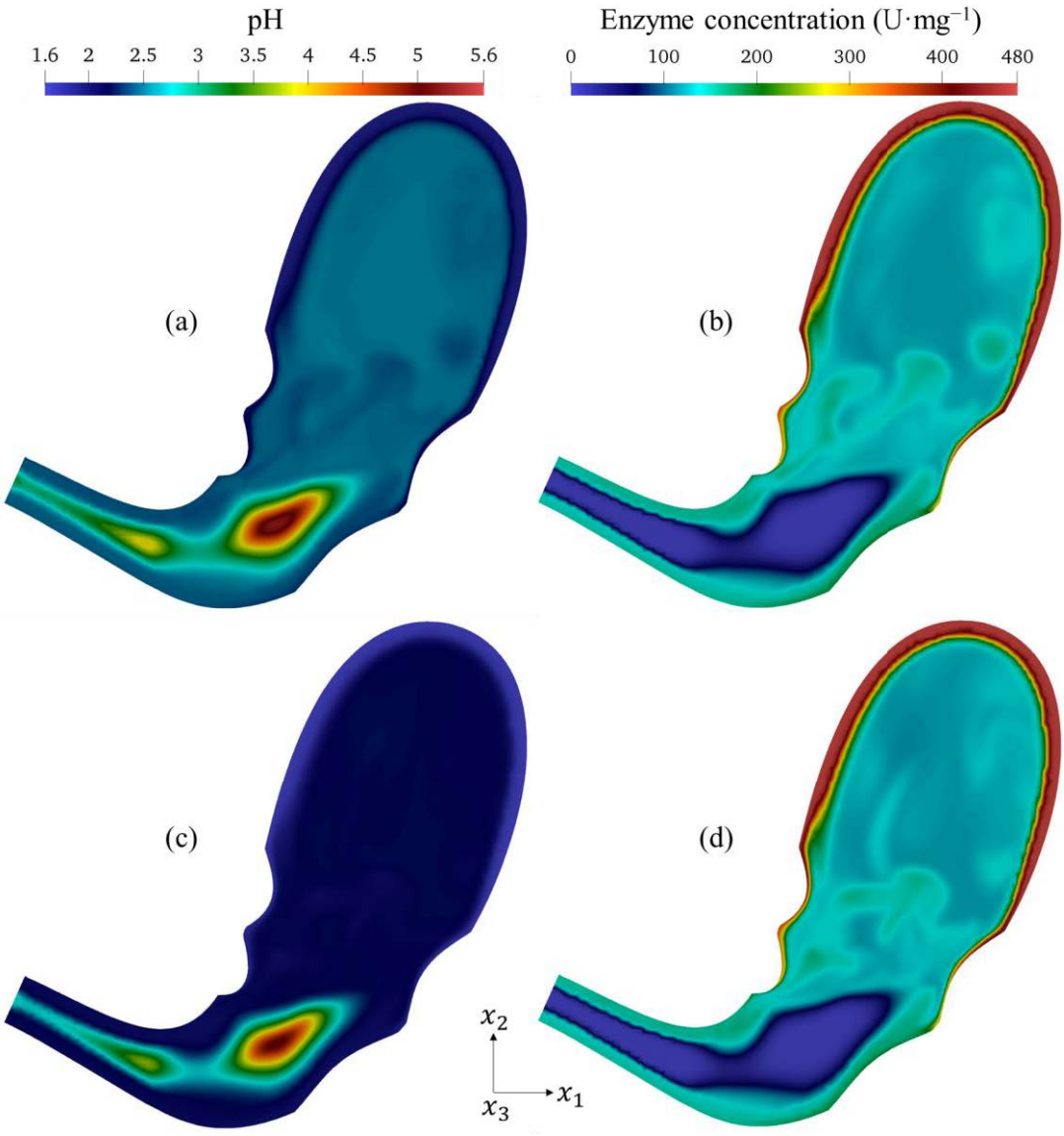

Fig. 5.12. pH and enzyme distribution on a cross-sectional plane at t = 1800 s. Half H^+ secretion: (a) pH, (b) enzyme; normal H^+ secretion: (c) pH, (d) enzyme.

The actual pH within food bolus can be higher than the pH measured in the liquid fraction of the stomach, which can be also seen in (a) and (c) of Fig. 5.9 and Fig. 5.12. This buffering effect reduces enzyme inactivation at low pH, e.g., salivary amylase, which inactivated when pH < 4, in this case, the activity of salivary amylase is potentially prolonged, so starch can be still digested in stomach. The phenomenon found here is in line with the statement in Capuano and Janssen (2021).

5.7 Conclusion

The CFD model has been further developed to analyze the digestion of solid food particles in human-stomach in an acid environment. The gastric motility, including the TCs, ACWs and TACs are modeled using a dynamic mesh. The chemical reaction, i.e., the disintegration of large meat particles in an acidic environment, is accounted for using a reaction-diffusion-convection model developed by Sicard et al. (2018).

Based on the numerical results, the digestion and emptying of meat-proteins with different heating temperatures in normal and disordered stomachs are investigated. The numerical results show that meat-proteins heated with a higher temperature are faster disintegrated and emptied. Reduced stomach-motility amplitude or secretion rate of hydrogen ions result in a slower digestion rate and emptying rate. These are in accordance with the observations in *in vivo* experiments.

An interesting finding obtained from my CFD results is that, much more large food- particles are disintegrated in the region close to the stomach inner-wrinkles than in the central region. This is due to the flow resistance by the food matrix made of large food particles. If this is true, in a 0D model, the size of food matrix instead of the size of food particles should be used as the characteristic length scale of mass transfer (for hydrogen ions or enzymes). It should be noted that the dynamics of large particles are approximated with moving mesh in this chapter, while the real particle dynamics might have more significant effects on the mass transport. The characteristic length scale of mass transfer still deserves deeper investigation.

The numerical results show that TACs stimulate strong retropulsive backflows which enhance the transport of enzymes and hydrogen ions. When the stomach-motility amplitude is reduced by a half, the maximum kinetic energy is reduced by 75.5% while the digestion rate of large particles is reduced by 43.8%. When the secretion rate of hydrogen ions is reduced by a half, the maximum kinetic energy is unchanged but the digestion rate of large particles is reduced by 9.7%. These results are helpful for estimating the gastric emptying rate in human-stomach.

CHAPTER 6

Summary and Outlook

6.1 Conclusion of This Thesis

The dynamics of the human-stomach, filled with a mixture of liquids and food particles, generates a complex and unsteady flow field. A CFD model for simulating the digestion process in human stomach was developed to understand the dynamics in human-stomach in this thesis. The muscle movements including TCs, ACWs, and TACs are accounted for using a dynamic mesh. The wrinkles of the stomach surfaces are treated as a porous medium zone, which is used to ensure mass conservation and to simulate the motility of wrinkles (expansion/shrinking) by adjusting its porosity. The secretion of gastric juice, which is a mixture of water, hydrogen ions and pepsins (considered in the simulation of protein digestion), is modeled by adding source terms in the mass and species transport equations. The gastric contents are approximated as mixtures of water and food species with different properties. The large deposited food boluses form the food matrix, which is modelled as another porous medium zone. The small food particles are treated as passive scalars. The emptying rates are determined according to the calorie amount of gastric contents.

The developed CFD model is used to simulate three typical processes with respect to gastric digestion to demonstrate its application and carry out qualitative analyses. These processes are the dynamics of liquid gastric contents, the mechanism of the Magenstrasse and the digestion of solid foods. The numerical results show that the mixing patterns vary among the liquid foods (water, orange juice and whole milk) due to their difference in physical properties, i.e., acidity, H^+ diffusion, density, viscosity and energy density. The pH value at the stomach outlet (pylorus) drops

more slowly as the emptying rate rises. Slower emptying rate leads to more efficient mixing of the water and gastric juice. The hydrogen ions are transported from the top region to the bottom region when the liquid food is heavier than the gastric juice. However, if the liquid food has the same density as the gastric juice, the hydrogen ions are transported from the acid-secretion region to the inner lumen of the stomach.

TAC forces the gastric contents back into the proximal antrum, leading to the retropulsive jet-like motion. This motion was also observed in previous studies (Ferrua et al., 2011; Pal et al., 2004; Schulze, 2006). When retropulsive jet pushes hydrogen ions and enzymes back to the proximal stomach, decreasing their emptying rate. It also enhances the mixing of them with the gastric contents. These characteristics are favorable for the digestion in the stomach. The retropulsive flow induces a strongly transient and 3D flow. The numerical results show that the TAC can significantly increase the averaged kinetic energy in the stomach. Compared to the case without the TAC, the maximum velocity is almost doubled. The interaction between the retropulsive jet and the relatively stagnant fluid in the stomach creates a high shear field at boundaries of the jet. Two types of large vortices, “crown-shaped” and “bulk-shaped” vortices, are found in the central region of stomach. Besides these large vortices, small vortical structures are also found close to the wrinkles of the stomach surfaces.

The TAC not only increases the maximum velocity in the stomach, but also makes the flow more chaotic. More small vortical structures can be observed in the upper region of the stomach after the TAC starts. These small vortices might help to grind the large food particles and enhance the mixing of gastric contents, consistent with Chen et al. (2016) and Wang et al. (2019). These vortices are important for lifting food particles from the stomach wall and transporting them towards the stomach center. TACs enhance the mixing of light food boluses, however, they have limited effects on heavy boluses.

From the numerical results of water emptying, hydrogen ions close to the lesser curvature are found to be transported faster to the pylorus than hydrogen ions close to the greater curvature, this phenomenon is in line with the observations of Pal et al. (2007). The arrival of hydrogen ions

released together with the gastric juice to the pylorus indicate the time scale of the fast pathway of emptying. However, water is not emptied faster than the gastric contents which are made of food species with a higher (than water) viscosity. This suggests that gastric motility and high viscosity of foods are not sufficient for the formation of the Magenstrasse.

The deposited food particles are further modelled as a food matrix, the food matrix has smaller permeability than stomach wrinkles since food particles are stickier. Fast emptying of water occurs when the food matrix is considered. The food matrix and stomach wrinkles have larger flow resistance to light food boluses, due to their higher viscosity than that of the water. In addition, since the large solid food particles cannot perfectly fill the stomach wrinkles, the region close to the stomach inner-surface has lower flow resistance than the food matrix region. As a result, the water is emptied rapidly close to the stomach inner-surface and around the chyme, leading to the Magenstrasse. My numerical results support that the Magenstrasse arises due to the gastric motility, high viscosity of food boluses, and the food matrix made of heavy food particles. The observation in previous *in vivo* experiments (Koziolek et al., 2016; Scheunert, 1912), which stated that the water can flow around the chyme, might be explained by this mechanism.

The enzymatic digestion of proteins in an acidic environment has been investigated with different heating temperatures in normal and disordered stomachs. The numerical results show that meat-proteins treated with a higher temperature are faster disintegrated and emptied. Reduced stomach-motility amplitude or secretion rate of hydrogen ions result in a slower digestion and emptying. Due to the flow resistance from the food matrix made of large meat particles, gastric digestion is limited by the diffusion of the pepsin inside the food matrix. The digestion starts form the out layer of the food matrix, therefore, the size of food matrix instead of the size of food particles should be used as the characteristic length scale for the mass transfer in a 0D model.

6.2 Open Questions and Further Work

The numerical study in this thesis demonstrates the potential of using a CFD model to better understand the physics of gastric digestion in human-stomach. However, the CFD model still needs to be further improved in the future.

First of all, it is still necessary to further validate the numerical results with experimental data. This is a challenging task for both experimentalists and CFD analysists. With respect to experiments, it is necessary to measure more details of the flow in stomach precisely and provide more reliable properties of the gastric contents.

With respect to numerical simulation, the CFD model should be further improved to approach the real digestion process. One important aspect is to implement the model of pylorus contraction, which can reach a contraction rate of 90% and thus lead to more complicated flow patterns (Skamniotis et al., 2020). In addition, real food boluses are non-Newtonian fluids which often have high viscosity and their properties are closer to those of soft solids. They are more often simulated using the Eulerian finite element method (Skamniotis and Charalambides, 2020; Skamniotis et al., 2017), or the discrete element method (Sinnott et al., 2017). The complexity of the food properties and chemical reaction renders the uncertainty of the numerical results. More efforts should be focused on coupling the current CFD model with the methods for simulating soft solid foods.

Another deficiency of the current CFD model is that it is still not able to simulate the full digestion process, which might take several hours. A technical barrier is that large deformation of stomach cannot be represented by the current dynamic mesh method. In addition, real stomach geometries are much more complicated than the stomach model in the present thesis. Deformation of such complicated geometries makes the simulation even more difficult. These problems need to be addressed in future work.

Finally, a potential field of research is about the influences of reduced gravity on gastric digestion. The research in this field still have not received much attention, although it may be related to space adaptation syndrome and the loss of the body mass after long space travel. A

possible reason for neglecting this problem is that foods still can be digested under reduced gravity through the movement of muscles. This is similar to the fact that human can still eat when they are on their heads (upside down), however, the digestion process is neither comfortable nor healthy. Weightlessness may have serious effect on human's health through deteriorating the digestion. Extensive studies are necessary to clearly understand human's gastric digestion under reduced gravity. Through the studies, we may find the ways with which astronauts and/or tourists may enjoy more comfortable and healthy meals during the journal to outer space.

Appendix: A 0D Model for Gastric Emptying Rate

A 0D model for the gastric emptying may be proposed. The first mechanism controlling the emptying rate is the food caloric content. Kong and Singh (2008) suggested that gastric emptying is controlled that about 2 to 4 kcal·min^{-1} (8.4 to 16.8 kJ·min^{-1}) caloric content is delivered to the duodenum through a negative feedback mechanism mediated by the duodenal receptors. The caloric flow rate is assumed to be a constant $\dot{q}$ which has the dimension kcal·s^{-1}, then the emptying rate is

$$\frac{\dot{m}}{\rho_g} = -\frac{dV}{dt} = \frac{\dot{q}}{q_g}. \tag{A.1}$$

Where $\dot{m}$ (kg·s^{-1}) is the mass flow rate of the gastric contents, ρ_g (kcal·m^{-3}) is the density of the gastric contents. q_g (kcal·m^{-3}) is the caloric density of the gastric contents. Another mechanism is about the net effects of propulsive forces and the flow resistance. According to mass conservation, the emptying rate is calculated as

$$\frac{\dot{m}}{\rho_g} = -\frac{dV}{dt} = u_e A_e, \tag{A.2}$$

where u_e (m·s^{-1}) and A_e (m^2) are the velocity and area at the outlet (pylorus), respectively. According to the energy conservation, the work done by the surface tension force at the stomach inner-surface $T_{is}u_{is}A_{is}/\rho_g$ is identical to the energy flow rate at the exit, expressed as

$$\frac{T_{is}u_{is}A_{is}}{\rho_g} = \frac{1}{2}u_e^3 A_e, \tag{A.3}$$

where T_{is} (Pa), u_{is} (m·s^{-1}) and A_{is} (m^2) are the surface tension force, velocity and surface of the stomach inner-surface, respectively. Considering $u_{is}A_{is} = u_e A_e$ and substituting Eq. (A.3) into Eq. (A.2), I have

$$\frac{dV}{dt} = -A_e\sqrt{2\,T_{is}/\rho_g}. \tag{A.4}$$

The following model is assumed for calculating T_{is},

$$T_{is} = \gamma V^{\beta}, \tag{A.5}$$

where β is a model constant. Substituting Eq. (A.5) into Eq. (A.4), I have

$$-\frac{dV}{dt} = \eta V^{\beta/2}, \tag{A.6}$$

where $\eta = \sqrt{\frac{2\gamma}{\rho_g}} A_e$ is the model coefficient. It appears that the stomach empties foods at a rate determined by the volume of gastric contents. Eq. (A.6) has the analytical solution:

$$V = \begin{cases} V_0 \mathrm{e}^{-\eta t} & \beta = 2 \\ \left[V_0^{\frac{2-\beta}{2}} - \eta \left(1 - \frac{\beta}{2}\right) t \right]^{\frac{2}{2-\beta}} & \beta \neq 2 \end{cases}, \tag{A.7}$$

here V_0 (m^3) is the initial volume of gastric contents. The normalized form of Eq. (A.7) is the retention fraction in the stomach:

$$r = \begin{cases} \mathrm{e}^{-\eta t} & \beta = 2 \\ \left[1 - \eta V_0^{\frac{\beta-2}{2}} \left(1 - \frac{\beta}{2}\right) t \right]^{\frac{2}{2-\beta}} & \beta \neq 2 \end{cases}. \tag{A.8}$$

Considering both Eq. (A.1) and Eq. (A.6), I have

$$-\frac{dV}{dt} = min\left(\frac{\dot{q}}{q_g}, \eta V^{\beta/2}\right). \tag{A.9}$$

Based on Eq. (A.9), two different emptying patterns for liquid foods are analyzed. One has a constant emptying rate of calorie content (see Eq. A.1), which I have $\dot{q}$ = 3.55 × 10^{-2} kcal·s^{-1} for glucose solutions of three different concentrations, they have energy amount of 0.2 kcal·ml^{-1}, 0.5 kcal·ml^{-1} and 1.0 kcal·ml^{-1} respectively. As shown in Fig. A.1a, the analytical predictions for the faction of gastric contents in the stomach (solid lines) agree well with physiological data from experiments. The emptying rate is slower as the caloric concentration increases since the indistinguishable emptying-rate of calories is used. The others don't have a constant energy emptying rate, their emptying rates are determined by Eq. (A.7). The model coefficients (η) for saline, water and ethanol are around 1.58 × 10^{-3}, 1.36 × 10^{-3} and 1.04 × 10^{-3} s^{-1} respectively, and

the model constant $\beta = 2$. As can be seen in Fig. A.1b, the analytical results fit the experiments well, gastric emptying of three subjects show a similar trend, the rate changes from their previous rapid pattern to a much slower one. They follow the typical exponential pattern, and the rate of emptying is determined by the volume of remained contents in the stomach.

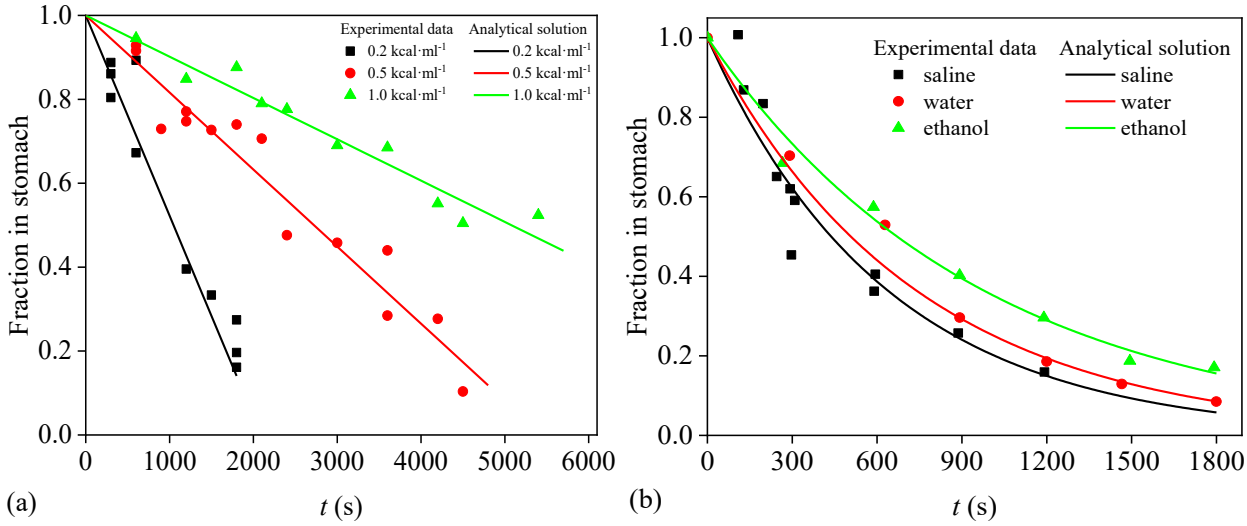

Fig. A.1. The retention fraction of gastric contents in the human stomach: (a) Three glucose solutions; (b) the physiological saline (0.9% w/v NaCl), water and ethanol. The discrete points are from in vivo experiments, see Brener et al. (1983) for glucose and saline, see Cooke (1970) for water and ethanol. The solid lines indicate analytical solutions predicted by the 0D model (see Eq. A.8).

Our model reflects mechanisms of gastric emptying. The emptying curve of a caloric food has a constant slope, which means that calorie amounts are delivered with a constant rate into the duodenum. This is consistent with the statement that the gastric emptying is in “steady state”, balanced by the intestinal inhibition (Brener et al., 1983). The emptying of non-nutrient foods is little impeded by the inhibition, it primarily depends on the distention of the stomach, and the surface tension from the inner wall plays a leading role. It’s said that ethanol is water soluble so it would not activate controlling receptors of emptying in the duodenum (Cooke, 1970). Thus the

emptying of ethanol is determined by the remnant volume of the gastric load. The differences of emptying curves in Fig. A.1b also indicate that there are other factors influencing the emptying, e.g., osmolality and stomach absorption. Comparing water and saline, it can be found that a higher osmolality gives a faster emptying. Between the water and the ethanol, the retention of the ethanol is higher in the stomach even through there are absorption effects of the ethanol.

In this thesis, the simplified situation of Eq. (A.9) has been used in CFD simulations. The emptying was assumed to be determined with the constant calorie emptying rate for foods with calories, namely $-\frac{dV}{dt} = \frac{\dot{q}}{q_g}$. The emptying rate was assumed to be constant for water, i.e., $-\frac{dV}{dt}$ remains unchanged in a simulation.

References

Abell, T.L., Camilleri, M., Donohoe, K., Hasler, W.L., Lin, H.C., Maurer, A.H., McCallum, R.W., Nowak, T., Nusynowitz, M.L., Parkman, H.P., 2008. Consensus recommendations for gastric emptying scintigraphy: a joint report of the American Neurogastroenterology and Motility Society and the Society of Nuclear Medicine. *Journal of nuclear medicine technology* 36, 44-54.

Abrahamsson, B., Alpsten, M., Bake, B., Larsson, A., Sjögren, J., 1998. In vitro and in vivo erosion of two different hydrophilic gel matrix tablets. *European journal of pharmaceutics and biopharmaceutics* 46, 69-75.

Abrahamsson, B., Pal, A., Sjöberg, M., Carlsson, M., Laurell, E., Brasseur, J.G., 2005. A novel in vitro and numerical analysis of shear-induced drug release from extended-release tablets in the fed stomach. *Pharmaceutical research* 22, 1215-1226.

Abuhelwa, A.Y., Foster, D.J., Upton, R.N., 2016. A quantitative review and meta-models of the variability and factors affecting oral drug absorption—part I: gastrointestinal pH. *The AAPS Journal* 18, 1309-1321.

Acharya, S., Halder, S., Kou, W., Kahrilas, P.J., Pandolfino, J.E., Patankar, N.A., 2021. A Fully Resolved Multiphysics Model of Gastric Peristalsis and Bolus Emptying in the Upper Gastrointestinal Tract. *arXiv preprint arXiv:2103.14814*.

Adams, C.P., Callaghan-Patrachar, N., Peyronel, F., Barker, J., Pink, D.A., Marangoni, A.G., 2019. Small and ultra-small angle neutron scattering studies of commercial milk. *Food Structure* 21, 100120.

Ajaj, W., Goehde, S., Papanikolaou, N., Holtmann, G., Ruehm, S., Debatin, J., Lauenstein, T., 2004. Real time high resolution magnetic resonance imaging for the assessment of gastric motility disorders. *Gut* 53, 1256-1261.

Alokaily, S., Feigl, K., Tanner, F.X., 2019. Characterization of peristaltic flow during the mixing process in a model human stomach. *Physics of Fluids* 31, 103105.

Alokaily, S.A., 2017. Modeling and simulation of the peristaltic flow of Newtonian and non-Newtonian fluids with application to the human body. Michigan Technological University.

Avvari, R.K., 2021. Theoretical modeling of the resistance to gastric emptying and duodenogastric reflux due to pyloric motility alone, presuming antral and duodenal quiescence. *Journal of Theoretical Biology* 508, 110460.

Baniabedalruhman, A., 2015. Dynamic meshing around fluid-fluid interfaces with applications to droplet tracking in contraction geometries. Michigan Technological University.

Bardonnet, P., Faivre, V., Pugh, W., Piffaretti, J., Falson, F., 2006. Gastroretentive dosage forms: Overview and special case of Helicobacter pylori. *Journal of controlled release* 111, 1-18.

Barros, L., Retamal, C., Torres, H., Zúñiga, R.N., Troncoso, E., 2016. Development of an in vitro mechanical gastric system (IMGS) with realistic peristalsis to assess lipid digestibility. *Food Research International* 90, 216-225.

Barroso, E., Cueva, C., Peláez, C., Martínez-Cuesta, M.C., Requena, T., 2015. Development of human colonic microbiota in the computer-controlled dynamic SIMulator of the GastroIntestinal tract SIMGI. *LWT-Food Science and Technology* 61, 283-289.

Bax, M.-L., Aubry, L., Ferreira, C., Daudin, J.-D., Gatellier, P., Rémond, D., Santé-Lhoutellier, V., 2012. Cooking temperature is a key determinant of in vitro meat protein digestion rate: investigation of underlying mechanisms. *Journal of agricultural and food chemistry* 60, 2569-2576.

Beckett, E.A., McGeough, C.A., Sanders, K.M., Ward, S.M., 2003. Pacing of interstitial cells of Cajal in the murine gastric antrum: neurally mediated and direct stimulation. *The Journal of physiology* 553, 545-559.

Berry, R., Miyagawa, T., Paskaranandavadivel, N., Du, P., Angeli, T.R., Trew, M.L., Windsor, J.A., Imai, Y., O'Grady, G., Cheng, L.K., 2016. Functional physiology of the human terminal antrum defined by high-resolution electrical mapping and computational modeling. *American Journal of Physiology-Gastrointestinal and Liver Physiology* 311, G895-G902.

Bilecen, D., Scheffler, K., Seifritz, E., Bongartz, G., Steinbrich, W., 2000. Hydro-MRI for the visualization of gastric wall motility using RARE magnetic resonance imaging sequences. *Abdominal imaging* 25, 30-34.

Bornhorst, G.M., 2017. Gastric mixing during food digestion: Mechanisms and applications. *Annual review of food science and technology* 8, 523-542.

Bornhorst, G.M., Chang, L.Q., Rutherfurd, S.M., Moughan, P.J., Singh, R.P., 2013. Gastric emptying rate and chyme characteristics for cooked brown and white rice meals in vivo. *Journal of the Science of Food and Agriculture* 93, 2900-2908.

Bornhorst, G.M., Gouseti, O., Wickham, M.S., Bakalis, S., 2016. Engineering digestion: multiscale processes of food digestion. *Journal of Food Science* 81, R534-R543.

Bornhorst, G.M., Paul Singh, R., 2014. Gastric digestion in vivo and in vitro: how the structural aspects of food influence the digestion process. *Annual review of food science and technology* 5, 111-132.

Bornhorst, G.M., Rutherfurd, S.M., Roman, M.J., Burri, B.J., Moughan, P.J., Singh, R.P., 2014. Gastric pH distribution and mixing of soft and rigid food particles in the stomach using a dual-marker technique. *Food Biophysics* 9, 292-300.

Brandstaeter, S., Fuchs, S.L., Aydin, R.C., Cyron, C.J., 2019. Mechanics of the stomach: A review of an emerging field of biomechanics. *GAMM‐Mitteilungen*, e201900001.

Brener, W., Hendrix, T.R., Mchugh, P.R., 1983. Regulation of the gastric emptying of glucose. *Gastroenterology* 85, 76-82.

Brodkorb, A., Egger, L., Alminger, M., Alvito, P., Assunção, R., Ballance, S., Bohn, T., Bourlieu-Lacanal, C., Boutrou, R., Carrière, F., 2019. INFOGEST static in vitro simulation of gastrointestinal food digestion. *Nature protocols* 14, 991-1014.

Brun, R., Michalek, W., Surjanhata, B., Parkman, H., Semler, J., Kuo, B., 2012. Comparative analysis of phase III migrating motor complexes in stomach and small bowel using wireless motility capsule and antroduodenal manometry. *Neurogastroenterology & Motility* 24, 332-e165.

Burton, D.D., Kim, H.J., Camilleri, M., Stephens, D.A., Mullan, B.P., O'Connor, M.K., Talley, N.J., 2005. Relationship of gastric emptying and volume changes after a solid meal in humans. *American Journal of Physiology-Gastrointestinal and Liver Physiology* 289, G261-G266.

Bylund, G., 2003. Dairy processing handbook. Tetra Pak Processing Systems AB.

Camilleri, M., Brown, M.L., Malagelada, J.-R., 1986. Relationship between impaired gastric emptying and abnormal gastrointestinal motility. *Gastroenterology* 91, 94-99.

Camilleri, M., Malagelada, J., Brown, M., Becker, G., Zinsmeister, A., 1985. Relation between antral motility and gastric emptying of solids and liquids in humans. *American Journal of Physiology-Gastrointestinal and Liver Physiology* 249, G580-G585.

Camps, G., Mars, M., De Graaf, C., Smeets, P.A., 2016. Empty calories and phantom fullness: a randomized trial studying the relative effects of energy density and viscosity on gastric emptying determined by MRI and satiety. *The American journal of clinical nutrition* 104, 73-80.

Capuano, E., Janssen, A.E., 2021. Food Matrix and Macronutrient Digestion. *Annual review of food science and technology* 12, 193-212.

Cardoso-Júnior, A., Coelho, L.G.V., Savassi-Rocha, P.R., Vignolo, M.C., Abrantes, M.M., De Almeida, A.M., Dias, E.E., Júnior, G.V., De Castro, M.M., Lemos, Y.V., 2007. Gastric emptying of solids and semi-solids in morbidly obese and non-obese subjects: an assessment using the 13 C-octanoic acid and 13 C-acetic acid breath tests. *Obesity surgery* 17, 236-241.

Carrière, F., Renou, C., Ransac, S., Lopez, V., De Caro, J., Ferrato, F., De Caro, A., Fleury, A., Sanwald-Ducray, P., Lengsfeld, H., 2001. Inhibition of gastrointestinal lipolysis by Orlistat during digestion of test meals in healthy volunteers. *American Journal of Physiology-Gastrointestinal and Liver Physiology* 281, G16-G28.

Chen, J., 2009. Food oral processing—A review. *Food Hydrocolloids* 23, 1-25.

Chen, L., Xu, Y., Fan, T., Liao, Z., Wu, P., Wu, X., Chen, X.D., 2016. Gastric emptying and morphology of a 'near real'in vitro human stomach model (RD-IV-HSM). *Journal of food engineering* 183, 1-8.

Chvasta, T.E., Cooke, A.R., 1971. Emptying and absorption of caffeine from the human stomach. *Gastroenterology* 61, 838-843.

Collins, P., Horowitz, M., Maddox, A., Myers, J., Chatterton, B., 1996. Effects of increasing solid component size of a mixed solid/liquid meal on solid and liquid gastric emptying. *American Journal of Physiology-Gastrointestinal and Liver Physiology* 271, G549-G554.

Collins, P., Houghton, L., Read, N., Horowitz, M., Chatterton, B., Heddle, R., Dent, J., 1991. Role of the proximal and distal stomach in mixed solid and liquid meal emptying. *Gut* 32, 615-619.

Cooke, A.R., 1970. The simultaneous emptying and absorption of ethanol from the human stomach. *The American journal of digestive diseases* 15, 449-454.

Davis, S.S., 2005. Formulation strategies for absorption windows. *Drug discovery today* 10, 249-257.

De Block, C.E., De Leeuw, I.H., Pelckmans, P.A., Van Gaal, L.F., 2006. Current concepts in gastric motility in diabetes mellitus. *Current diabetes reviews* 2, 113-130.

De Boer, A., Van der Schoot, M.S., Bijl, H., 2007. Mesh deformation based on radial basis function interpolation. *Computers & structures* 85, 784-795.

de La Pomélie, D., Santé-Lhoutellier, V., Sayd, T., Théron, L., Gatellier, P., 2019. Using a dynamic artificial digestive system to investigate heme iron nitrosylation during gastro-intestinal transit. *Food chemistry* 281, 231-235.

Demirdžić, I., Perić, M., 1988. Space conservation law in finite volume calculations of fluid flow. *International journal for numerical methods in fluids* 8, 1037-1050.

Desipio, J., Friedenberg, F., Korimilli, A., Richter, J., Parkman, H., Fisher, R., 2007. High‐resolution solid‐state manometry of the antropyloroduodenal region. *Neurogastroenterology & Motility* 19, 188-195.

Dikeman, C.L., Fahey Jr, G.C., 2006. Viscosity as related to dietary fiber: a review. *Critical reviews in food science and nutrition* 46, 649-663.

Do, D.H.T., Kong, F., Penet, C., Winetzky, D., Gregory, K., 2016. Using a dynamic stomach model to study efficacy of supplemental enzymes during simulated digestion. *LWT-Food Science and Technology* 65, 580-588.

Dufour, D., Tanner, F., Feigl, K., Windhab, E., 2021. Investigation of the dispersing characteristics of antral contraction wave flow in a simplified model of the distal stomach. *Physics of Fluids* 33, 083101.

Dupont, D., Alric, M., Blanquet-Diot, S., Bornhorst, G., Cueva, C., Deglaire, A., Denis, S., Ferrua, M., Havenaar, R., Lelieveld, J., 2019. Can dynamic in vitro digestion systems mimic the physiological reality? *Critical reviews in food science and nutrition* 59, 1546-1562.

Dupont, D., Le Feunteun, S., Marze, S., Souchon, I., 2018. Structuring food to control its disintegration in the gastrointestinal tract and optimize nutrient bioavailability. *Innovative Food Science & Emerging Technologies* 46, 83-90.

Eckel, R.H., Grundy, S.M., Zimmet, P.Z., 2005. The metabolic syndrome. *The lancet* 365, 1415-1428.

Ehrlein, H., Schemann, M., 2005. Gastrointestinal motility. *Technische Universität München: Munich*, 1-26.

Engelen, L., Fontijn-Tekamp, A., van der Bilt, A., 2005. The influence of product and oral characteristics on swallowing. *Archives of Oral Biology* 50, 739-746.

Erickson, H.P., 2009. Size and shape of protein molecules at the nanometer level determined by sedimentation, gel filtration, and electron microscopy. *Biological procedures online* 11, 32-51.

Faas, H., Steingoetter, A., Feinle, C., Rades, T., Lengsfeld, H., Boesiger, P., Fried, M., Schwizer, W., 2002. Effects of meal consistency and ingested fluid volume on the intragastric distribution of a drug model in humans—a magnetic resonance imaging study. *Alimentary pharmacology & therapeutics* 16, 217-224.

Ferrua, M.J., Singh, R.P., 2010. Modeling the fluid dynamics in a human stomach to gain insight of food digestion. *Journal of Food Science* 75, R151-R162.

Ferrua, M.J., Kong, F., Singh, R.P., 2011. Computational modeling of gastric digestion and the role of food material properties. *Trends in Food Science & Technology* 22, 480-491.

Ferrua, M.J., Singh, R.P., 2011. Understanding the fluid dynamics of gastric digestion using computational modeling. *Procedia Food Science* 1, 1465-1472.

Ferrua, M.J., Singh, R.P., 2015. Computational modelling of gastric digestion: current challenges and future directions. *Current Opinion in Food Science* 4, 116-123.

Ferrua, M.J., Xue, Z., Singh, R.P., 2014. On the kinematics and efficiency of advective mixing during gastric digestion–A numerical analysis. *Journal of Biomechanics* 47, 3664-3673.

Fontijn-Tekamp, F., Van Der Bilt, A., Abbink, J., Bosman, F., 2004. Swallowing threshold and masticatory performance in dentate adults. *Physiology & behavior* 83, 431-436.

Garcia-Villalba, R., Vissenaekens, H., Pitart, J., Romo-Vaquero, M., Espín, J.C., Grootaert, C., Selma, M.V., Raes, K., Smagghe, G., Possemiers, S., 2017. Gastrointestinal simulation model TWIN-SHIME shows differences between human urolithin-metabotypes in gut microbiota composition, pomegranate polyphenol metabolism, and transport along the intestinal tract. *Journal of agricultural and food chemistry* 65, 5480-5493.

Glerup, H., Bluhme, H., Villadsen, G.E., Rasmussen, K., Ejskjaer, N., Dahlerup, J.F., 2007. Gastric emptying: a comparison of three methods. *Scandinavian journal of gastroenterology* 42, 1182-1186.

Gopirajah, R., Raichurkar, K.P., Wadhwa, R., Anandharamakrishnan, C., 2016. The glycemic response to fibre rich foods and their relationship with gastric emptying and motor functions: an MRI study. *Food & function* 7, 3964-3972.

Gray, G.M., 1975. Carbohydrate digestion and absorption: role of the small intestine. *New England Journal of Medicine* 292, 1225-1230.

Griffiths, M., 2012. Crash Course: Gastrointestinal System E-Book. Elsevier Health Sciences.

Grimm, M., Scholz, E., Koziolek, M., Kühn, J.-P., Weitschies, W., 2017. Gastric water emptying under fed state clinical trial conditions is as fast as under fasted conditions. *Molecular pharmaceutics* 14, 4262-4271.

Guerra, A., Denis, S., le Goff, O., Sicardi, V., François, O., Yao, A.F., Garrait, G., Manzi, A.P., Beyssac, E., Alric, M., 2016. Development and validation of a new dynamic computer‐controlled model of the human stomach and small intestine. *Biotechnology and bioengineering* 113, 1325-1335.

Guerra, A., Etienne-Mesmin, L., Livrelli, V., Denis, S., Blanquet-Diot, S., Alric, M., 2012. Relevance and challenges in modeling human gastric and small intestinal digestion. *Trends in biotechnology* 30, 591-600.

Hao, S., Wang, B., Wang, Y., 2015. Density-dependent gastroretentive microparticles motion in human gastric emptying studied using computer simulation. *European Journal of Pharmaceutical Sciences* 70, 72-81.

Harrison, S.M., Cleary, P.W., Sinnott, M.D., 2018. Investigating mixing and emptying for aqueous liquid content from the stomach using a coupled biomechanical-SPH model. *Food & function* 9, 3202-3219.

Helkimo, E., Carlsson, G.E., Helkimo, M., 1978. Chewing efficiency and state of dentition: a methodologic study. *Acta Odontologica Scandinavica* 36, 33-41.

Hirano, I., Yamada, T., Hirano, I., 2015. Esophagus: Anatomy and Structural Anomalies, Yamada's Textbook of Gastroenterology. John Wiley & Sons, Ltd Oxford, UK, pp. 42-59.

Ho, H.V.T., Jovanovski, E., Zurbau, A., Blanco Mejia, S., Sievenpiper, J.L., Au-Yeung, F., Jenkins, A.L., Duvnjak, L., Leiter, L., Vuksan, V., 2017. A systematic review and meta-analysis of randomized controlled trials of the effect of konjac glucomannan, a viscous soluble fiber, on LDL cholesterol and the new lipid targets non-HDL cholesterol and apolipoprotein B. *The American journal of clinical nutrition* 105, 1239-1247.

Hogben, C.A.M., Schanker, L.S., Tocco, D.J., Brodie, B.B., 1957. Absorption of drugs from the stomach. II. The human. *Journal of pharmacology and experimental therapeutics* 120, 540-545.

Holz, M., Heil, S.R., Sacco, A., 2000. Temperature-dependent self-diffusion coefficients of water and six selected molecular liquids for calibration in accurate 1H NMR PFG measurements. *Physical Chemistry Chemical Physics* 2, 4740-4742.

Huh, C., Bhutani, M., Farfan, E., Bolch, W., 2003. Individual variations in mucosa and total wall thickness in the stomach and rectum assessed via endoscopic ultrasound. *Physiological measurement* 24, N15.

Hunt, J., Smith, J., Jiang, C., 1985. Effect of meal volume and energy density on the gastric emptying of carbohydrates. *Gastroenterology* 89, 1326-1330.

Hunt, J.C.R., Wray, A., Moin, P., 1988. Eddies, stream, and convergence zones in turbulent flows, Center for turbulence research report CTR-S88, pp. 193-208.

Imai, Y., Kobayashi, I., Ishida, S., Ishikawa, T., Buist, M., Yamaguchi, T., 2013. Antral recirculation in the stomach during gastric mixing. *American Journal of Physiology: Gastrointestinal and Liver Physiology* 304, G536-G542.

Indireshkumar, K., Brasseur, J.G., Faas, H., Hebbard, G.S., Kunz, P., Dent, J., Feinle, C., Li, M., Boesiger, P., Fried, M., 2000. Relative contributions of “pressure pump” and “peristaltic pump” to gastric emptying. *American Journal of Physiology: Gastrointestinal and Liver Physiology* 278, G604-G616.

Ishida, S., Miyagawa, T., O'Grady, G., Cheng, L.K., Imai, Y., 2019. Quantification of gastric emptying caused by impaired coordination of pyloric closure with antral contraction: a simulation study. *Journal of the Royal Society Interface* 16, 20190266.

Islam, M., Kitamura, Y., Kokawa, M., Monalisa, K., Tsai, F.-H., Miyamura, S., 2017. Effects of micro wet milling and vacuum spray drying on the physicochemical and antioxidant properties of orange (Citrus unshiu) juice with pulp powder. *Food and bioproducts processing* 101, 132-144.

Jalabert-Malbos, M.-L., Mishellany-Dutour, A., Woda, A., Peyron, M.-A., 2007. Particle size distribution in the food bolus after mastication of natural foods. *Food Quality and Preference* 18, 803-812.

Jasak, H., 2009. Dynamic mesh handling in OpenFOAM, 47th AIAA aerospace sciences meeting including the new horizons forum and aerospace exposition, p. 341.

Jasak, H., Jemcov, A., Tukovic, Z., 2007. OpenFOAM: A C++ library for complex physics simulations, International workshop on coupled methods in numerical dynamics. IUC Dubrovnik Croatia, pp. 1-20.

Jasak, H., Tukovic, Z., 2006. Automatic mesh motion for the unstructured finite volume method. *Transactions of FAMENA* 30, 1-20.

Jaspersen, D., 2000. Drug-induced oesophageal disorders. *Drug safety* 22, 237-249.

Ji, H., Hu, J., Zuo, S., Zhang, S., Li, M., Nie, S., 2021. In vitro gastrointestinal digestion and fermentation models and their applications in food carbohydrates. *Critical reviews in food science and nutrition*, 1-23.

Johnson, A.A., Tezduyar, T.E., 1994. Mesh update strategies in parallel finite element computations of flow problems with moving boundaries and interfaces. *Computer methods in applied mechanics and engineering* 119, 73-94.

Johnson, G.B., Brusca, G.J., 1994. Biology, visualizing life. Holt, Rinehart and Winston Austin.

Kamaltdinov, M., 2014. 3D modeling of antroduodenal zone motility of digestive track for the purpose of health risks evaluation with peroral exposition to chemicals. *АНАЛИЗ РИСКА ЗДОРОВЬЮ*, 75.

Kamaltdinov, M., Trusov, P., Zaitseva, N., 2018. A multiphase flow in the antroduodenum: some results of the mathematical modelling and computational simulation, MATEC Web of Conferences. EDP Sciences, p. 04002.

Kamaltdinov, M., Zaitseva, N., Shur, P., 2017a. Numerical modeling of acidity distribution in antroduodenum aimed at identifying anomalous zones at consuming drinks with different pH level. *Health*, 36.

Kamaltdinov, M.R., Trusov, P.V., Zaitseva, N.V., 2020. A mathematical model for multiphase flow in the antroduodenum with the consideration of the neurohumoral regulation, AIP Conference Proceedings. AIP Publishing LLC, p. 060003.

Kamaltdinov, M.R., Trusov, P.V., Zaitseva, N.V., 2021. A mathematical model of flow in the antroduodenum: Changes in the density and viscosity in relation to the component composition, AIP Conference Proceedings. AIP Publishing LLC, p. 060003.

Kamaltdinov, M., Trusov, P., Zaitseva, N., 2017b. Multi-component mixture flow in the stomach and duodenum allowing for functional disorders: results of numeric modelling for determining acidity. *Russian Journal of Biomechanics* 21.

Kamba, M., Seta, Y., Kusai, A., Nishimura, K., 2001. Evaluation of the mechanical destructive force in the stomach of dog. *International journal of pharmaceutics* 228, 209-217.

Kamba, M., Seta, Y., Kusai, A., Nishimura, K., 2002. Comparison of the mechanical destructive force in the small intestine of dog and human. *International journal of pharmaceutics* 237, 139-149.

Katelaris, P., Seow, F., Lin, B., Napoli, J., Ngu, M., Jones, D., 1993. Effect of age, Helicobacter pylori infection, and gastritis with atrophy on serum gastrin and gastric acid secretion in healthy men. *Gut* 34, 1032-1037.

Kaunitz, J., Akiba, Y., 2006. duodenal bicarbonate–mucosal protection, luminal chemosensing and acid–base balance. *Alimentary pharmacology & therapeutics* 24, 169-176.

Kelly, K.A., 1980. Gastric emptying of liquids and solids: roles of proximal and distal stomach. *American Journal of Physiology-Gastrointestinal and Liver Physiology* 239, G71-G76.

King, P., Adam, R., Pryde, A., McDicken, W., Heading, R., 1984. Relationships of human antroduodenal motility and transpyloric fluid movement: non-invasive observations with real-time ultrasound. *Gut* 25, 1384-1391.

Kobayashi, I., Kozu, H., Wang, Z., Isoda, H., Ichikawa, S., 2017. Development and fundamental characteristics of a human gastric digestion simulator for analysis of food disintegration. *Japan Agricultural Research Quarterly: JARQ* 51, 17-25.

Kondjoyan, A., Daudin, J.-D., Santé-Lhoutellier, V., 2015. Modelling of pepsin digestibility of myofibrillar proteins and of variations due to heating. *Food chemistry* 172, 265-271.

Kong, F., Singh, R.P., 2008. Disintegration of solid foods in human stomach. *Journal of Food Science* 73, R67-R80.

Kong, F., Singh, R.P., 2010. A human gastric simulator (HGS) to study food digestion in human stomach. *Journal of Food Science* 75, E627-E635.

Koziolek, M., Garbacz, G., Neumann, M., Weitschies, W., 2013. Simulating the postprandial stomach: physiological considerations for dissolution and release testing. *Molecular pharmaceutics* 10, 1610-1622.

Koziolek, M., Grimm, M., Garbacz, G., Kühn, J.-P., Weitschies, W., 2014. Intragastric volume changes after intake of a high-caloric, high-fat standard breakfast in healthy human subjects investigated by MRI. *Molecular pharmaceutics* 11, 1632-1639.

Koziolek, M., Grimm, M., Schneider, F., Jedamzik, P., Sager, M., Kühn, J.-P., Siegmund, W., Weitschies, W., 2016. Navigating the human gastrointestinal tract for oral drug delivery: uncharted waters and new frontiers. *Advanced Drug Delivery Reviews* 101, 75-88.

Kozu, H., Kobayashi, I., Nakajima, M., Neves, M.A., Uemura, K., Isoda, H., Ichikawa, S., 2017. Mixing characterization of liquid contents in human gastric digestion simulator equipped with gastric secretion and emptying. *Biochemical Engineering Journal* 122, 85-90.

Kozu, H., Kobayashi, I., Nakajima, M., Uemura, K., Sato, S., Ichikawa, S., 2010. Analysis of flow phenomena in gastric contents induced by human gastric peristalsis using CFD. *Food Biophysics* 5, 330-336.

Kozu, H., Kobayashi, I., Neves, M.A., Nakajima, M., Uemura, K., Sato, S., Ichikawa, S., 2014a. PIV and CFD studies on analyzing intragastric flow phenomena induced by peristalsis using a human gastric flow simulator. *Food & function* 5, 1839-1847.

Kozu, H., Nakata, Y., Nakajima, M., Neves, M.A., Uemura, K., Sato, S., Kobayashi, I., Ichikawa, S., 2014b. Development of a human gastric digestion simulator equipped with peristalsis

function for the direct observation and analysis of the food digestion process. *Food Science and Technology Research* 20, 225-233.

Krehbiel, C., Matthews, J., 2003. Absorption of amino acids and peptides. *Amino acids in animal nutrition* 5, 41.

Kunz, P., Feinle‐Bisset, C., Faas, H., Boesiger, P., Fried, M., Steingötter, A., Schwizer, W., 2005. Effect of ingestion order of the fat component of a solid meal on intragastric fat distribution and gastric emptying assessed by MRI. *Journal of Magnetic Resonance Imaging: An Official Journal of the International Society for Magnetic Resonance in Medicine* 21, 383-390.

Kunz, P., Feinle, C., Schwizer, W., Fried, M., Boesiger, P., 1999. Assessment of gastric motor function during the emptying of solid and liquid meals in humans by MRI. *Journal of Magnetic Resonance Imaging: An Official Journal of the International Society for Magnetic Resonance in Medicine* 9, 75-80.

Kwiatek, M.A., Menne, D., Steingoetter, A., Goetze, O., Forras-Kaufman, Z., Kaufman, E., Fruehauf, H., Boesiger, P., Fried, M., Schwizer, W., 2009. Effect of meal volume and calorie load on postprandial gastric function and emptying: studies under physiological conditions by combined fiber-optic pressure measurement and MRI. *American Journal of Physiology-Gastrointestinal and Liver Physiology* 297, G894-G901.

Kwiatek, M.A., Steingoetter, A., Pal, A., Menne, D., Brasseur, J.G., Hebbard, G.S., Boesiger, P., Thumshirn, M., Fried, M., Schwizer, W., 2006. Quantification of distal antral contractile motility in healthy human stomach with magnetic resonance imaging. *Journal of Magnetic Resonance Imaging: An Official Journal of the International Society for Magnetic Resonance in Medicine* 24, 1101-1109.

Lafond, M., Bouza, B., Eyrichine, S., Rouffineau, F., Saulnier, L., Giardina, T., Bonnin, E., Preynat, A., 2015. In vitro gastrointestinal digestion study of two wheat cultivars and evaluation of xylanase supplementation. *Journal of animal science and biotechnology* 6, 1-14.

Langer, P., 1988. The mammalian herbivore stomach: comparative anatomy, function and evolution. Gustav Fischer.

Laulicht, B., Tripathi, A., Schlageter, V., Kucera, P., Mathiowitz, E., 2010. Understanding gastric forces calculated from high-resolution pill tracking. *Proceedings of the National Academy of Sciences* 107, 8201-8206.

Le Feunteun, S., Barbé, F., Rémond, D., Ménard, O., Le Gouar, Y., Dupont, D., Laroche, B., 2014. Impact of the dairy matrix structure on milk protein digestion kinetics: mechanistic modelling based on mini-pig in vivo data. *Food and bioprocess technology* 7, 1099-1113.

Le Feunteun, S., Mackie, A.R., Dupont, D., 2020. In silico trials of food digestion and absorption: how far are we? *Current Opinion in Food Science* 31, 121-125.

Levitt, M.D., Li, R., Demaster, E.G., Elson, M., Furne, J., Levitt, D.G., 1997. Use of measurements of ethanol absorption from stomach and intestine to assess human ethanol metabolism. *American Journal of Physiology-Gastrointestinal and Liver Physiology* 273, G951-G957.

Li, C., Gasow, S., Jin, Y., Xiao, J., Chen, X.D., 2021. Simulation based investigation of 2D soft-elastic reactors for better mixing performance. *Engineering Applications of Computational Fluid Mechanics* 15, 1229-1242.

Li, C., Yu, W., Wu, P., Chen, X.D., 2020. Current in vitro digestion systems for understanding food digestion in human upper gastrointestinal tract. *Trends in Food Science & Technology* 96, 114-126.

Li, Y., Fortner, L., Kong, F., 2019. Development of a Gastric Simulation Model (GSM) incorporating gastric geometry and peristalsis for food digestion study. *Food Research International* 125, 108598.

Liu, W., Fu, D., Zhang, X., Chai, J., Tian, S., Han, J., 2019. Development and validation of a new artificial gastric digestive system. *Food Research International* 122, 183-190.

Liu, W., Jin, Y., Wilde, P.J., Hou, Y., Wang, Y., Han, J., 2020. Mechanisms, physiology, and recent research progress of gastric emptying. *Critical reviews in food science and nutrition*, 1-14.

Löhner, R., Yang, C., 1996. Improved ALE mesh velocities for moving bodies. *Communications in numerical methods in engineering* 12, 599-608.

Lorkowski, G., 2012. Gastrointestinal absorption and biological activities of serine and cysteine proteases of animal and plant origin: review on absorption of serine and cysteine proteases. *International journal of physiology, pathophysiology and pharmacology* 4, 10.

Mackie, A., Mulet-Cabero, A.-I., Torcello-Gómez, A., 2020. Simulating human digestion: developing our knowledge to create healthier and more sustainable foods. *Food & function* 11, 9397-9431.

Malagelada, J.-R., Go, V.L., Summerskill, W., 1979. Different gastric, pancreatic, and biliary responses to solid-liquid or homogenized meals. *Digestive diseases and sciences* 24, 101-110.

Malagelada, J.-R., Longstreth, G., Summerskill, W., Go, V., 1976. Measurement of gastric functions during digestion of ordinary solid meals in man. *Gastroenterology* 70, 203-210.

Marciani, L., Gowland, P.A., Fillery-Travis, A., Manoj, P., Wright, J., Smith, A., Young, P., Moore, R., Spiller, R.C., 2001a. Assessment of antral grinding of a model solid meal with echo-planar imaging. *American Journal of Physiology-Gastrointestinal and Liver Physiology* 280, G844-G849.

Marciani, L., Gowland, P.A., Spiller, R.C., Manoj, P., Moore, R.J., Young, P., Al-Sahab, S., Bush, D., Wright, J., Fillery-Travis, A.J., 2000. Gastric response to increased meal viscosity assessed by echo-planar magnetic resonance imaging in humans. *The Journal of nutrition* 130, 122-127.

Marciani, L., Gowland, P.A., Spiller, R.C., Manoj, P., Moore, R.J., Young, P., Fillery-Travis, A.J., 2001b. Effect of meal viscosity and nutrients on satiety, intragastric dilution, and emptying assessed by MRI. *American Journal of Physiology-Gastrointestinal and Liver Physiology* 280, G1227-G1233.

Marciani, L., Hall, N., Pritchard, S.E., Cox, E.F., Totman, J.J., Lad, M., Hoad, C.L., Foster, T.J., Gowland, P.A., Spiller, R.C., 2012. Preventing gastric sieving by blending a solid/water meal enhances satiation in healthy humans. *The Journal of nutrition* 142, 1253-1258.

Marciani, L., Wickham, M., Singh, G., Bush, D., Pick, B., Cox, E., Fillery-Travis, A., Faulks, R., Marsden, C., Gowland, P.A., 2007. Enhancement of intragastric acid stability of a fat emulsion

meal delays gastric emptying and increases cholecystokinin release and gallbladder contraction. *American Journal of Physiology-Gastrointestinal and Liver Physiology*.

Marze, S., 2017a. Bioavailability of nutrients and micronutrients: advances in modeling and in vitro approaches. *Annual review of food science and technology* 8, 35-55.

Marze, S., 2017b. Modeling of Food Digestion, Modeling of Microscale Transport in Biological Processes. Elsevier, pp. 353-374.

Mason, K.L., Huffnagle, G.B., Noverr, M.C., Kao, J.Y., 2008. Overview of gut immunology. *GI microbiota and regulation of the immune system*, 1-14.

Mayer, E.A., 2011. Gut feelings: the emerging biology of gut–brain communication. *Nature Reviews Neuroscience* 12, 453-466.

McDonald, K., Sun, D.-W., 2001. The formation of pores and their effects in a cooked beef product on the efficiency of vacuum cooling. *Journal of food engineering* 47, 175-183.

Ménard, O., Cattenoz, T., Guillemin, H., Souchon, I., Deglaire, A., Dupont, D., Picque, D., 2014. Validation of a new in vitro dynamic system to simulate infant digestion. *Food chemistry* 145, 1039-1045.

Mennah-Govela, Y.A., Cai, H., Chu, J., Kim, K., Maborang, M.-K., Sun, W., Bornhorst, G.M., 2020. Buffering capacity of commercially available foods is influenced by composition and initial properties in the context of gastric digestion. *Food & function* 11, 2255-2267.

Miralles, B., Del Barrio, R., Cueva, C., Recio, I., Amigo, L., 2018. Dynamic gastric digestion of a commercial whey protein concentrate. *Journal of the Science of Food and Agriculture* 98, 1873-1879.

Miyagawa, T., Imai, Y., Ishida, S., Ishikawa, T., 2016. Relationship between gastric motility and liquid mixing in the stomach. *American Journal of Physiology-Gastrointestinal and Liver Physiology* 311, G1114-G1121.

Molly, K., Woestyne, M.V., Verstraete, W., 1993. Development of a 5-step multi-chamber reactor as a simulation of the human intestinal microbial ecosystem. *Applied microbiology and biotechnology* 39, 254-258.

Morell, P., Fiszman, S., Varela, P., Hernando, I., 2014. Hydrocolloids for enhancing satiety: Relating oral digestion to rheology, structure and sensory perception. *Food Hydrocolloids* 41, 343-353.

Mosca, A.C., Chen, J., 2016. Food oral management: Physiology and objective assessment. *Current Opinion in Food Science* 9, 11-20.

Mukai, J., Tsuge, Y., Yamada, M., Otori, K., Atsuda, K., 2017. Effects of resistant dextrin for weight loss in overweight adults: a systematic review with a meta-analysis of randomized controlled trials. *Journal of pharmaceutical health care and sciences* 3, 1-7.

Musselman, M.M., 1951. The Esophagus and Pharynx in Action: a Study of Structure in Relation to Function. Oxford University Press Oxford, UK.

Nguyen, H., Silny, J., Albers, D., Roeb, E., Gartung, C., Rau, G., Matern, S., 1997. Dynamics of esophageal bolus transport in healthy subjects studied using multiple intraluminal impedancometry. *American Journal of Physiology-Gastrointestinal and Liver Physiology* 273, G958-G964.

Ortiz Araque, L.C., Darré, M., Ortiz, C.M., Massolo, J.F., Vicente, A.R., 2018. Quality and yield of Ricotta cheese as affected by milk fat content and coagulant type. *International journal of dairy technology* 71, 340-346.

Osmanoglou, E., Van Der Voort, I., Fach, K., Kosch, O., Bach, D., Hartmann, V., Strenzke, A., Weitschies, W., Wiedenmann, B., Trahms, L., 2004. Oesophageal transport of solid dosage forms depends on body position, swallowing volume and pharyngeal propulsion velocity. *Neurogastroenterology & Motility* 16, 547-556.

Owen, D.A., 1986. Normal histology of the stomach. *The American journal of surgical pathology* 10, 48-61.

Pal, A., Brasseur, J.G., Abrahamsson, B., 2007. A stomach road or “Magenstrasse” for gastric emptying. *Journal of Biomechanics* 40, 1202-1210.

Pal, A., Indireshkumar, K., Schwizer, W., Abrahamsson, B., Fried, M., Brasseur, J.G., 2004. Gastric flow and mixing studied using computer simulation. *Proceedings of the Royal Society of London, Series B: Biological Sciences* 271, 2587-2594.

Parkman, H., Urbain, J.C., Knight, L., Brown, K., Trate, D., Miller, M., Maurer, A., Fisher, R., 1998. Effect of gastric acid suppressants on human gastric motility. *Gut* 42, 243-250.

Peng, Z., Wu, P., Wang, J., Dupont, D., Menard, O., Jeantet, R., Chen, X.D., 2021. Achieving realistic gastric emptying curve in an advanced dynamic in vitro human digestion system: experiences with cheese—a difficult to empty material. *Food & function* 12, 3965-3977.

Pera, P., Bucca, C., Borro, P., Bernocco, C., De Lillo, A., Carossa, S., 2002. Influence of mastication on gastric emptying. *Journal of dental research* 81, 179-181.

Piper, D., Fenton, B.H., 1965. pH stability and activity curves of pepsin with special reference to their clinical importance. *Gut* 6, 506.

Podolsky, D.K., Camilleri, M., Fitz, J.G., Kalloo, A.N., Shanahan, F., Wang, T.C., 2015. Yamada's textbook of gastroenterology. John Wiley & Sons.

POPESCU, A., ANGEL, E., 2019. Cow raw milk quality and its factors of influence in relationship with milk price. *Scientific Papers: Management, Economic Engineering in Agriculture & Rural Development* 19.

Pullan, A., Cheng, L., Yassi, R., Buist, M., 2004. Modelling gastrointestinal bioelectric activity. *Progress in biophysics and molecular biology* 85, 523-550.

Quillin, M.L., Matthews, B.W., 2000. Accurate calculation of the density of proteins. *Acta Crystallographica Section D: Biological Crystallography* 56, 791-794.

Rickett, L., 2013. A mathematical analysis of digestive processes in a model stomach. University of East Anglia.

Sarna, S.K., 1985. Cyclic motor activity; migrating motor complex: 1985. *Gastroenterology* 89, 894-913.

Sauter, M., Curcic, J., Menne, D., Goetze, O., Fried, M., Schwizer, W., Steingoetter, A., 2012. Measuring the interaction of meal and gastric secretion: a combined quantitative magnetic

resonance imaging and pharmacokinetic modeling approach. *Neurogastroenterology & Motility* 24, 632-e273.

Savoye-Collet, C., Savoye, G., Smout, A., 2003. Determinants of transpyloric fluid transport: a study using combined real-time ultrasound, manometry, and impedance recording. *American Journal of Physiology-Gastrointestinal and Liver Physiology* 285, G1147-G1152.

Scheunert, A., 1912. Über den Magenmechanismus des Hundes bei der Getränkaufnahme. *Pflüger's Archiv für die gesamte Physiologie des Menschen und der Tiere* 144, 569-576.

Schneeman, B.O., 2002. Gastrointestinal physiology and functions. *British Journal of Nutrition* 88, S159-S163.

Schubert, M.L., 2008. Hormonal regulation of gastric acid secretion. *Current Gastroenterology Reports* 10, 523-527.

Schulze, K., 2006. Imaging and modelling of digestion in the stomach and the duodenum. *Neurogastroenterology & Motility* 18, 172-183.

Schwizer, W., Maecke, H., Michael, F., 1992. Measurement of gastric emptying by magnetic resonance imaging in humans. *Gastroenterology* 103, 369-376.

Schwizer, W., Steingötter, A., Fox, M., Zur, T., Thumshirn, M., Bösiger, P., Fried, M., 2002. Non-invasive measurement of gastric accommodation in humans. *Gut* 51, i59-i62.

Sensoy, I., 2021. A review on the food digestion in the digestive tract and the used in vitro models. *Current research in food science*.

Seo, J.H., Mittal, R., 2022. Computational Modeling of Drug Dissolution in the Human Stomach. *Frontiers in Physiology*, 2080.

Shang, L., Wang, Y., Ren, Y., Ai, T., Zhou, P., Hu, L., Wang, L., Li, J., Li, B., 2020. In vitro gastric emptying characteristics of konjac glucomannan with different viscosity and its effects on appetite regulation. *Food & function* 11, 7596-7610.

Sicard, J., Mirade, P.-S., Portanguen, S., Clerjon, S., Kondjoyan, A., 2018. Simulation of the gastric digestion of proteins of meat bolus using a reaction–diffusion model. *Food & function* 9, 6455-6469.

Singh, S., Singh, R.P., 2010. Gastric digestion of foods: mathematical modeling of flow field in a human stomach, Food engineering interfaces. Springer, pp. 99-117.

Singh, S.K., 2007. Fluid flow and disintegration of food in human stomach. University of California, Davis.

Sinnott, M.D., Cleary, P.W., Harrison, S.M., 2017. Peristaltic transport of a particulate suspension in the small intestine. *Applied Mathematical Modelling* 44, 143-159.

Skamniotis, C., Charalambides, M., 2020. Development of computational design tools for characterising and modelling cutting in ultra soft solids. *Extreme Mechanics Letters* 40, 100964.

Skamniotis, C., Edwards, C.H., Bakalis, S., Frost, G., Charalambides, M., 2020. Eulerian-Lagrangian finite element modelling of food flow-fracture in the stomach to engineer digestion. *Innovative Food Science & Emerging Technologies* 66, 102510.

Skamniotis, C., Elliott, M., Charalambides, M., 2017. On modeling the large strain fracture behaviour of soft viscous foods. *Physics of Fluids* 29, 121610.

Smeets, P.A., Deng, R., van Eijnatten, E.J., Mayar, M., 2021. Monitoring food digestion with magnetic resonance techniques. *Proceedings of the Nutrition Society* 80, 148-158.

Stobdan, T., Chaurasia, O.P., Korekar, G., Yadav, A., Singh, S.B., 2010. Attributes of Seabuckthorn (Hippophae rhamnoides L.) to Meet Nutritional Requirements in High Altitude. *Defence Science Journal* 60, 226.

Sun, W., Smout, A., Malbert, C., Edelbroek, M., Jones, K., Dent, J., Horowitz, M., 1995. Relationship between surface electrogastrography and antropyloric pressures. *American Journal of Physiology-Gastrointestinal and Liver Physiology* 268, G424-G430.

Takahashi, T., 2012. Mechanism of interdigestive migrating motor complex. *Journal of Neurogastroenterology and Motility* 18, 246.

Takahashi, T., 2013. Interdigestive migrating motor complex-its mechanism and clinical importance. *Journal of Smooth Muscle Research* 49, 99-111.

Takahashi, T., Sakata, T., 2002. Large particles increase viscosity and yield stress of pig cecal contents without changing basic viscoelastic properties. *The Journal of nutrition* 132, 1026-1030.

Talukder, R., Fassihi, R., 2004. Gastroretentive delivery systems: A mini review. *Drug development and industrial pharmacy* 30, 1019-1028.

Tharakan, A., 2009. Modelling of physical and chemical processes in the small intestine. University of Birmingham.

Tortora, G.J., Derrickson, B., 2017. Principles of anatomy & physiology. John Wiley & Sons, Incorporated.

Tougas, G., Anvari, M., Dent, J., Somers, S., Richards, D., Stevenson, G., 1992. Relation of pyloric motility to pyloric opening and closure in healthy subjects. *Gut* 33, 466-471.

Treier, R., Steingoetter, A., Weishaupt, D., Goetze, O., Boesiger, P., Fried, M., Schwizer, W., 2006. Gastric motor function and emptying in the right decubitus and seated body position as assessed by magnetic resonance imaging. *Journal of Magnetic Resonance Imaging: An Official Journal of the International Society for Magnetic Resonance in Medicine* 23, 331-338.

Trusov, P., Zaitseva, N., Kamaltdinov, M., 2013. Simulation of digestion processes in consideration of functional disorders in a human organism: conceptual and mathematical formulations, model structure. *Russian Journal of Biomechanics* 17, 60-74.

Trusov, P., Zaitseva, N.V., Kamaltdinov, M., 2016. A multiphase flow in the antroduodenal portion of the gastrointestinal tract: a mathematical model. *Computational and Mathematical Methods in Medicine* 2016.

Urbain, J.-L.C., Siegel, J.A., Charkes, N.D., Maurer, A.H., Malmud, L.S., Fisher, R.S., 1989. The two-component stomach: effects of meal particle size on fundal and antral emptying. *European journal of nuclear medicine* 15, 254-259.

Vantrappen, G., Janssens, J., Hellemans, J., Ghoos, Y., 1977. The interdigestive motor complex of normal subjects and patients with bacterial overgrowth of the small intestine. *The Journal of clinical investigation* 59, 1158-1166.

Vardakou, M., Mercuri, A., Barker, S.A., Craig, D.Q., Faulks, R.M., Wickham, M.S., 2011. Achieving antral grinding forces in biorelevant in vitro models: comparing the USP dissolution

apparatus II and the dynamic gastric model with human in vivo data. *Aaps Pharmscitech* 12, 620-626.

Vassallo, M.J., Camilleri, M., Prather, C.M., Hanson, R., Thomforde, G., 1992. Measurement of axial forces during emptying from the human stomach. *American Journal of Physiology-Gastrointestinal and Liver Physiology* 263, G230-G239.

Versantvoort, C.H.M., Van de Kamp, E., Rompelberg, C.J.M., 2004. Development and applicability of an in vitro digestion model in assessing the bioaccessibility of contaminants from food. Report RIVM, Report 320102002/2004, Inspectorate of Health Inspection, Bilthoven.

Villanueva-Carvajal, A., Bernal-Martínez, L.R., García-Gasca, M.T., Dominguez-Lopez, A., 2013. In vitro gastrointestinal digestion of Hibiscus sabdariffa L.: The use of its natural matrix to improve the concentration of phenolic compounds in gut. *LWT-Food Science and Technology* 51, 260-265.

Walter, C., Willett, M., David, S., Ludwig, M., 2020. Milk and health. *N. Engl. J. Med* 382, 644-654.

Wang, J., Wu, P., Liu, M., Liao, Z., Wang, Y., Dong, Z., Chen, X., 2019. An advanced near real dynamic in vitro human stomach system to study gastric digestion and emptying of beef stew and cooked rice. *Food & function* 10, 2914-2925.

Wang, J., Wu, P., Wang, J., Wang, J., Gu, B., Ge, F., Chen, X.D., 2022. In vitro gastric digestion and emptying of cooked white and brown rice using a dynamic human stomach system. *Food Structure* 31, 100245.

Wickham, M., Faulks, R., Mann, J., Mandalari, G., 2012. The design, operation, and application of a dynamic gastric model. *Dissolution Technol* 19, 15-22.

Wiking, L., Stagsted, J., Björck, L., Nielsen, J.H., 2004. Milk fat globule size is affected by fat production in dairy cows. *International Dairy Journal* 14, 909-913.

Wu, P., Chen, X.D., 2019. On designing biomimic in vitro human and animal digestion track models: ideas, current and future devices. *Current Opinion in Food Science* 35, 10-19.

Xue, Z., Ferrua, M.J., Singh, P., 2012. Computational fluid dynamics modeling of granular flow in human stomach. *Alimentos hoy* 21, 3-14.

Ye, Q., Ge, F., Wang, Y., Wu, P., Chen, X.D., Selomulya, C., 2022. Digestion of curcumin-fortified yogurt in short/long gastric residence times using a near-real dynamic in vitro human stomach. *Food chemistry* 372, 131327.

Zhong, C., Langrish, T., 2020. A comparison of different physical stomach models and an analysis of shear stresses and strains in these system. *Food Research International* 135, 109296.